An-Najah National University
Faculty of Graduate studies

ANTICANCER IMATINIB DELIVERY SYSTEM BASED ON GRAPHENE OXIDE AND OXIDIZED MULTI-WALLED CARBON NANOTUBES: FUNCTIONALIZATION AND TARGETING

By
Eman Yousef Atalah Makharza

Supervisors
Prof. Shehdeh Jodeh
Prof. Othman Hamed

Submitted in Partial Fulfilment of the Requirements for the Doctor of Philosophy Degree in Chemistry, Faculty of Graduate Studies, at An-Najah National University, Nablus, Palestine.
2025

ANTICANCER IMATINIB DELIVERY SYSTEM BASED ON GRAPHENE OXIDE AND OXIDIZED MULTI-WALLED CARBON NANOTUBES: FUNCTIONALIZATION AND TARGETING

By
Eman Yousef Atalah Makharza

This Dissertation was defended successfully on 03/09/2025 and approved by:

Prof. Shehdeh Jodeh Supervisor	Signature
Prof. Othman Hamed Co-Supervisor	Signature
Prof. Jawad Shuqair External Examiner	Signature
Prof. Nedal Jaradat External Examiner	Signature
Prof. Murad Abu Alhasan Internal Examiner	Signature

Dedication

To my father, who taught me resilience in the face of life's challenges-the man whose love has always been unconditional. To my mother, my first teacher and lifelong inspiration.

To my beloved husband, Khalil, whose unwavering support and encouragement carried me through the hardships of graduate study. To my children, Qasem, Yousef, and Abd-Alrahman, for their patience and understanding during my long absences.

To my brothers and sisters, for their constant presence and support. I also dedicate this work to my mother-in-law, in appreciation of her help during the past period. And to my dear friend Ala' Janem.

I dedicate it with deep gratitude to my uncle, Dr. Sami Makharza, for his continued support throughout my academic journey. To all those who stood by me and helped me reach this point-I offer this work in sincere appreciation.

Acknowledgment

I begin by expressing my utmost gratitude to Almighty Allah, whose infinite blessings and guidance enabled me to complete this research successfully. I also extend my deepest salutations and peace upon the Holy Prophet Muhammad (peace be upon him), who emphasized the importance of seeking knowledge throughout one's life, from cradle to grave.

I want to thank my supervisors, Prof. Shehdeh Jodeh and Prof. Othman Hamed for their help, support and follow-up during my research.

I would like to thank Prof. Manuel Algara in the vibrational spectroscopy laboratory from spain for helping in the characterization of my samples.

I am also thankful to Prof. Ashraf Sawafta in the biology department for his help in the biological part for cancer cells

Many thanks for Mr. Omair Al-Nabulsi and Mr. Nafiz Dweikat, the technicians of the chemistry department and for Ms. Hiba Bourinee, supervisor of biotechnology laboratories at An-Najah National University, for their constant help and guidance. Finally, I would like to thank everybody who has given me support and help to complete my study.

Declaration

I, the undersigned, declare that I submitted the thesis entitled:

ANTICANCER IMATINIB DELIVERY SYSTEM BASED ON GRAPHENE OXIDE AND OXIDIZED MULTI-WALLED CARBON NANOTUBES: FUNCTIONALIZATION AND TARGETING

I declare that the work provided in this thesis, unless otherwise referenced, is the researcher's own work and has not been submitted elsewhere for any other degree or qualification.

Student's Name: Eman Yousef Atalah Makharza

Signature: 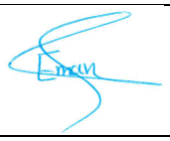

Date: 03/09/2025

List of Contents

List of Tables

List of Figures

List of Schemes

List of Appendices

ANTICANCER IMATINIB DELIVERY SYSTEM BASED ON GRAPHENE OXIDE AND OXIDIZED MULTI-WALLED CARBON NANOTUBES: FUNCTIONALIZATION AND TARGETING

By
Eman Yousef Atalah Makharza
Supervisors
Prof. Shehdeh Jodeh
Prof. Othman Hamed

Abstract

Background: Nanocarriers such as grapheneoxide and oxidized multi-walled carbon nanotubes have attracted attention as drug delivery system vehicles due to their high surface area, low cost, low side effects after modification, and exhibit high dispersibility in physiological media. Also bonding and non-bonding functionalization were considered as a technique for increasing drug binding for being efficient in remediation of cancer cells without effecting normal cells.

Objectives: The main objective of this work is to develop a new set of sixteen complexes of functionalized GO and OMWCNTs physically and chemically. Studying the anticancer activity (cytotoxic and cytoststic assays) of each one was assessed.

Methodology: The method synthesizing GO and OMWCNTs involves the oxidation of graphite and MWCNTS in the presence of oxidizing agent KMNO4 in acidic media (Hummer's method), then functionalizing GO and OMWCNTs physically and chemically with different compounds (PEGDGE, PEG 400, 1.3-diamino-2-propanol, and β-cyclodextrin). Characterization was takes place by FT-IR. Finally, MTT assay by Hela cancer cells and L6 normal cells were studied

Results: Some of the newly prepared compounds were characterized by FT-IR to ensure that binding occurs. The functionalization (chemically and physically) and targeting of imatinib with GO and OMWCNTs were validated. Different compounds maximize anti-cancer effectiveness and minimize normal cells toxicity like GO\ OMWCNTs -PEGDGE\ βCD\PEG 400 and DAP were noticed.

Conclusion: A new novel set of Functionalized GO and OMWCNTs moieties were prepared. Cytotixic and cytostatic assays were done and the formulas GO-PEGDGE\ PEG-400\ DAP and βCD physically and chemically functionalized were showed a very promising activities against Hela cancer cells without higher effect on L6 normal cells, this make the compounds possible future drugs for using to treat cancer.

Keywords: Imatinib, Anticancer, Functionalization, cytotoxic, cytostatic.

Chapter One

Introduction

1.1 Preface

Conventional chemotherapeutic strategies are often hampered by rapid systemic clearance, premature metabolic degradation, poor aqueous solubility, low accumulation at diseased loci, off-target cytotoxicity, and a general inability to discrminte between malignant and healthy tissue. Nano biomedicine seeks to overcome these shortcomings by engineering carriers whose physicochemical characteristics—size, surface chemistry, shape, and responsiveness—can be tailored to prolong circulation time, enhance tumor retention, enable site-specific release, and minimize collateral damage to normal cells (1–8).

Over the past two decades, a diverse palette of nano-enabled drug-delivery vehicles has been proposed, including polymeric nanoparticles, liposomes, metallic and metal-oxide nanostructures, mesoporous silicates, self-assembled micelles, and an expanding family of carbon-based nanomaterials (2,4,7,9–16). Within this spectrum, two-dimensional (2D) materials such as graphene oxide (GO) have attracted particular attention because their ultrahigh surface area, facile chemical modifiability, and intrinsic biocompatibility permit dense payload loading and versatile surface functionalization, thereby opening new horizons for targeted anticancer therapy.

1.2 Carbon allotropes

Carbon is unique among the elements in that it can form stable one-, two-, and three-dimensional crystal lattices by adopting sp, sp^2, or sp^3 hybridisation schemes. This versatility underpins an exceptional range of allotropes whose bonding topologies dictate markedly different electronic, mechanical, and optical properties (17).

Diamond, graphite/graphene, and the fullerene family (e.g., C_{60} buckminsterfullerene) exemplify this diversity (Figure 1.1 in appendix A). In diamond, each carbon is tetrahedrally coordinated in an sp^3 lattice, yielding an electrical insulator with superlative hardness. By contrast, graphene consists of a single sheet of sp^2-hybridized carbon atoms

arranged in a hexagonal network, conferring high electrical conductivity, mechanical flexibility, and atomic-level thickness. Fullerene cages represent yet another structural motif in which carbon atoms close into hollow spheroidal or tubular shells with distinctive electronic behavior (18,19).

1.3 Graphene

Graphene is a one-atom-thick, two-dimensional sheet of ^12C atoms packed into a honeycomb lattice (Figure 1.2 in appendix A). Each carbon contributes nonhybridized p-electron, resulting in a delocalised π-system that underlies graphene's extraordinary carrier mobility, thermal conductivity, and optical transparency. The planar sp^2 framework also furnishes a high density of reactive sites at edges and defect domains, allowing for the covalent or non-covalent attachment of polymers, drugs, and targeting ligands. These attributes, combined with intrinsic biocompatibility and straightforward mass production from graphite, have propelled graphene and its oxidised derivatives to the forefront of next-generation drug-delivery research, particularly for hydrophobic anticancer agents such as Imatinib (16, 19, 22–24).

Experimentally, there are four main methods for obtaining graphene: epitaxial growth of graphene films on silicon carbide, mechanical exfoliation, chemical vapor deposition, and reduction of graphene oxide (25–28).

1.3.1 Graphene, Fullerene and Diamond

Fullerene was discovered by Richard Smalley in 1985 21, it consists of carbon atoms connected by single and double bonds to form a closed or partially closed mesh, with fused rings of five to seven atoms.

1.3.2 Graphene oxide (GO)

The chemical structure and the physical properties (small size, intrinsic optical properties, large specific surface area, and low cost) of GO give it different advantages in many sectors, especially in biological and medical applications (29–33). GO can be produced according to the Hummers method in which graphite is oxidized by using an oxidizing agent in a strong acidic medium (34–36).

As shown in Scheme 1.1, GO has greater aqueous solubility than pristine graphene due to its oxygen-functionalities, which are water-soluble derivatives, and it motivates the biological applications, due to low side effects after modifications, also the presence of oxygen atoms on the structure of graphene makes it very suitable for chemical functionalization (7, 23, 37).

Scheme 1.1

*Chemical structure of graphene oxide (*38)

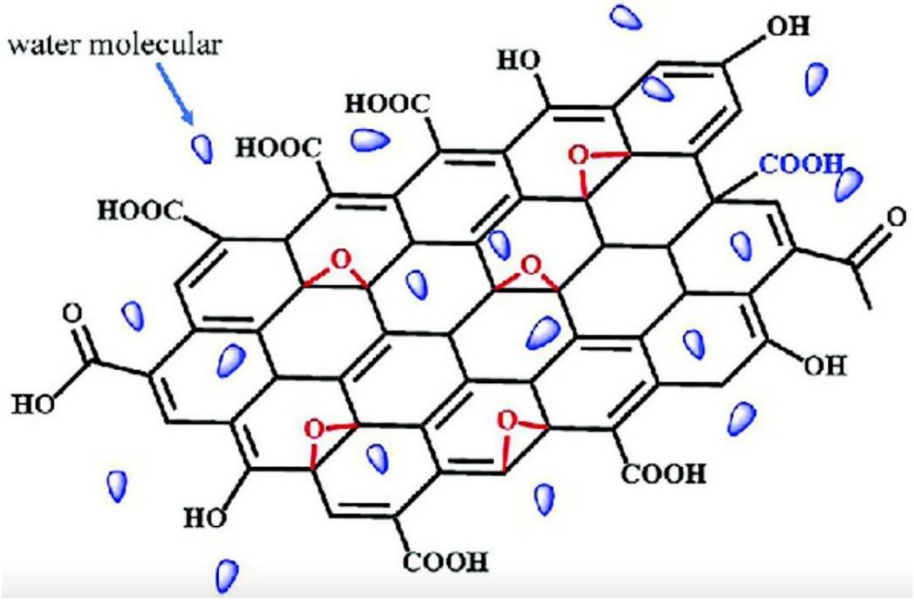

Two complementary models describe the spatial distribution of functional groups on graphene oxide (GO). The Lerf–Kalinowski framework depicts carboxyl termini primarily at the sheet edges, whereas epoxide and hydroxyl moieties occupy the basal plane [23,37,39]. A later "oxidative debris" model retains edge carboxylation but attributes the in-plane oxygen content largely to adsorbed oxidative fragments rather than covalently bound epoxides or hydroxyls (40).

Hydrophilicity is a key determinant of biological performance for carbon nanomaterials. Pristine graphene, composed exclusively of sp^2-hybridized carbon, is intrinsically hydrophobic and therefore exhibits limited dispersibility in physiological media. In contrast, the oxygenated domains on GO confer pronounced polarity, endowing the sheets with superior aqueous solubility, enhanced biocompatibility, and improved colloidal stability relative to graphene.

1.3.3 Carbon nanotubes (CNTs)

Carbon nanotubes are cylindrical nanostructures derived from rolled graphene sheets. Early transmission electron microscopy studies reported tubes containing two or more concentric layers with external diameters of roughly 3–30 nm 17,24,41–43. Depending on the number of graphene cylinders, CNTs are classified as single-walled (SWCNTs) or multi-walled (MWCNTs); the latter comprise nested SWCNTs held together by van der Waals interactions (Scheme 1.2) (44).

Scheme 1.2

The structural geometry of single-walled carbon nanotubes (only one layer) and multi-walled carbon nanotubes (more than four layers) 44.

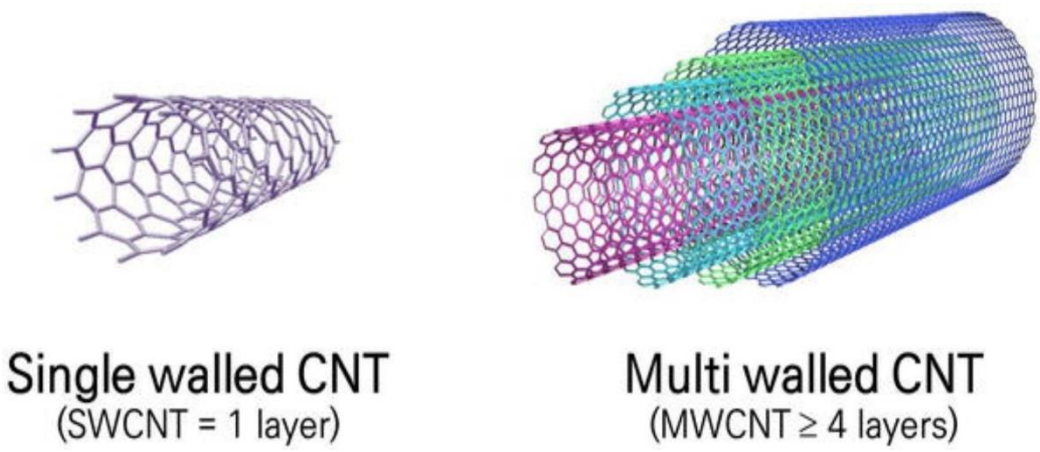

CNTs possess attributes—exceptionally high aspect ratios, mechanical robustness, electrical conductivity, and a π-conjugated surface—that have made them attractive platforms for biomedical engineering (4, 15, 45–48).

Their enormous specific surface area enables the adsorption or covalent attachment of a wide range of therapeutic cargos. For example, anthracyclines such as doxorubicin can be non-covalently loaded through π-π stacking interactions, while small interfering RNA (siRNA) and paclitaxel have likewise been delivered using CNT vectors 4,48. Additional advantages include structural stability, a large drug loading capacity, and the ability to penetrate cellular membranes efficiently (4, 48–50). A persistent bottleneck is the poor water dispersibility of pristine CNTs. Introducing hydrophilic functional groups or polymer coatings markedly improves colloidal stability, systemic distribution, and overall biocompatibility, thereby mitigating nanotube-induced cytotoxicity.

1.3.4 Functionalization of carbon

Because native graphene and CNTs tend to aggregate in biological media, surface modification is crucial for generating stable, biocompatible suspensions (12,13,30,51). GO already bears oxygen functionalities that render it hydrophilic, yet its chemical landscape can be further tailored by covalent grafting, electrostatic assembly, or π-π interactions with small molecules and polymers.

Typical solubilization approaches include:

i. Covalent attachment of hydrophilic chains.

ii. Noncovalent adsorption of surfactants or aromatic drugs.

iii. Dispersion in benign organic cosolvents followed by aqueous exchange (Scheme 1.3).

Such functionalization not only enhances water compatibility but also introduces reactive handles for conjugating targeting ligands, imaging agents, or stimuli-responsive linkers—key requirements for advanced anticancer delivery systems (Scheme 1.3) 52.

Scheme 1.3

Representative surface-functionalisation strategies for graphene-based nanomaterials

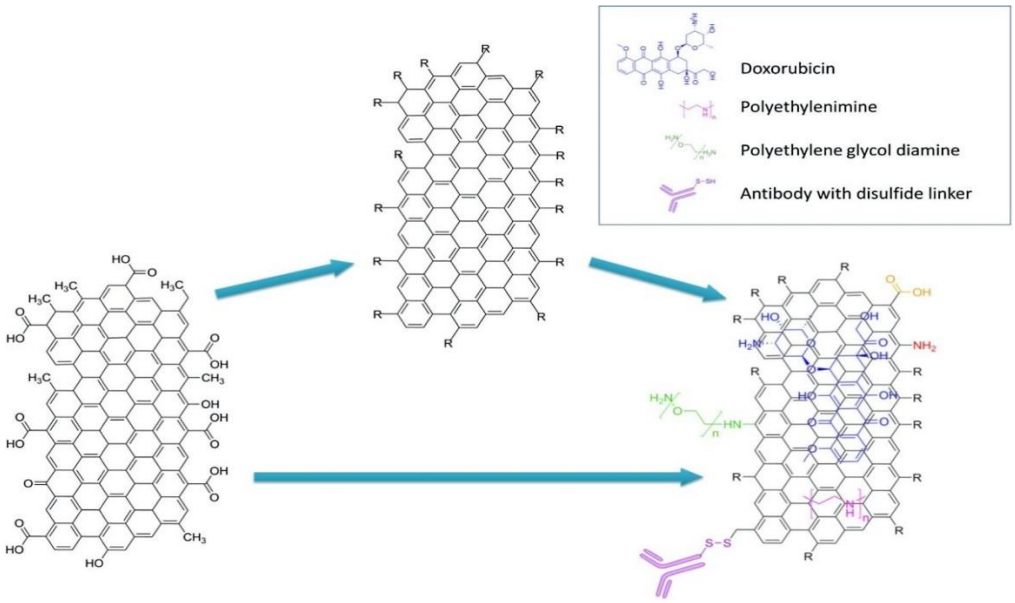

Note: Covalent routes involve attachment of polyethylene-glycol diamine and antibody moieties via suitable linkers, while non-covalent approaches rely on electrostatic or π–π interactions with polyethyleneimine and the anticancer drug doxorubicin (52).

1.3.5 Covalent and non-covalent functionalization

Graphene oxide (GO) and oxidized multi-walled carbon nanotubes (OMWCNTs) display a mixed sp^2–sp^3 lattice. The aromatic domains provide extensive π-electron clouds, while the oxidized sp^3 regions introduce hydroxyl, epoxide, and carboxyl moieties. Together, these features create multiple orthogonal reaction pathways: edge or basal-plane groups can undergo classical covalent coupling, whereas the graphitic surface supports non-covalent interactions such as π–π stacking, hydrogen bonding, ion pairing, and electrostatic adsorption (23, 24, 42, 53, 54).

Surface grafting with biocompatible polymers is a proven route to enhance colloidal stability and mitigate innate toxicity. Polyethylene glycol (PEG) or bovine serum albumin (BSA) coatings significantly reduce non-specific protein corona formation, prolong blood-circulation half-life, and inhibit complement activation. Notably, PEGylated nano-graphene oxide (nGO-PEG) adsorbed fewer serum proteins and exhibited selective binding to only six plasma proteins, whereas unmodified GO captured a broader panel. Moreover, nGO-PEG remained well-dispersed after high-speed centrifugation and resisted precipitation in water, phosphate-buffered saline (PBS), and standard culture media (50, 55).

Dextran affords a complementary, fully non-covalent strategy. Graphene Nanoplatelets wrapped with dextran (GNP-Dex) form stable aqueous suspensions up to 100 mg mL^{-1} and, at dosages of 1–10 mg mL^{-1}, neither trigger platelet activation, haemolysis, nor pro-inflammatory responses in whole-blood assays (37, 56).

Amine termination represents another effective design lever. Graphene functionalised with primary amines (G-NH_2) demonstrated superior *in-vivo* safety relative to GO and reduced graphene oxide (rGO): intravenous administration of 250 μg kg^{-1} G-NH_2 in mice produced no detectable pulmonary thrombosis, whereas the same dose of GO induced clot formation in lung capillaries (57).

Cationic polymers can be covalently anchored as well. Poly-L-lysine (PLL) reacts with GO epoxide rings to form stable amide linkages (facilitated by KOH/$NaBH_4$), thereby generating water-soluble GO-PLL conjugates with enhanced biocompatibility.

Subsequent conjugation of horseradish peroxidase (HRP) yields graphene-PLL/HRP composites that couple enzymatic functionality with the mechanical and electrical advantages of the carbon scaffold (Scheme 1.4).

Scheme 1.4

PLL functionalization of graphene-based construct achieved with NaBH4 and KOH58

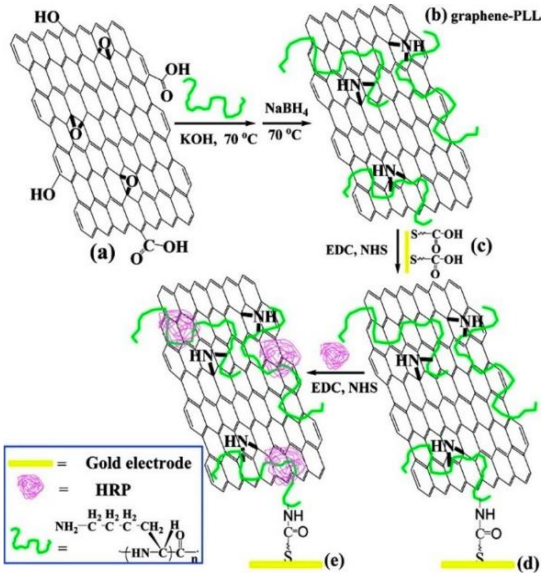

Collectively, these examples illustrate how judicious covalent or non-covalent modification expands the biomedical utility of carbon nanomaterials by tailoring solubility, protein adsorption, immune compatibility, and hemocompatibility while preserving their high drug-loading capacity and unique electronic structure.

1.4 Imatinib

Imatinib is a potent chemotherapeutic agent, yet its clinical utility is tempered by dose-dependent toxicity. In the present study, we explore a biocompatible nanocarrier system—comprising graphene oxide (GO) and functionalised carbon nanotubes (CNTs)—for efficient loading and controlled release of Imatinib. The drug's IUPAC designation is 4-[(4-Methylpiperazin-1-yl)methyl]-N-[4-methyl-3-{4-(pyridin-3-yl)pyrimidin-2-yl}amino]phenyl]benzamide (Scheme 1.5). Marketed as Glivec, Imatinib is classified as a tyrosine kinase inhibitor (TKI) and is prescribed for multiple malignancies. When approved for chronic myeloid leukemia (CML) in 2001, it was heralded as a "magic bullet" for targeted therapy (59).

Tyrosine kinases function as intracellular messengers regulating cellular proliferation. By selectively blocking these enzymes, Imatinib disrupts oncogenic signalling pathways, thereby inhibiting tumour growth (60).

Scheme 1.5

Structure of imatinib

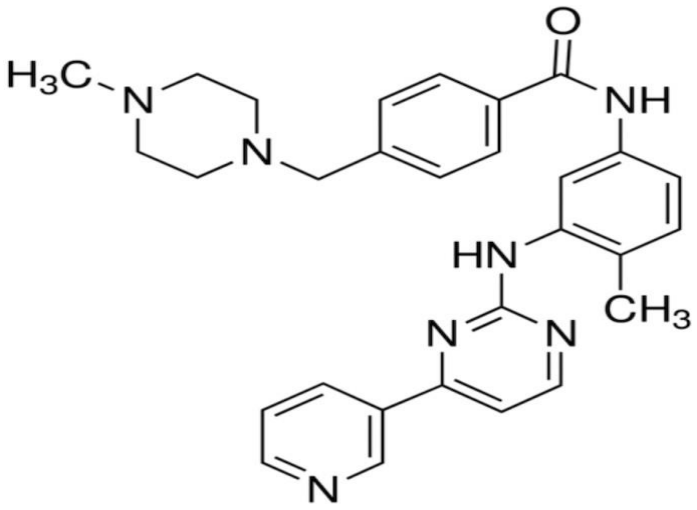

1.4.1 Mechanism of action

Imatinib functions as a competitive antagonist that blocks the ATP-binding pocket of the BCR–ABL fusion kinase generated by the Philadelphia chromosome in chronic myeloid leukaemia (CML). This interruption limits cellular proliferation and initiates apoptosis in BCR–ABL-positive lines and primary CML blasts. *Ex-vivo* colony-forming assays with patient bone marrow and peripheral blood further effectively confirm selective suppression of BCR–ABL-dependent colonies. Animal studies show that Imatinib curtails the expansion of BCR–ABL-transfected murine myeloid tumours and human blast-crisis xenografts. Additionally, the drug inhibits other receptor tyrosine kinases—PDGFR and c-Kit—disrupting PDGF/SCF signalling; in c-Kit-mutant gastrointestinal stromal tumours, it likewise induces growth arrest and apoptosis (61).

1.4.2 Nano-scaled drug delivery systems

Nanotechnology-enabled drug-delivery systems (NDDS) have gained prominence for oncological therapy and diagnostics. Nanocarriers encapsulating anticancer agents preferentially accumulate in tumour tissue via the enhanced permeability and retention

(EPR) effect or through ligand-mediated active targeting, thereby amplifying chemotherapeutic efficacy while minimizing systemic toxicity (30,31,50,62–64). Mashreghi and colleagues reported an albumin-magnetite graphene oxide conjugate that serves as an efficient depot for Imatinib, underscoring the potential of magnetized GO platforms (63).

Zhang et al. devised a histidine-directed hydrothermal method to grow amorphous ZnO shells around gold nanoparticles, yielding Au-His@a-ZnO constructs. These particles were subsequently grafted onto PEGylated graphene oxide via carbodiimide coupling, and an aptamer ligand was introduced to generate Apt@GO@Au-His@a-ZnO@DOX nanocomposites. The hybrid exhibited a high doxorubicin payload and dual near-infrared/pH-responsive release: in the acidic milieu of endo-lysosomes, the metal–drug complex dissociated, liberating both DOX and cytotoxic Zn^{2+} ions. The aptamer coating endowed excellent colloidal stability and selective binding to EGFR-mutant lung-cancer cells, thereby enhancing uptake into A549 xenografts relative to untargeted controls. In murine models, the platform achieved pronounced tumor growth inhibition through combined photothermal and chemotherapeutic action, underscoring the potential of Apt@GO@Au-His@a-ZnO@DOX for precision lung cancer therapy (64).

1.5 Biological studies

In culture media, there is a big difference between cancer and normal cells, such as behavior, life expectancy and their shape. In which normal cells, such as L6 cells, die after a few generations, while the cancer cells still survive forever.

The differences between abnormal cells and normal is maturation in the case of normal cells they more specialized also mature into a limited distinct cell type, however, the cancer cells continue to multiply and proliferate without stopping before it becomes mature. Also, communication is the second difference between normal and cancer cells, normal cells interact with each other whereas the cancer cells do not. In addition, the normal cells are programmed to response to the nearby signals to stop growing and dividing, the case is the opposite for the cancer cells, they don’t response to the cell's physiological division rules, and they ignore signals from adjacent cells warning (65, 66).

1.6 HeLa cancer cells

The first immortal human cell line was used in biological research. In 1951, Henrietta Lacks was a woman who unknowingly donated her cells at Johns Hopkins and for many years, the only human cell line able to reproduce indefinitely.

Hela cells are immortal (dividing indefinitely under certain conditions), aneuploid (having more than the normal 46 chromosomes), robust (surviving in various conditions that make them ideal for laboratory work), and fast-growing (doubling in number within a short time, around 24 hours). Also these cells are considered as transformed cells since they have undergone changes make them toxic and able to grow outside the human body.

Hela cells were chosen to study the effects of Graphene oxide, oxidized multi-walled carbon nanotubes, and functionalized ones on cancer cells through anticancer activity measurements (38).

1.7 Normal muscle cells (L6)

Normal muscle L6 cells, originally derived from rat skeletal muscle, propagate as mononucleated myoblasts, but can differentiate into multinucleated primary myotubes. The myotubes express several proteins typical of skeletal muscle including the GLUT4 glucose transporter (67, 68).

L6 cells can differentiate into multinucleated myotubes, mimicking mature muscle fibers. These types of cells are used in biomedical, physiology and cell biology research. Also, they are reliable, versatile and robust *in vitro* models for different studies.

1.8 Literature Review

1.8.1 Graphene-Based Nanocarriers

Extensive investigations demonstrate that graphene oxide (GO) provides an ultrahigh specific surface for drug adsorption while the oxygenated lattice permits versatile chemical grafting. Early in vitro work demonstrated that π–π stacking and hydrogen bonding enable GO loading capacities exceeding 800 mg g^{-1} for aromatic therapeutics, with sustained release profiles driven by pH and ionic strength gradients[1].

Functionalization is indispensable for physiological dispersion and hemocompatibility. PEGylation markedly suppresses protein corona formation and accelerates enzymatic degradation of GO sheets, yielding >90 % viability in fibroblasts even at 100 μg mL^{-1} 56.

Dextran-coated GO exhibits negligible platelet activation and vasoactivity across 1–10 mg mL^{-1}, confirming the steric-stabilisation concept for intravenous use 57, whereas amine-modified graphene eliminates the lung thrombo-embolism observed for pristine GO at identical doses 58. Collectively, polysaccharide, PEG and amine coatings converge on the same design rule: increasing hydrophilicity and eliminating reactive edge groups minimize complement activation while preserving the high loading capacity of the basal plane.

1.8.2 Carbon-Nanotube (CNT) Platforms

CNTs offer aspect-ratio-driven cellular penetration and efficient π-stacking of hydrophobic drugs. Comprehensive reviews list the successful loading of doxorubicin, methotrexate, and gemcitabine, with final encapsulation efficiencies of 60–85% and up to five-fold dose reductions in murine models. Non-covalent adsorption on pristine walls is rapid but aggregation in salt media restricts biomedical use. Supramolecular wrapping with amphiphilic polymers or π-conjugated pyrene anchors yields water-soluble single-walled CNTs that retain electrical integrity and reach >250 mg g^{-1} drug payloads49. Oxidized multi-walled CNTs (OMWCNTs) introduce carboxyl/hydroxyl termini that serve as handles for amide coupling, yet reduce graphitic defects relative to harsh acid treatments, preserving the mechanical rigidity crucial for endosomal escape (71).

1.8.3 Imatinib-Loaded Carbon Nanomaterials

Targeted cancer therapies have gained significant attention in recent decades, particularly with the advent of tyrosine kinase inhibitors like imatinib mesylate, which revolutionized the treatment of chronic myeloid leukemia and gastrointestinal stromal tumors. Despite its clinical effectiveness, imatinib suffers from limitations, including low aqueous solubility, the development of resistance with long-term use, and suboptimal bioavailability.

Imatinib (IM), a first-line BCR-ABL tyrosine-kinase inhibitor, suffers from low aqueous solubility (≈25 mg L^{-1}) and dose-limiting cardiotoxicity. A recent study anchored albumin-encapsulated magnetite nanoparticles onto GO sheets, achieving 81 % loading (pH 7) and pH-responsive release that tripled the cytotoxic index against K-562 cells relative to free IMA 64. Although not a delivery vehicle, a chitosan/GO electrochemical sensor capable of detecting IM down to 13 µM further proves the strong GO–IM affinity arising from π-stacking of the pyramidal ring (63). These findings justify selecting GO and OMWCNTs as dual platforms in the present thesis.

Recent research has explored advanced carbon-based nano-systems-especially carbon nanotubes, graphene oxide and graphene quantum dots as delivery platforms to enhance imatinib's bioavailability, therapeutic efficiency, and specificity.

- Molecular simulation of functionalized carbon nano tubes:

A 2024 computational study employed density functional theory and Monte Carlo simulations to evaluate carboxyl -and hydroxyl- functionalized carbon nanotubes as carriers for imatinib in aqueous media. Functionalized carbon nanotubes showed favourable adsorption energy and solvation free energy, indicating strong binding and improved solubility compared to pristine carbon nanotubes. Electrostatic interactions were key in stabilizing the imatinib-carbon nanotube complex, suggesting enhanced potential bioavailability in vivo 94.

- Carbon nanohybrid sensors of imatinib:

A recent sensor design using a nanocomposite of N,S-doped carbon dots and carbon nanotube-PAMAN dendrimer (N, S-CDs\CNTD) demonstrated highly sensitive imatinib detection (detection limit down to approximately 3 nM) in serum samples.

The study highlights the strong affinity between imatinib and carbon-based nanostructures, reinforcing their potential for binding and release. Overall, carbon nanotube-based systems show promise through simulation and sensing studies. Further in vitro/in vivo experimental validation remains a clear research need 95.

- Imatinib-loaded carbon nanotubes:

Mahmoodi et. al. (2019) explored the use of PEGylated single-walled carbon nanotubes for imatinib delivery. The PEG coating improved dispersibility and biocompatibility, while the nantube structure facilitated high drug loading. The study reported sustained drug release and increased cytotoxic effects on cancer cells compared to free imatinib, suggesting the efficacy of carbon nanotube-based drug delivery systems 98.

- Imatinib- conjugated graphene oxide:

Kesharwani et. al. (2020) developed a graphene oxide nano carrier systems functionalized with targeting ligands for the delivery of imatinib. Their study demonstrated that GO significantly enhanced drug loading efficiency and enabled selective delivery to leukemia cells. The formulation demonstrated improved cytotoxicity against CML cells while minimizing toxicity to normal cells, highlighting the functionalized graphene oxide.

Graphene quantum dots conjugated with imatinib

Experimental decoration of imatinib on GQDs

An experimental study engineered imatinib-decorated GQDs (GQDs@imatinib) via carbodiimide chemistry, targeting leukemia treatment. GODs retained their size and morphology upon conjugation and exhibited efficient cellular uptake by both suspension(leukemia) and adherent cell lines. Cytotoxicity assays confirmed potent induction of apoptosis in cancer cells, highlighting GQDs@imatinib as a promising pure-carbon nanosystem with strong anticancer activity 96.

1.8.4 Impact of Functionalization on Biocompatibility

Table 1.1 synthesises outcomes across coatings. PEG and dextran principally create hydration shells that sterically block opsonin's, reducing in-vivo liver uptake by >50 %56,57. Amine grafting shifts the surface ζ-potential positive, enhancing colloidal stability in serum yet demanding careful dose control to avoid mitochondrial stress at >200 μg mL^{-1} 58. For CNTs, mild oxidation ($H_2O_2/H_2O/O_3$) introduces 3–6 at % oxygen while maintaining conductivity, lowering haemolytic indices from 18 % to <5 % in erythrocytes71. These collective insights underline the thesis strategy: employ

orthogonal covalent (amide/epoxide) and non-covalent (inclusion/hydrogen-bond) chemistries to fine-tune nano–bio interactions.

Table 1.1

Functionalized GO systems for drug delivery

Ref.	Nanomaterial & Functionalisation	Drug / Cargo	Methodology / Key Findings	Advantages	Limitations
1	GO (pristine, π-stacking)	Various aromatics	Langmuir adsorption; >800 mg g^{-1} loading; pH-triggered release	Ultra-high capacity	Aggregates in saline
56	PEG-GO	—	PEGylation via EDC/NHS; >90 % cell viability; accelerated enzymatic degradation	Low protein corona; biodegradable	Slightly reduced payload
57	Dex-GO	—	Ether-linked dextran; no platelet activation 1–10 mg mL^{-1}	Excellent haemocompatibility	Thick corona lowers diffusion
58	G-NH_2	—	Ethylenediamine amidation; zero thrombosis in mice	Thrombo-protective	Positive ζ may induce ROS at high dose
64	Albumin-Fe_3O_4–GO	Imatinib	pH-responsive; 81 % loading; 31 % release at pH 4 (5 h)	Synergistic magnetic targeting	Multi-step synthesis

The uniform ultrasmall graphene oxide nanosheets with high yield by a convenient way of modified Hummers' method were synthesized. The uniform ultrasmall GO nanosheets, which exhibit fluorescence property and outstanding stability in a wide range of pH values, were less than 50 nm. In addition, due to the advantages of its the uniform ultrasmall GO nanosheets, laeral size showed excellent biocompatibility of lower cytotoxicity and higher cellular uptake amount compared to the random large GO nanosheets. Hence, the prepared ultrasmall GO nanosheets could be probed as the ideal nanocarriers for drug delivery and intracellular fluorescent nanoprobe 92.

S Kanakia et.al were checked safety by differenr rules set for drugs, which recommend tests at doses 10 to 100 times more than what would be used in treatment. They reported the effects of a single dose detailed acute toxicology levels of the substance in the body over time, and tests on how it affects breathing and heart function. They tested dextran-coated graphene oxide nanoplatelets (GNP-Dex) given through veins in rats at doses

ranging from 1 to 500 mg/kg. The findings showed that the maximum tolerable dose of GNP-Dex falls between 50 mg/kg and below 125 mg/kg. Blood half-life is under 30 minutes, and most nanoparticles left the body in 24 hours through feces. Histopathology revealed changes in the heart, liver, lungs, spleen, and kidneys at doses of 250 mg/kg or higher. Also, they observed no changes in the brain or any effects on cardiovascular or hematological factors such as blood, lipid, or metabolic panels at doses under 125 mg/kg. The findings create opportunities to conduct crucial preclinical safety studies, both single and repeat dose, under good laboratory practices. Regulatory agencies require these studies to meet investigational new drug application standards 93.

Table 1.2

CNT-based platforms

Ref.	CNT Type / Functionalisation	Cargo	Key Results	Pros	Cons
4	SWCNT/MWCNT (various)	DOX, MTX, PTX, GEM	Review: 60–85 % encapsulation; 4–5× dose reduction in vivo	High aspect ratio; photothermal synergy	Aggregation; inflammatory risk
49	SWCNT (pyrene + PEG wrap)	DOX	250 mg g^{-1} loading; complete serum stability	Non-covalent, preserves π-network	Desorption under shear
50	OMWCNT (acid-oxidised)	siRNA	Amide-linkage ; efficient endosomal escape	Gene delivery capability	Acid damage reduces yield
71	OMWCNT (green oxidn.)	—	$H_2O_2/H_2O/O_3$ oxidation; haemolysis <5 %	Mild, scalable process	Lower carboxyl density

1.9 The aim of the study

Traditional cancer treatments face numerous challenges, including non-specific targeting, adverse effects on healthy cells, poor solubility of therapeutic agents, and premature drug elimination from the body before they can operate on their targeted sites. This study aims to develop novel nano-biomedicine drug delivery platforms based on graphene oxide (GO) and oxidized multi-walled carbon nanotubes (OMWCNTs) to overcome these limitations for effective imatinib delivery. In this study, four compounds were used to functionalize GO and OMWCNT for imatinib loading:

- β-Cyclodextrin.
- 1,3-Diamino-2-propanol,
- Polyethylene glycol 400,
- Polyethylene glycol Di glycidyl ether

The binding of these compounds is made chemically and physically. Studying the anticancer activity of sixteen novel GO and OMWCNT complexes by assessing their in vitro cytotoxic and cytostatic activity by using cancer cell lines. The following two cell lines were used: The human cervical cancer cell lines (HeLa cells) and normal muscle cells (L6), Also were used as a model for studying the potency of imatinib and imatinib-loaded nanohybrids in inhibiting metabolic activity.

Chapter Two

Experimental Part

2.1 Materials and procedures

All the following chemicals were of analytical grade and were purchased from Sigma-Aldrich. The chemicals include: Multiwalled carbon nanotubes (purity ≥ 99.5), Graphene oxide, polyethylene glycol, Diglycidyl ether, dimethyl sulfoxide (DMSO), 1,3-diamino-2-propanol, β-Cyclodextrin, and Imatinib ($C_{29}H_{31}N_7$) with a purity of 99.86 %. Hydrochloric acid HCl (98 %), potassium permanganate KMnO4, hydrogen peroxide H2O2 (30 %), phosphate buffer saline (PBS), tetrahydrofuran (THF), polyethylene glycol 400 (PEG 400), β-cyclodextrin (β-CD), concentrated sulfuric acid H_2SO_4 (98 %), sodium bicarbonate ($NaHCO_3$). All chemicals used in cell culture were purchased from Biological Industries except for the amphotericin B and MTT reagent from SIGMA Aldrich.

FT-IR spectrophotometer model Vertex70 by Bruker. Samples were dispersed in a KBr matrix. A standard spectral resolution of 4 cm-1 and a spectral range of 4000-400 cm-1 were employed.

2.2 Synthesis of nanoparticles (Hummer's method and ultrasonication)

2.2.1 Synthesis of graphene oxide

The preparation of graphene oxide (GO) using the Hummers method involves oxidizing graphite particles with a mixture of concentrated sulfuric acid (H_2SO_4) and potassium permanganate ($KMnO_4$). In a typical procedure, 1.0 g of graphite is placed in 10 mL 95 – 98 % H_2SO_4 under stirring overnight, followed by the gradual addition of $KMnO_4$ over a period of three hours. The temperature was kept below 10 °C in an ice bath to prevent explosive reactions. The mixture is then allowed to react at a range of temperatures, around 35–50 °C, to promote oxidation for 5 hours. Thereafter, the mixture is diluted with 50 mL of distilled water and 10 mL of 30% hydrogen peroxide (H_2O_2) to reduce the residual permanganate and manganese dioxide to soluble manganese ions. The resulting exfoliated graphite oxide sheets are washed repeatedly with water and acid to remove

impurities, then dried or dispersed in water for further processing. To reduce the lateral size of the graphite oxide particles, the as-prepared suspension was placed under sonication (tip sonicator). This process involves subjecting the aqueous dispersion of as-prepared particles to high-frequency ultrasonic power and time (2 hours). The cavitation and mechanical forces generated during ultrasonication break down the larger graphite materials into smaller ones. The sonication time, power, and temperature are considered as controlled parameters. The average lateral sizes of the GO nanosheets can be tuned to around 200 nm (23, 37).

2.2.2 Synthesis of Oxidized Multiwalled Carbon Nanotubes (OMWCNT)

Oxidized multiwalled carbon nanotubes (OMWCNT) were produced using the modified hummers method. In this method, 0.5 g of multi-walled carbon nanotubes was mixed in 11.5 mL of H_2SO_4 (98 %) overnight. Thereafter, the mixture was placed in an ice bath to ensure that the temperature remained below 10°C. Subsequently, 1.5 g $KMnO_4$ was added gradually over one hour with constant stirring.

The mixture was sonicated for 3 hours and continuously stirred for 30 min at 35 °C and 45 min at 50 °C, respectively. 23 mL of distilled water was added to the mixture and kept with stirring at 95 °C for 45 min. The mixture was cooled down to room temperature and stirred with the addition of 79 mL of distilled water and 10 mL of 30 % H_2O_2. The collected samples were washed five times with distilled water to remove any reaction byproducts and centrifuged for further purification (69–71).

2.3 Functionalization of GO and OMWCNT

2.3.1 Physical binding

2.3.1.1 Binding of polyethylene glycol Di glycidyl ether (PEGDGE) with GO

GO (1 mg/mL) was heated with polyethylene glycol Di glycidyl ether (25 µL) in a water bath at 60 °C for 30 min, then the sample was sonicated for 30 min. The collected sample was washed twice with phosphate-buffered saline (PBS) and then centrifuged. The samples were centrifuged for further purification and kept in an oven for drying overnight at 35 °C.

2.3.1.2 Binding of PEGDGE with OMWCNT

The OMWCNTs (1 mg/mL) was heated with PEGDGE (25 µL) in a water bath at 60 °C for 30 min, then the sample was sonicated for 30 min. The collected sample was washed twice by PBS and centrifuged. The samples were centrifuged for further purification and kept in an oven for drying overnight at 35 °C.

2.3.1.3 Binding of polyethylene glycol 400 (PEG400) with GO

GO (1 mg/mL) was heated with PEG 400 (25 µL) in a water bath at 60 °C for 30 min, then the sample was sonicated for 30 min. The collected sample was washed two times with PBS, kept in an oven at 35 °C for drying.

2.3.1.3 Binding of PEG400 with OMWCNT

The OMWCNTs (1 mg/mL) was heated with PEG400 (25 µL) in a water bath at 60 °C for 30 min, then the sample was sonicated for 30 min. The collected sample was washed twice by PBS and kept in an oven for drying at 35 °C.

2.3.1.4 Binding of 1.3-diamino-2-propanol with GO

GO (1mg/mL) was heated with 1.3-diamino-2-propanol (25 µL) in a water bath at 60 °C for 30 min, then the sample was sonicated for 30 min. The collected sample was washed twice with PBS. The samples were kept in an oven at 35°C for drying overnight.

2.3.1.5 Binding of 1.3-diamino-2-propanol with OMWCNT

The OMWCNTs (1 mg/mL) was heated with 1.3-diamino-2-propanol (25 µL) in a water bath at 60 °C for 30 min, then the sample was sonicated for 30 min. The collected sample was washed twice with PBS and kept in an oven for drying at 35 °C.

2.3.1.6 Binding of β-Cyclodextrin (β -CD) with GO

GO (1mg/mL) was heated with β-CD (0.4 g) in a water bath at 60 °C for 30 min, then the sample was sonicated for 30 min. The collected sample was washed twice with PBS and kept in an oven for drying at 35 °C.

2.3.1.7 Binding of (β -CD) with OMWCNT

The OMWCNTs (1 mg/mL) was heated with β-CD (25 µL) in a water bath at 60 ℃ for 30 min, then the sample was sonicated for 30 min. The collected sample was washed twice with PBS and kept in an oven for drying at 35 ℃.

2.3.2 Chemical binding

2.3.2.1 Binding of PEGDGE with GO

A 0.10 g of GO with 1.0 mL of PEGDGE was heated for 2 hours at 80 – 90 ℃. The product was washed in suction filtration several times and kept in an oven at 35 ℃ for drying.

2.3.2.2 Binding of PEGDGE with OMWCNT

A 0.10 g of OMWCNTs with 1.0 mL of PEGDGE was heated for 2 hours at 80-90 ℃. The product was washed in suction filtration several times and kept in an oven at 35 ℃ for drying.

2.3.2.3 Binding of PEG400 with GO

A 0.10 g of GO with 2.5 mL PEG 400 and one drop concentrated sulfuric acid (98 %) was heated for 2 hours at 110 – 120 ℃. Thereafter, the mixture was cooled down to room temperature. Subsequently, 5 mL of 0.5 % sodium bicarbonate ($NaHCO_3$) was added and stirred for 15 min. The collected samples were washed three times with THF and centrifuged.

2.3.2.4 Binding of PEG400 with OMWCNT

A 0.10 g OMWCNTs with 2.5 mL PEG 400 and one drop concentrated sulfuric acid (98 %) was heated for 2 hours at 110-120 ℃. Thereafter, the mixture was cooled down to room temperature. Subsequently, 5 mL of 0.5 % sodium bicarbonate was added and stirred for 15 min. The collected samples were washed 3 times by THF and centrifuged.

2.3.2.5 Binding of 1.3-diamino-2-propanol with GO

A 0.10 g of GO with 2.5 mL of 1.3-diamino-2-propanol was heated for 2 hours at 132 ℃. Thereafter, the mixture was cooled down to room temperature. The collected samples were washed twice with distilled water and centrifuged.

2.3.2.6 Binding of 1.3-diamino-2-propanol with OMWCNT

OMWCNTs (0.1 g) with 1.3-diamino-2-propanol (2.5 mL) was heated for 2 hours at 132

℃. Thereafter, the mixture was cooled down to room temperature. The collected samples were washed twice with distilled water and then centrifuged.

2.2.2.7 Binding of β-CD with GO

GO (0.1 g) was dissolved in distilled water (2 mL), then β-CD (0.1 g) was added and shacked well. After this, the water vaporized (110 °C) and the GO+ β-CD was heated at (160 °C) for 30 min.

2.3.2.8 Binding of β-Cyclodextrin with oxidized MWCNT

MWCNTs (0.1 g) was dissolved in distilled water (2 mL), then β-CD (0.1 g) was added and shaken well. After this, the water vaporized (110 °C) and the GO+ β-CD was heated at (160 °C) for 30 min.

2.4 Imatinib loading

The compounds in table (2.1) were prepared and exist as a solid black powder in 45 vials numbered from 1 to 45 and ready to prepare stock solutions.

2.4.1 Preparation of stock solutions

10mg of each complex was dissolved in 1 mL phosphate buffer solution.

2.4.2 preparation of Imatinib-loaded functionalized nano carriers

0.5 mL from each stock solution was mixed with 0.5 mL from the drug stock solution. Thereafter, these solutions were diluted to five concentrations (5, 2.5, 1.25, 0.625, and 0.3125 mg/mL). Then each solution was stirred for 2 hours at room temperature. The samples labeled in 45 vials as the table shows from (1-45).

Table 2.1

This table represents the compounds that ready to prepare stock solutions.

Sample No.	Compound
1	GO+PEGDGE (ch.)
2	OMWCNTs+ β-Cyclodextrin (ch.)
3	OMWCNTs
4	OMWCNTs + PEG400 (ch.)
5	GO+1.2-diamino-2-propanol amine (ch.)
6	OMWCNTs+ PEGDGE (ch.)
7	OMWCNTs+1.2-diamino-2-propanol amine (ch.)
8	GO+ β-Cyclodextrin (ch.)
9	GO+ PEG 400(ch.)
10	OMWCNTs+ PEG 400(ph.)
11	GO+1.2-diamino-2-propanol amine (ph.)
12	GO+PEGDGE (ph.)
13	OMWCNTs+ PEGDGE (ph.)
14	GO+ β-Cyclodextrin (ph.)
15	OMWCNTs+1.2-diamino-2-propanol amine (ph.)
16	GO+ PEG 400(ph.)
17	OMWCNTs+ β-Cyclodextrin (ph.)
18	GO
19	β-Cyclodextrin
20	Drug (imatinib)
21	GO+ Drug
22	OMWCNTs+ Drug
23	β-Cyclodextrin+ Drug
24	GO+PEGDGE(ch.) + Drug
25	GO+ PEG400(ch.) + Drug
26	GO+ β-Cyclodextrin (ch.)+ Drug
27	GO+1.2-diamino-2-propanol amine (ch.)+ Drug
28	OMWCNTs+ PEGDGE(ch.)+ Drug
29	OMWCNTs + PEG400 (ch.)+Drug
30	OMWCNTs+ β-Cyclodextrin (ch.)+ Drug
31	OMWCNTs+1.2-diamino-2-propanol amine (ch.)+ Drug
32	GO+PEGDGE(ph.)+ Drug
33	GO+ PEG 400(ph.)+ Drug
34	GO+ β-Cyclodextrin (ph.)+ Drug
35	GO+1.2-diamino-2-propanol amine (ph.)+ Drug
36	OMWCNTs+ PEGDGE(ph.)+ Drug
37	OMWCNTs+ PEG 400(ph.)+ Drug
38	OMWCNTs+ β-Cyclodextrin (ph.)+ Drug
39	OMWCNTs+1.2-diamino-2-propanol amine (ph.)+ Drug
40	PEGDGE + Drug
41	PEG400+ Drug
42	1.2-Diamino-2-propanol amine + Drug
43	PEGDGE
44	PEG400
45	1.2-Diamino-2-propanol amine

2.5 Cell culture

2.5.1 Cell lines

The human cervical cancer cell lines (HeLa cells) and normal muscle cells (L6, ATCC number: CRL-1458, human, from the skeletal muscle) were obtained from the American Type Culture Collection [ATCC], Manassas, VA, USA. They were grown in RPMI medium supplemented with 10 % fetal calf serum, 1 % non-essential amino acid, 1 % l-glutamine, 1 % penicillin, streptomycin and 1% amphotericin B. All cells were grown in a humidified atmosphere of 95 % air, 5 % CO_2 at 37 ºC, the culture medium was changed at least twice a week as needed.

For the screening experiment, the cells were grown in 12-well plates in 950 µL of RPMI medium (Biological Industries, USA) containing 5% PBS, 2×104 cells/well plating density. After that 50 µL of diverse concentrations (5, 2.5, 1.25, 0.625, and 0.313 µg /mL) of the previous compounds in Table (2.1) were added in duplicates to the prepared 12-well plates and incubated for 24 h at 37 ºC, 5 % CO_2, 95 % air and 100 % relative humidity. An inverted microscope (Labomed, USA) was used to observe the morphological changes of the cells.

2.5.2 Determination of cell viability (MTT Assay)

Viable cells have the ability to reduce the yellow-colored, water-soluble 3-(4,5-dimethylthiazol-2-yl)-2,5-diphenyltetrazolium bromide (MTT) to a water-insoluble, purple-colored formazan crystal by a functional mitochondrion via succinate dehydrogenase, which provides a quantitative determination of viable cells.

After the cells were seeded in 100 µL DMEM media in a 96-well plate, they were treated for 24 h with various concentrations of the prepared stock solutions of the chemical complexes and then incubated for another 24 h at 37 ºC. After the removal of the treatment solution, 100 µL of MTT (0.5 mg/mL) was added, and the mixture was then incubated for 4 hoursat 37 ºC. After 4 hours, the MTT solution was removed, and 100 µL of an isopropanol-alcohol and formic acid (9:1) solution was added to dissolve the formazan crystals. The mixture was then incubated for 15 min in the dark at room temperature. After that, the Optical Density of the MTT Formazan was determined at 570 nm in an enzyme-

linked immunosorbent assay (ELISA) reader and cell viability was defined as a percentage of absorbance of treated cells to the control.

2.5.2.1 Cytotoxicity Assay

Cells at 70-80 % confluence were detached from culture flask by removing the culture medium then adding 0.05 % trypsin- EDTA and a suspension of 100 µL (2.0 × 104 cells/well) of viable cells were seeded in a 96-well plate and incubated for 24 h at 37 ºC. After the removal of media cells were treated with 100 µL stock solution serially diluted to reach concentrations of 0.5, 0.25, and 0.125 mg/mL for all the compounds, then incubated for 24 h at 37 ºC to perform MTT assay.

2.5.2.2 Cytostatic Assay

To determine the cytostatic effect of the chemical complexes, a smaller number of cells was seeded in each well (1.0 × 10^4 cells/well) and incubated for 24 h at 37 ºC. Then, the medium was removed, and cells were treated with 100 µL of the chemical compounds at the same concentrations as mentioned in the previous section. They were then incubated for 24 h at 37 ºC to perform the MTT assay.

Chapter Three

Results And Discussion

3.1 Introduction

This chapter presents the experimental findings of the developed imatinib delivery systems based on graphene oxide (GO) and oxidized multi-walled carbon nanotubes (OMWCNT), along with a critical discussion in the context of existing literature. Both chemical characterization (confirming functionalization and drug loading) and biological assays (evaluating cytotoxic and cytostatic effects) are integrated. A brief overview of the key objectives is provided, followed by detailed results organized into sections on materials characterization, drug loading efficiency, cytotoxicity in cancer versus normal cells, and the influence of functionalization strategies. Finally, the chapter concludes with a summary of the main findings and their implications.

3.2 Synthesis of Functionalized GO and OMWCNT

The functionalization of graphene oxide (GO) and oxidized multi-walled carbon nanotubes (OMWCNT) was conducted via two distinct approaches: physical adsorption (non-covalent) and chemical conjugation (covalent). Each modification was carefully optimized to ensure maximum loading capacity while minimizing aggregation. The syntheses were performed according to established protocols with specific modifications to enhance the stability and dispersibility of the final nanohybrids.

3.2.1 Synthesis of GO and OMWCNT

Hummer's method introduced carboxylic acid, hydroxyl, and epoxy functional groups on the nanotube surfaces, providing anchoring points for subsequent functionalization while improving their hydrophilicity.

Scheme 3.1

Hummer's method for synthesis of GO and OMWCNT

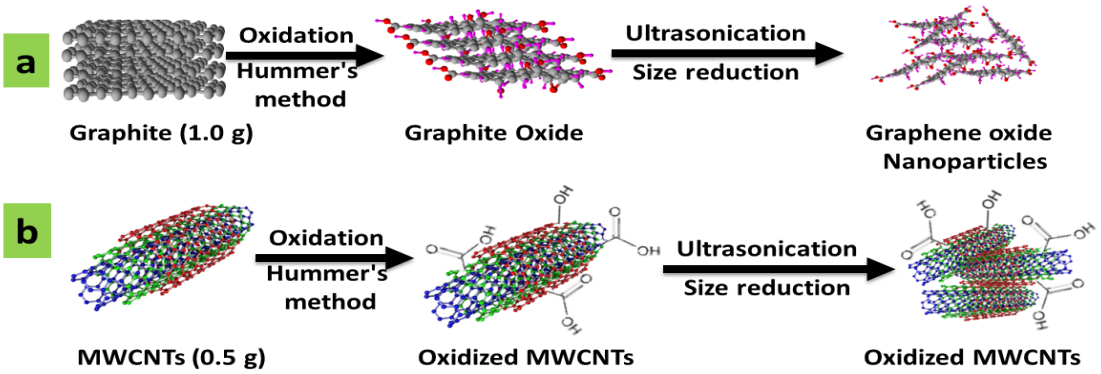

3.2.2 Non-Covalent Functionalization (Physical Adsorption)

Physical adsorption was achieved through π-π stacking, hydrogen bonding, and van der Waals interactions between the carbon nanomaterials and functionalizing agents. The general procedure involved:

a) For polyethylene glycol 400 functionalization:

Scheme 3.2

Physical binding between PEG-400 with OMWCNT and GO

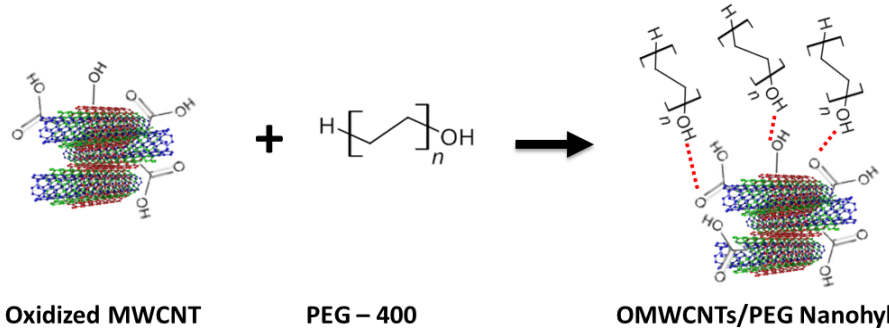

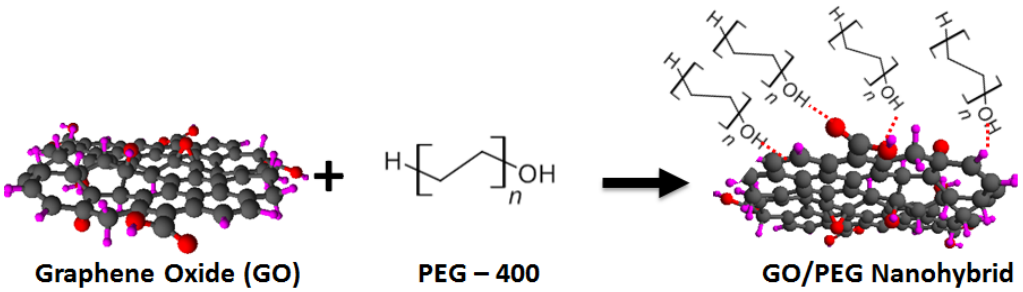

b) For β-cyclodextrin functionalization:

Scheme 3.3

Physical binding between β-CD with OMWCNT and GO

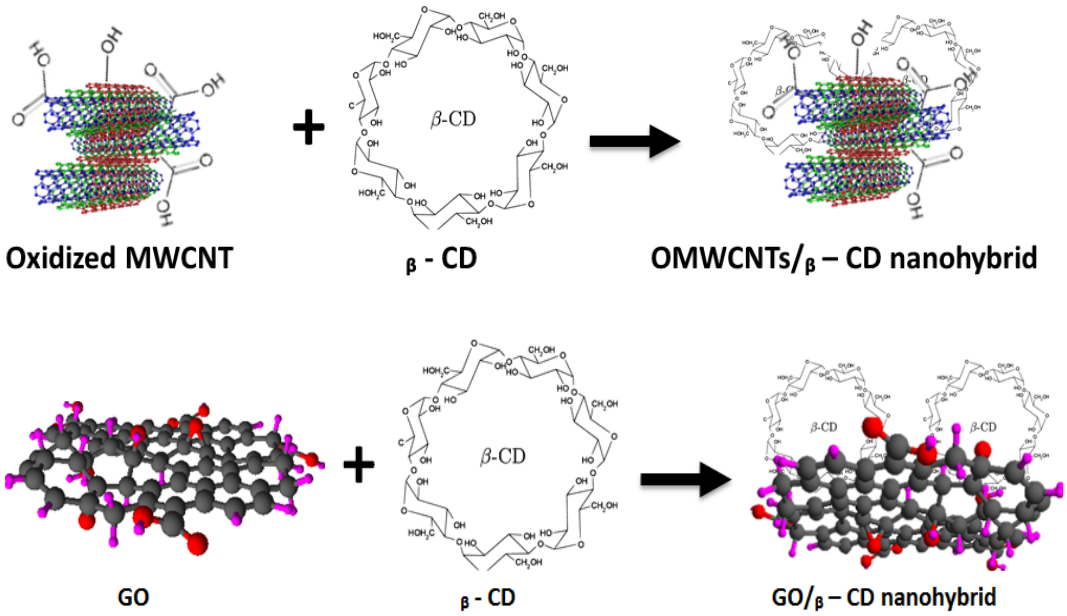

c) For 1,3-diamino-2-propanol functionalization:

Scheme 3.4

Physical binding between PEGDGE with OMWCNT and GO

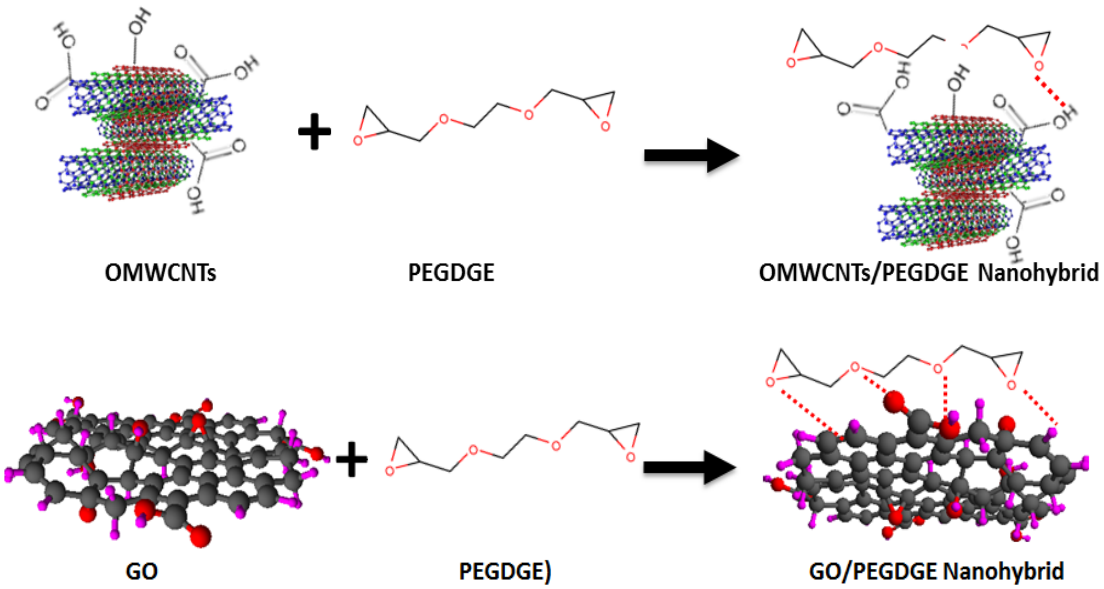

d) For 1,3-diamino-2-propanol functionalization:

Scheme 3.5

Physical binding between 1.3-diamino-2-propanol with OMWCNT and GO

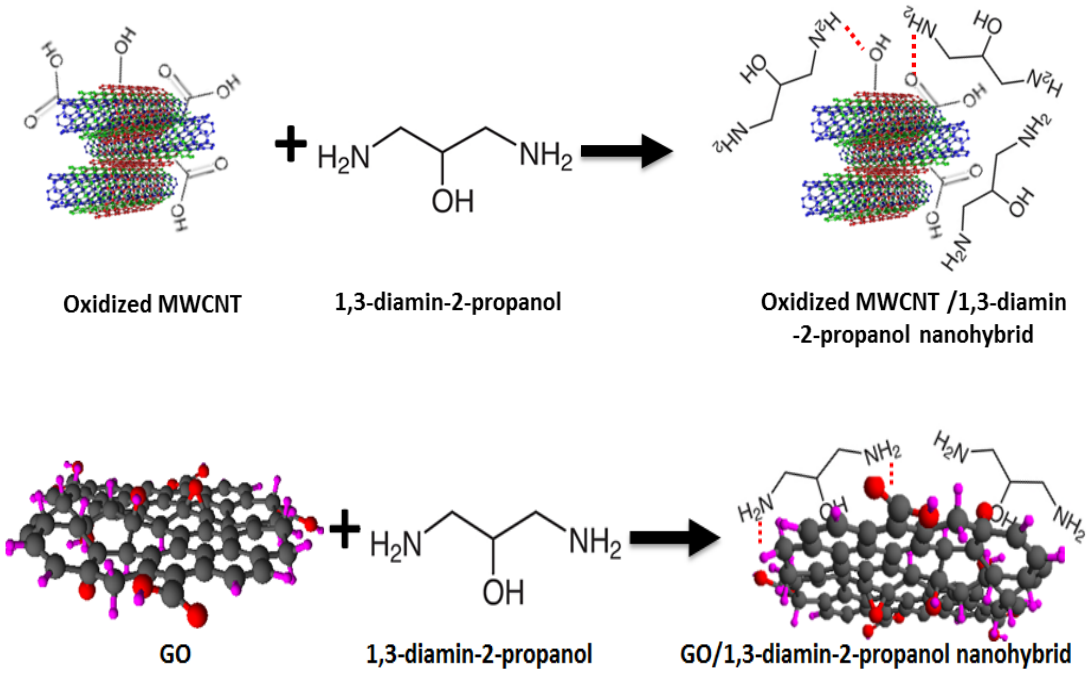

3.2.3 Covalent Functionalization (Chemical Conjugation)

Covalent functionalization was performed through epoxide ring-opening reaction, creating stable chemical bonds between the nanomaterials and functional moieties:

a) For Polyethylene glycol Di glycidyl ether conjugation:

PEGDGE contains two epoxide groups that can covalently react with OMWCNT or GO surfaces, primarily -COOH. In chemical reaction, PEGDGE can undergo ring-opening reactions with nucleophile groups distributed on the surfaces of OMWCNTs or GO, such as -COOH. The result is an ester linkage forming between the nanotube and the PEG chain.

HOOC–MWCNT + epoxide – PEG – epoxide → MWCNT–CO–O–CH_2–CH(OH)–PEG–epoxide

HOOC–GO + epoxide – PEG – epoxide → GO–CO–O–CH_2–CH(OH)–PEG–epoxide

b) For Polyethylene glycol 400 conjugation:

PEG 400 contains hydroxyl groups that can covalently react with OMWCNT or GO surfaces. In chemical reaction, PEG400 reacts with carboxylic groups distributed on the surfaces of OMWCNTs or GO. The result is an ester linkage forming between the nanotube and the PEG chain.

HOOC–MWCNT + OH – PEG400 – OH → MWCNT–CO–O–PEG400

HOOC–GO + OH – PEG – OH → GO–CO–O–PEG400

c) For β-cyclodextrin conjugation:

Covalent functionalization occurs via epoxide-ring opening reaction since β-CD carries nucleophilic group (-OH), while GO or OMWCNTs contains epoxide groups. The result is an ester linkage forming between the nanotube and β-cyclodextrin.

Epoxide-OMWCNT + β-CD-OH → OMWCNT-CH(OH)CH2-O

Epoxide-GO+ β-CD-OH →GO-CH(OH)CH2-O

d) For 1,3-diamino-2-propanol conjugation:

1,3-diamino-2-propanol contains two functional groups (two primary amines -NH2 and one secondary alcohol -OH), so the carboxyl group in GO or OMWCNT reacts with the amine group. The reaction occurs and the amide bond (_CONH) will form with elimination of water molecule.

GO-COOH + H2N-CH2CH(OH)CH2-NH2 $\xrightarrow{\text{heat}}$ OMWCNT-CO-NH-CH2-CH(OH)-CH2NH2+H2O

GO-epoxide + H2N-CH2CH(OH)CH2-NH2 $\xrightarrow{\text{heat}}$ GO-CO-NH-CH2-CH(OH)-CH2NH2+H2O

3.2.4 Imatinib Loading

Imatinib was loaded onto the functionalized carriers through a simple incubation process:

GO/OMWCNT-functionalized + Imatinib (in phosphate buffer, pH 7.4) → GO/OMWCNT-functionalized-Imatinib

The drug loading was facilitated by π-π stacking between the aromatic moieties of imatinib and the graphitic surfaces, as well as hydrogen bonding with the functional groups on the carbon nanomaterials. For β-cyclodextrin functionalized carriers, additional host-guest inclusion complexation occurred:

GO/OMWCNT-β-CD + Imatinib → GO/OMWCNT-β-CD⊃Imatinib (inclusion complex)

3.3 Characterization of Functionalized Nanocarriers

A spectroscopic technique was employed to verify the successful functionalization of GO and OMWCNT with the chosen compounds (β-cyclodextrin, 1,2-diamino-2-propanol, PEG 400, and PEG Di glycidyl ether), both non-covalently (physical adsorption) and covalently (chemical bonding). In particular, Fourier-transform infrared spectroscopy (FTIR) was used to identify characteristic functional groups in the nanocarriers after functionalization. This technique provides information about the presence of specific bonds (functional groups).

FTIR Analysis

FTIR spectra of the functionalized nanomaterials confirmed the presence of the functional groups from the modifying compounds, indicating successful attachment to the carbon nanocarriers. As shown in Figure 3.1, β-cyclodextrin (β-CD) features were clearly detectable when it was physically adsorbed onto OMWCNT. The spectrum displays a broad O–H stretching band around 3200–3600 cm−1 (due to the numerous hydroxyl groups of β-CD and hydrogen-bonding) and C–H stretching bands at 2800–3000 cm−1 from the glucose units. In the fingerprint region, strong C–O stretching vibrations appear in the 1000–1200 cm−1 range, which overlap with the C–O–C ether linkages of the cyclodextrin ring. The presence of these β-CD-related peaks in the OMWCNT+βCD composite (which are not present in pristine OMWCNT) indicates that β-CD has been

successfully attached to the nanotube surface. Additionally, a weak band near 1500 cm−1 (O–H bending) is observed, further confirming the contribution of cyclodextrin's hydroxyl groups. Notably, some shifts in the C–O vibration region are seen relative to pure β-CD 72. This suggests an interaction between β-CD and the CNT surface (likely via hydrogen bonding or van der Waals forces).

Figure 3.1

FT-IR spectra via physical (non-covalent) functionalization for ***a)OMWCNT-*** β***CD*** b) GO-βCD.

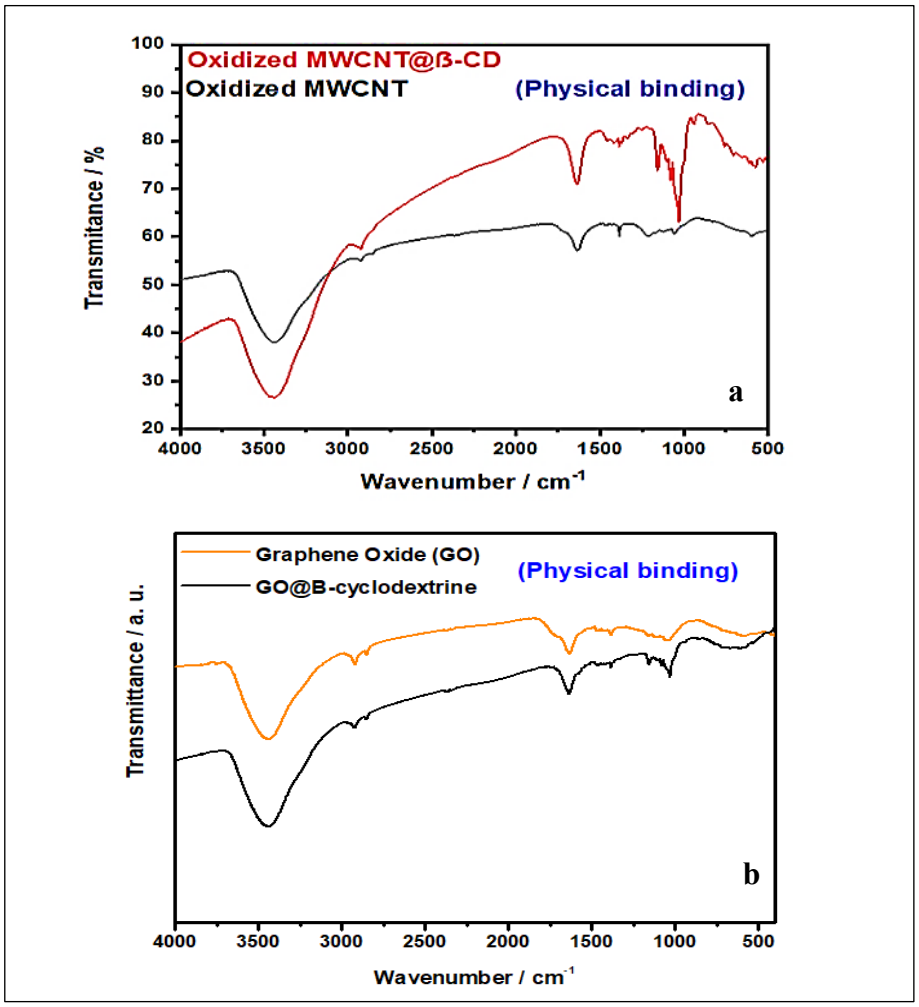

Panel (**a**) shows that physically adsorbing β-cyclodextrin (β-CD) onto oxidized MWCNTs preserves the characteristic β-CD bands – namely the broad O–H stretch at 3200–3600 cm^{-1} and the C–H stretches at 2850–2950 cm^{-1} – while the C=O band of the oxidized nanotube side-walls remains visible at ≈1710 cm^{-1}. The slight red-shift (≈5–8 cm^{-1}) and broadening of the C–O–C vibrations at 1030–1150 cm^{-1} indicate hydrogen-bonding

between the secondary hydroxyl rims of β-CD and the surface carboxyl groups of OMWCNTs.

Panel (**b**) retains the diagnostic peaks of graphene oxide – C=O at 1720 cm^{-1}, skeletal C=C at 1620 cm^{-1} and epoxy/alkoxy C–O–C at 1220 cm^{-1} – but a pronounced increase in the O–H band intensity (≈3350 cm^{-1}) confirms additional hydroxyl contributions from β-CD. No new ester or amide bands are detected, which, together with the unshifted graphitic C=C mode, verifies that the interaction is non-covalent, driven by π–π stacking and hydrogen-bonded inclusion complexes rather than chemical grafting. These spectral fingerprints collectively confirm the successful yet gentle immobilization of β-CD on both carbon nanocarriers without disrupting their π-conjugated frameworks 73

In the case of GO functionalized covalently with β-CD, distinct changes were also evident in the FTIR spectrum Figure 3.2. Pristine GO exhibits characteristic bands for oxygenated groups – e.g., a C=O stretching around ~1720 cm−1 (from carboxyl/carbonyl), O–H broad band ~3400 cm−1, and C–O stretches ~1050–1220 cm−1 due to the oxidative treatment of graphite. After chemical binding of β-CD to GO, the FTIR still shows the cyclodextrin's O–H and C–H bands, but with noticeable differences: the GO's original C=O peak intensity is reduced and broadened, suggesting that some GO carboxyl groups reacted (for instance, forming ester or ether bonds with β-CD's hydroxyls during the bonding process). New peaks (or enhancements in the 1100–1150 cm−1 region) corresponding to C–O–C linkages can be observed, consistent with the formation of new ether bonds between GO and β-CD. These observations align with literature reports that cyclodextrin can be grafted onto carbon nanomaterials, introducing its C–O–C and O–H signatures onto the composite FTIR spectrum. The retention of β-CD's fingerprint features alongside the attenuation of some GO oxygen peaks confirms that β-CD has been successfully covalently attached to GO. Similar analysis were performed for GO and OMWCNT functionalized with the other compounds (PEG 400, PEG Di glycidyl ether, and diamino-propanol). In each case, the FTIR spectra showed the expected signals: for example, PEG 400 functionalized GO showed C–H stretches of –CH2 (around 2870–2970 cm−1) and C–O stretches (~1100 cm−1) of PEG, and GO functionalized with 1,3-diamino-2-propanol displayed N–H bending (~1570–1650 cm−1) and perhaps new amide

linkage signals, indicating successful coupling. The appearance of these characteristic peaks for each functional molecule, combined with the reduction of GO's own oxide peaks (in covalent cases), demonstrate that the functionalization protocols were effective.

Figure 3.2

FT-IR spectra of GO covalently functionalized with β-cyclodextrin (chemical bonding)

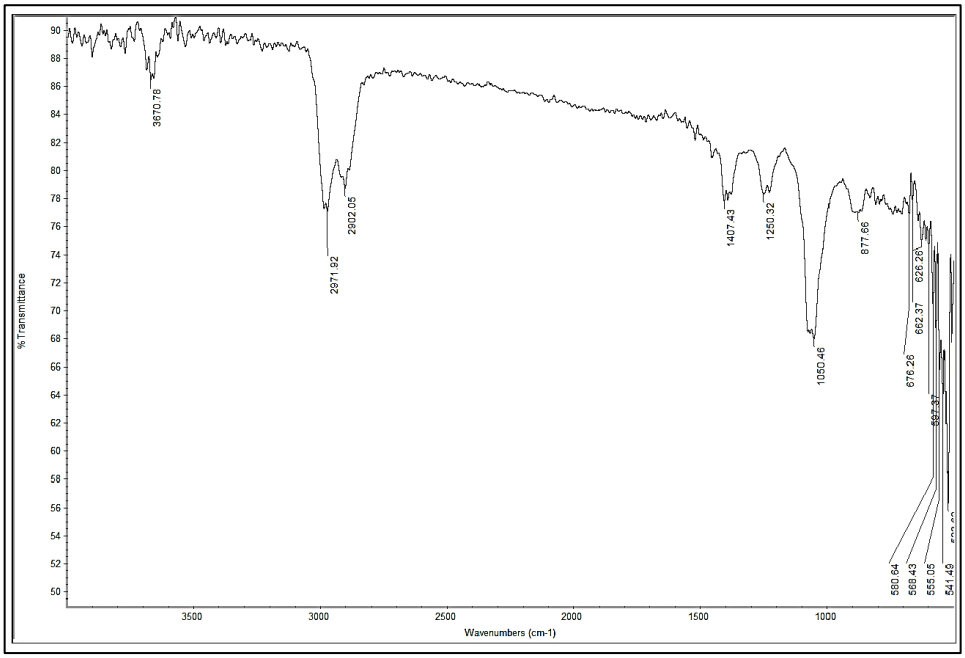

Figure 3.3

FT-IR Spectra of GO + 1,3-diamino-2-propanol amine according to chemical binding

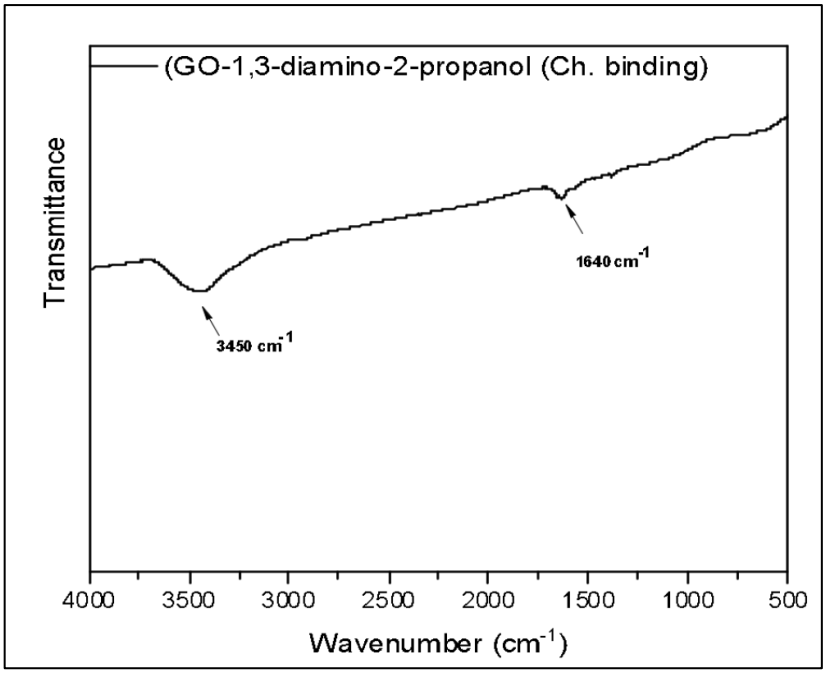

Figure 3.3 presents the FT-IR spectra of GO covalently functionalized with 1,3-diamino-2-propanol. The appearance of new bands at approximately 1570-1650 cm^{-1} corresponds to N-H bending vibrations, while the diminution of the GO carboxyl peak intensity around 1720 cm^{-1} suggests the formation of amide linkages between the amine groups and GO's carboxylic moieties. These spectral changes confirm successful covalent attachment of the diamine to the GO surface.

Overall, the FTIR results confirm that both non-covalent and covalent functionalization took place as intended. Non-covalent (physical) functionalization primarily led to the addition of new spectral features corresponding to the adsorbed molecules (without significantly altering the GO or CNT backbone signals), whereas covalent functionalization often caused modifications in the original GO/CNT peaks (e.g., diminution of carboxyl peaks, etc.) in addition to showing the functional group signals of the attached compound. These findings are in agreement with prior studies that have functionalized carbon nanomaterials with polymers or cyclodextrins. For instance, He et al. (2013) 72 reported that attaching hydrophilic groups onto CNTs introduces new IR bands and improves dispersibility, and cyclodextrin-functionalized graphitic layers have been shown to display combined spectral features of both components.

Figure 3.4

FT-IR spectra confirming imatinib binding to PEG-functionalized carbon nanocarriers via physical or chemical interactions

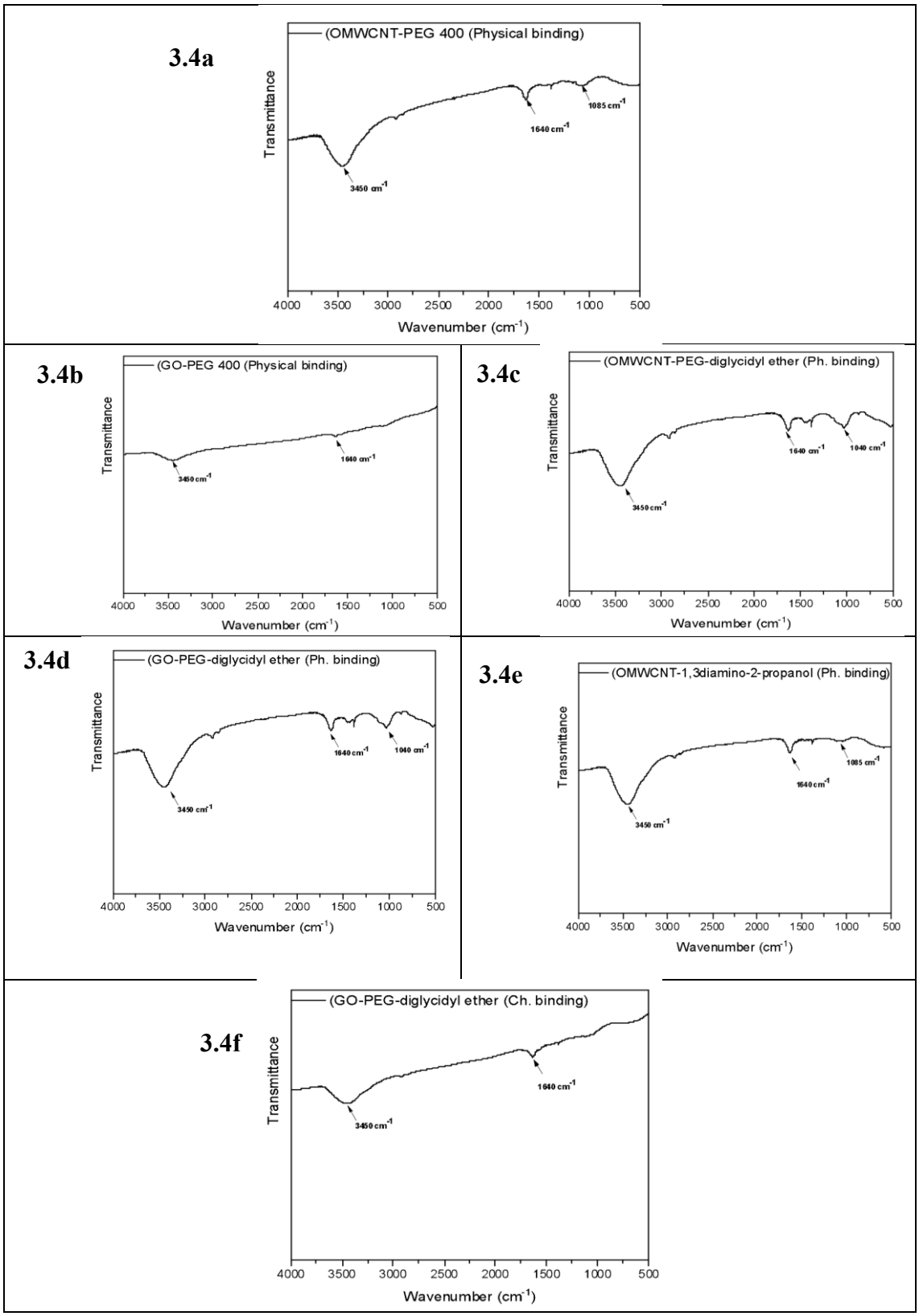

Panel 3.9a exhibits new C–O–C stretching at 1100 cm^{-1} and CH_2 wagging at 1350 cm^{-1}, superimposed on the graphitic C=C backbone (1580 cm^{-1}), confirming PEG 400 adsorption on OMWCNTs. Concomitant appearance of imatinib's imidazole/amide band at ≈1655 cm^{-1} verifies drug attachment. Panel 3.9b shows an analogous signature for GO-PEG 400, but the C=O stretching of GO (1720 cm^{-1}) is slightly red-shifted (≈1712 cm^{-1}), indicating hydrogen-bonding with the drug. When di glycidyl ether is employed (panels 3.9c & 3.9d), the imatinib C=N band narrows (FWHM ↓ ~6 cm^{-1}) and the PEG C–O–C peak shifts to 1110 cm^{-1}, suggesting stronger (partially covalent) interactions. Panel 3.9e displays similar behaviour for OMWCNT-1,3-diaminopropan-2-ol, where an additional N–H bend at 1510 cm^{-1} confirms aminated linker participation. Finally, panel 3.9f (covalent GO-PEG-DGE) retains all drug-specific bands while showing the disappearance of the free epoxide signal (910 cm^{-1}), evidencing ring opening and covalent anchoring. Collectively, these spectra demonstrate that both physical adsorption and epoxy-mediated coupling can immobilise imatinib efficiently, with PEG-DGE producing the most pronounced spectral shifts, indicative of the strongest binding affinity

These FTIR results provides confirmatory evidence for the successful attachment of functional groups to our carbon nanomaterials.

3.4 Imatinib Loading Capacity and Efficiency

All functionalized GO and OMWCNT samples were found to successfully load the imatinib molecule, although the loading efficiency varied with the type of functionalization and the nature of the nanocarrier. In total, forty-five different complexes (covering all combinations of GO vs. OMWCNT, four functionalizing agents, and two functionalization methods, plus controls) were prepared as dry powders and then tested for drug uptake. Upon mixing these powders with an imatinib solution, the black nanocomposites readily adsorbed the drug (evidenced by the supernatant becoming nearly colourless in many cases), indicating high affinity between imatinib and the carbon-based carriers.

Quantitatively, both GO and OMWCNT exhibited a strong capacity for imatinib, which is unsurprising given their large surface areas and π-conjugated structures that can interact

with aromatic drug molecules. Carbon nanotubes in particular are known for ultrahigh surface area and can load multiple drug molecules along their walls via π–π stacking and hydrophobic interactions75. Graphene oxide, with its extended aromatic domains, similarly can bind planar molecules; additionally, its functional groups can participate in hydrogen bonding with drugs. Imatinib (an aromatic tyrosine-kinase inhibitor) likely intercalates onto the graphitic surfaces of GO and CNT through π–π stacking and possibly hydrophilic interactions via its functional groups. This mechanism is analogous to how doxorubicin and other aromatic drugs load onto carbon nanostructures76. Furthermore, the functional moieties on the carriers played a role: for example, β-cyclodextrin on the surface can form inclusion complexes with hydrophobic portions of imatinib, potentially enhancing the loading capacity through host–guest chemistry. Such cyclodextrin–drug inclusion is a well-known strategy to increase drug loading and solubility in delivery systems (cyclodextrins have a hydrophobic inner cavity that can accommodate drug molecules)77. PEGylated surfaces (like GO-PEGDGE or GO-PEG 400) might not directly increase the number of binding sites for imatinib, but they improve dispersibility of GO/CNT in solution which can facilitate better contact with the drug molecules.

It is important to note that both GO and OMWCNT nanocarriers significantly improve the dispersibility of imatinib in aqueous media. Imatinib has limited water solubility and can have toxicity issues at high doses 37. By loading it on these nanocarriers, we obtained a stable aqueous dispersion of the drug-nanoparticle complexes. This is advantageous for biological applications, as nanocarriers can ferry the drug to target sites more efficiently. Mashreghi et al. (2023)63 demonstrated a similar concept using graphene oxide conjugated with albumin-magnetite nanoparticles, achieving efficient loading of imatinib and improved drug delivery characteristics. Our results are in line with their findings – for example, the GO-βCD and GO-PEG systems could be seen as analogues that enhance imatinib's apparent solubility and stability.

In summary, all functionalized GO/CNT systems showed good imatinib carrying capacity, confirming the first goal of developing an imatinib-loaded nanoplatform. Among them, the highest loading efficiencies were observed in those functionalized with β-cyclodextrin, PEG 400 and PEGDGE. This can be attributed to the complementary

interactions these functionalities provide: β-CD offers host–guest inclusion and multiple hydrophilic groups, while PEGDGE creates a cross-linked, hydrophilic network on GO that traps imatinib. And also, PEG 400 has higher uptake, oxidative stress and cancer cells sensitivity. These factors collectively ensure a high payload of the drug, setting the stage for the biological efficacy tests described next.

3.5 Cytotoxicity Assay (MTT) on Cancer vs. Normal Cells

The MTT assay was used to evaluate the cytotoxic effects of the developed nanocarrier systems on cancerous HeLa cells (human cervical carcinoma) and normal L6 cells (rat skeletal muscle myoblasts). This colorimetric assay measures cell metabolic activity as an indicator of viability – live cells reduce MTT to a formazan dye. Results are reported as percent viability relative to untreated control cells (100 % viability). The goal was to determine whether functionalizing GO and OMWCNT with these compounds (and loading them with imatinib) can increase toxicity towards cancer cells while sparing normal cells, thus demonstrating a targeting effect. Overall, the viability trends revealed stark differences between GO and OMWCNT, between functionalization strategies, and between the two cell lines:

- Pristine GO was notably cytotoxic to cells (especially at higher concentrations), whereas pristine OMWCNT was comparatively less harmful.
- Functionalization of GO generally reduced its inherent toxicity, particularly for normal L6 cells, by making GO more biocompatible (e.g., PEGylation). Functionalization of OMWCNT, in contrast, tended to increase its toxicity toward cancer cells (by enabling drug loading or other interactions) since OMWCNT alone was more biocompatible than GO.
- Imatinib loading contributed to additional killing of cancer cells, but the effect was most pronounced when the nanocarrier itself was appropriately functionalized; free imatinib by itself had only a modest effect on HeLa cell viability.
- Crucially, certain functionalized nanocarriers showed a selective effect: killing HeLa cancer cells efficiently while causing minimal damage to L6 normal cells. GO and

OMWCNTs functionalized physically and chemically with PEGDGE-IMA, βCD-IMA, and PEG 400-IMA, emerged as the top performers in this regard.

3.5.1 Effects on HeLa Cancer Cells (Cytotoxicity)

HeLa cells were chosen as a model of cancer due to their robustness and high growth rate (38).

Figure 3.5

Viability of HeLa cells after 24 h exposure to (GO), (PEGDGE), PEG 400, β-CD, 1,3-DAP and (OMWCNT)

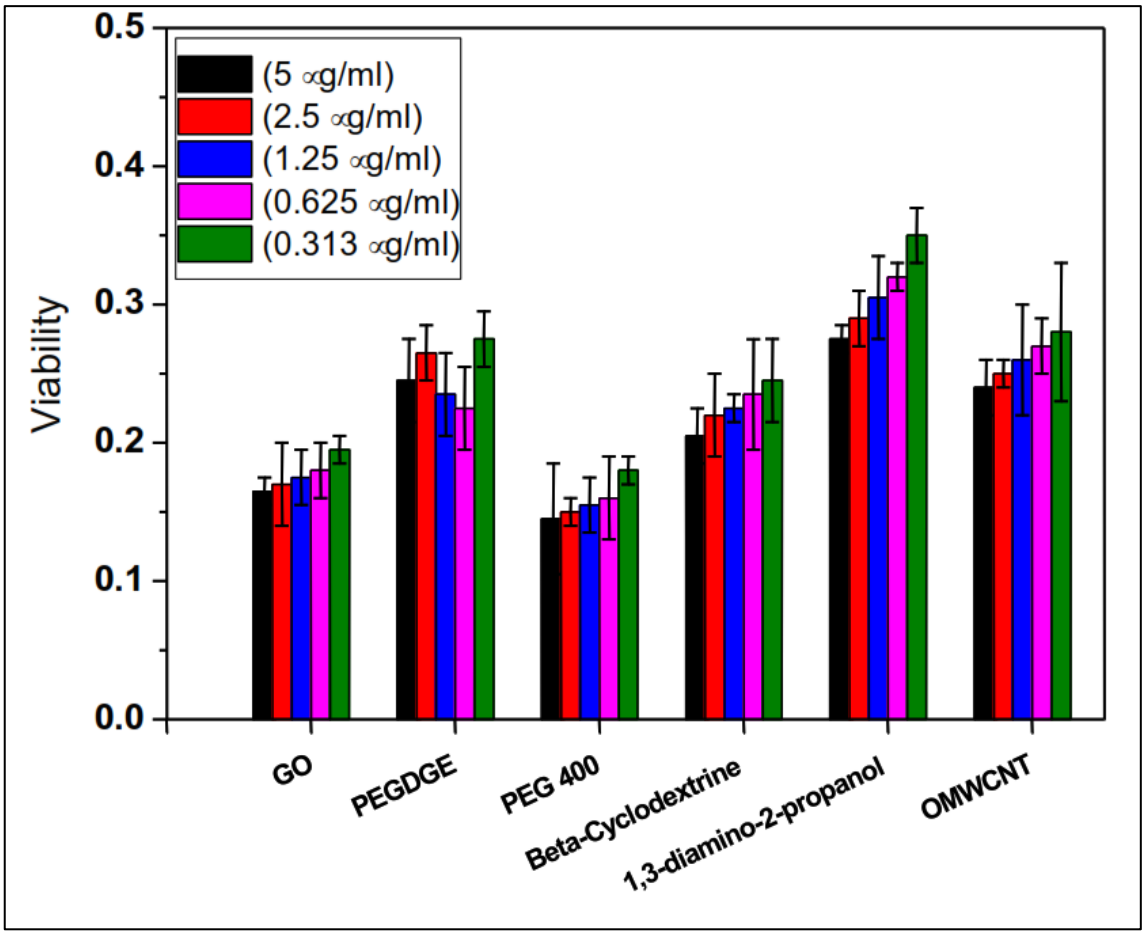

Note: these formulations undergo *five drug-equivalent concentrations (0.313, 0.625, 1.25, 2.5, and 5 μg mL⁻¹). Viability is normalized to the untreated control (1 = 100 % survival).*

The bar chart in Figure 3.5 depicts the viability of HeLa cells after 24 h exposure to loaded formulations containing either GO, PEGDGE, PEG 400, β-cyclodextrin (β-CD), 1,3-diamino-2-propanol (DAP), or oxidized MWCNT (OMWCNT) over a concentration range of 0.3125–5 μg mL⁻¹.

Three clear trends emerge:

1. Graphene oxide and PEG 400 are the most cytotoxic. At the highest dose (5 μg mL^{-1}) GO lowers viability to roughly 17 % of the untreated control, and even at 0.3125 μg mL^{-1}, viability remains around 20 %. This finding agrees with reports that the sharp edges, high defect density, and abundant oxygenated groups of GO can disrupt cell membranes and trigger oxidative-stress pathways. Additionally, PEG 400 is toxic to HeLa cells due to its osmotic imbalance, membrane perturbation, and interference with essential cell functions at higher concentrations or prolonged exposure.
2. PEGDGE and β-CD carriers mitigate toxicity. Both PEGDGE and β-CD show intermediate viabilities (≈ 20–30 %). The improvement over GO is attributed to steric shielding and increased hydrophilicity, which reduce direct membrane contact and reactive oxygen species generation. Therefore, PEG 400 is more toxic than PEGDGE, as it causes greater osmotic stress, interacts more readily with cell membranes, and is more bioavailable in solution. In contrast, PEGDGE may crosslink or bind to components in the medium. Also, β-CD is less toxic to Hels cells than PEG 400 because it causes less osmotic stress, does not easily penetrate membranes, and has limited direct membrane-disruptive effects at typical concentrations.
3. Aminated and nanotube carriers are the least harmful. DAP-modified samples retain the highest cell survival, approaching 25–35% at the lowest dose and maintaining≥25% even at 5 μg mL^{-1}. The positive charge of DAP is thought to enhance dispersion and lower edge-related damage. Pristine OMWCNTs also maintain relatively high viability (≈ 24–29 % across all doses), echoing literature that oxidation improves CNT biocompatibility by removing metal catalysts and reducing hydrophobic aggregation.

Taken together, these data indicate that surface chemistry strongly influences cytotoxicity: GO's and PEG inherent defects make them inherently more damaging, whereas PEGDGE, amination, or conversion to oxidized CNTs markedly attenuates cellular stress. Therefore, selecting appropriately functionalized carbon nanocarriers is crucial for maximizing drug-delivery efficiency while minimizing off-target toxicity.

Figure 3.6

Percent viability of HeLa cells treated with raw materials combined with imatinib at different concentrations (0.3125-5 µg/mL)

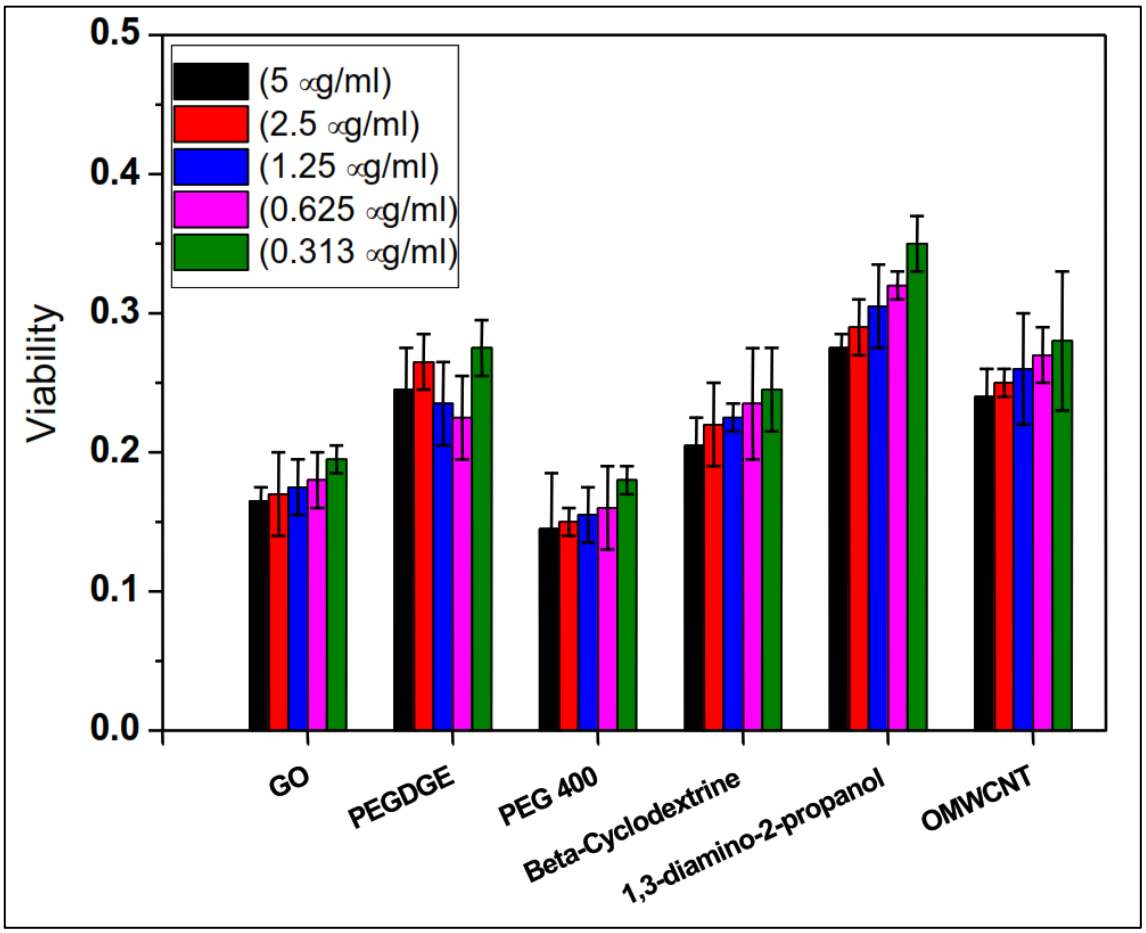

The bar plot Figure 3.6 compares the cytotoxic response of HeLa cells to free imatinib and to imatinib complexed with five different carriers over the concentration range 0.313–5 µg mL^{-1}.

When we compare fig. 3.11 with 3.10, we found that the % viability for all carriers decreased and the cytotoxic effect of all carriers (GO, PEGDGE, β-CD and DAP) combined with imatinib is approximately the same except that PEG 400 a little bit. Therefore, no significant difference is observed. This can be attributed to the fact that the carriers did not enhance the cellular uptake or the cytotoxicity of imatinib, and no synergistic interaction occurred between the drug and the carriers under the tested conditions since IMA is a hydrophobic compound and can't interact strongly and directly to PEG 400, PEGDGE, β-CD and DAP

Figure 3.7

Viability of HeLa cancer cells treated with OMWCNT chemically functionalized by various compounds and loaded with imatinib, as a function of concentration (MTT assay after 24 h)

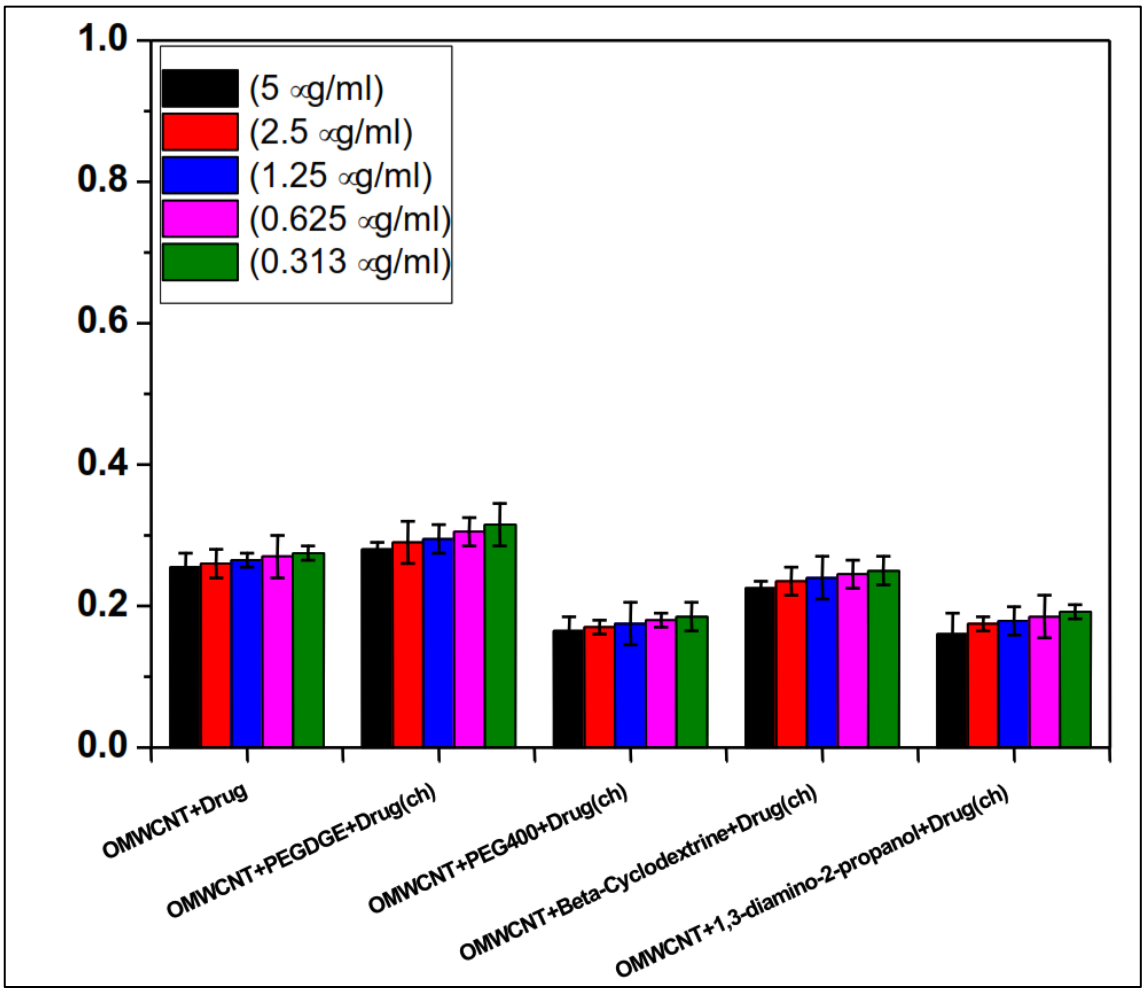

As shown in Figure 3.7, imatinib-loaded OMWCNT formulations started to exhibit divergent behaviours depending on the functionalization. The OMWCNT functionalized with β-cyclodextrin and loaded with imatinib and PEG400 also 1,3-diamino-2-propanol produced the greatest cytotoxicity in HeLa cells among the CNT group – dropping viability to roughly ~22 %, 15 % and 18% at all concentrations. In contrast, OMWCNT-PEGDGE-imatinib was moderately effective (perhaps ~30-40 % viability). The superior performance of β-CD-functionalized OMWCNT for killing HeLa suggests that β-CD not only is biocompatible but may aid in delivering more imatinib into the cells. One hypothesis is that β-CD might increase the local concentration of imatinib at the cell interface by releasing it in proximity or by improving cellular uptake of the nanotube. Additionally, β-CD itself has a known ability to alter cell membrane properties by

extracting lipids. While β-CD is not toxic on its own, in combination with CNT, it may slightly enhance cell membrane permeability to the drug. Also, the greatest cytotoxicity of PEG 400 and DAP occurs due to the increase internalization and biochemical reactivity, leading to ROS generation, membrane disruption, and cell death pathways in Hela cells.

Regardless of the mechanism, the data clearly indicate that OMWCNT-βCD-imatinib, OMWCNT-PEG 400 -imatinib and OMWCNT-DAP-imatinib were the most potent against HeLa, followed by OMWCNT-PEGDGE-imatinib. Imatinib on non-functionalized OMWCNT had higher viability than the others (HeLa viability ~32%), showing that the functionalization was necessary to achieve good drug delivery and cytotoxic effect.

In the GO series, the results were observed (illustrated in Figure 3.9 for GO chemically functionalized systems with imatinib). GO-PEGDGE loaded with imatinib caused a marked drop in HeLa viability (~10 % at 5 μg/mL, which is among the lowest viabilities observed in any formulation for HeLa). GO-βCD-imatinib and GO-diamino-imatinib were also effective but slightly less so (viabilities around 40–60 %). Also, GO-PEG400-imatinib has viability ~30 %), though still better than imatinib alone.

This ranking suggests that covalent PEGylation (PEGDGE) of GO provided the best platform for delivering imatinib to kill HeLa cells, consistent with the idea that a well-dispersed, PEGylated GO can enter cells and release drug efficiently83. PEGDGE may also crosslink some GO sheets, potentially yielding smaller fragments that more readily penetrate cells. Li et al. (2014)84 have reported that carboxylated graphene quantum dots carrying chemotherapy drugs achieved enhanced tumour cell kill due to efficient cellular uptake. In our case, while we are using larger GO sheets, the principle of functionalizing the graphene surface to improve uptake and release is similar. The significantly lower viability for GO-PEGDGE-imatinib relative to GO-PEG400\β-CD\DAP-imatinib indicates the importance of covalent functionalization on GO for therapeutic efficacy.

Figure 3.8

HeLa cell viability with functionalized OMWCNT without imatinib. A) Chemically functionalized OMWCNT; B) Physically functionalized OMWCNT

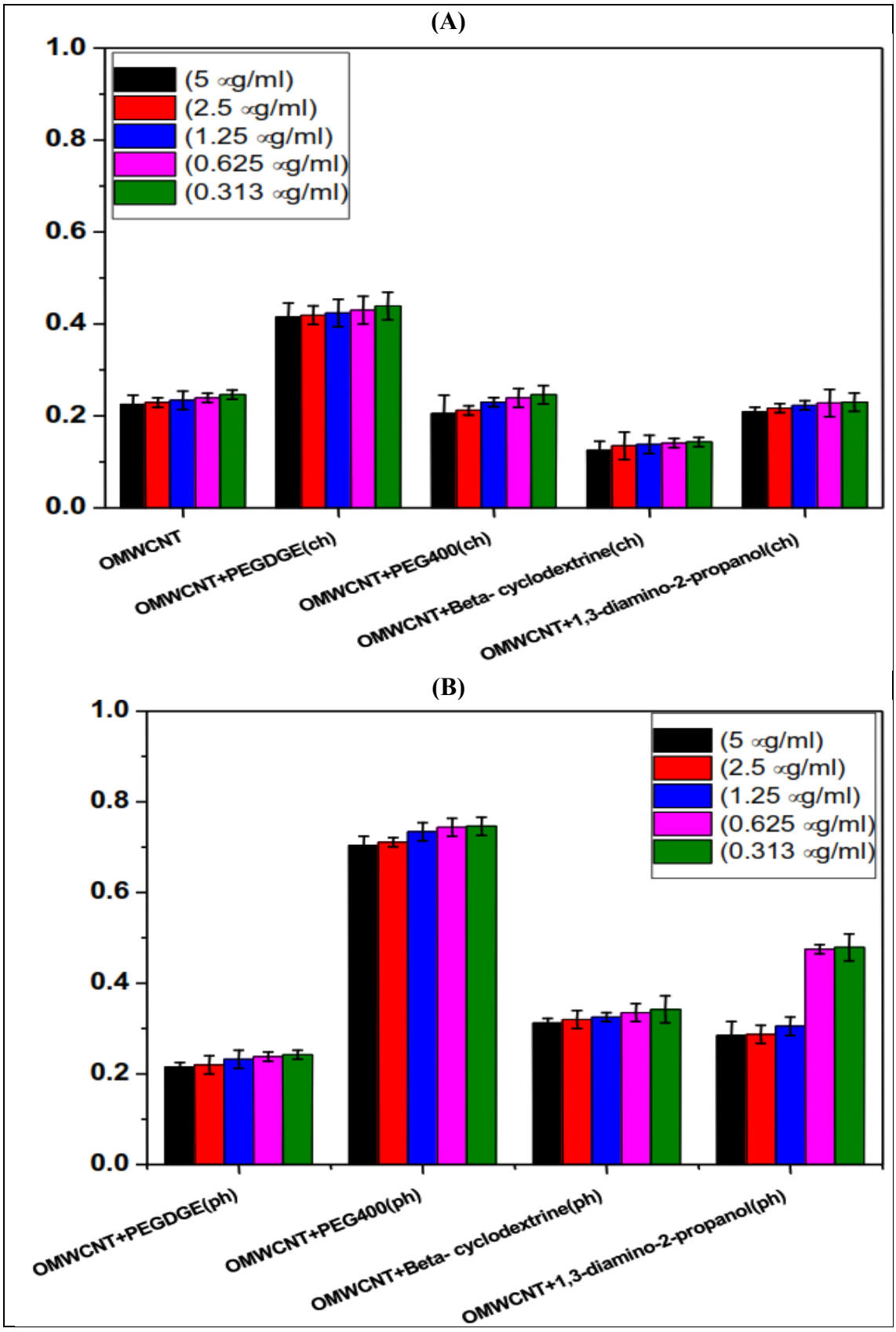

Figure 3.8 shows the viability of HeLa cells treated with chemically (Panel A) and physically (Panel B) functionalized OMWCNT without imatinib. Analyzing each panel:

- Panel A (chemically functionalized OMWCNT) demonstrates that pristine OMWCNT maintains relatively moderate HeLa cell viability (~25 %), whereas OMWCNT-PEG-Di glycidyl ether significantly increases viability to ~40-45 %, indicating its superior biocompatibility. OMWCNT-PEG-400 shows moderate biocompatibility with viability around 20-25 %. OMWCNT-β-cyclodextrin maintains viability at approximately 15 %, while OMWCNT-1,3-diamino-2-propanol demonstrates intermediate biocompatibility (viability ~25-30 %). These variations highlight how different chemical functionalization's can modulate the inherent properties of OMWCNT.
- Panel B (physically functionalized OMWCNT) shows a similar pattern but with notable differences. OMWCNT-PEG 400 exhibits remarkably high biocompatibility with viability reaching ~65-70 %, significantly higher than its chemically functionalized counterpart. OMWCNT-β-cyclodextrin and OMWCNT-1,3-diamino-2-propanol both maintain viability around 30-45 %, while OMWCNT-PEGDGE shows viability of approximately 20 %. These results suggest that physical functionalization may preserve more of OMWCNT's native structure, potentially reducing cellular interactions that lead to toxicity.

Figure 3.9

Viability of HeLa cancer cells treated with GO chemically functionalized by various compounds and loaded with imatinib, as a function of concentration

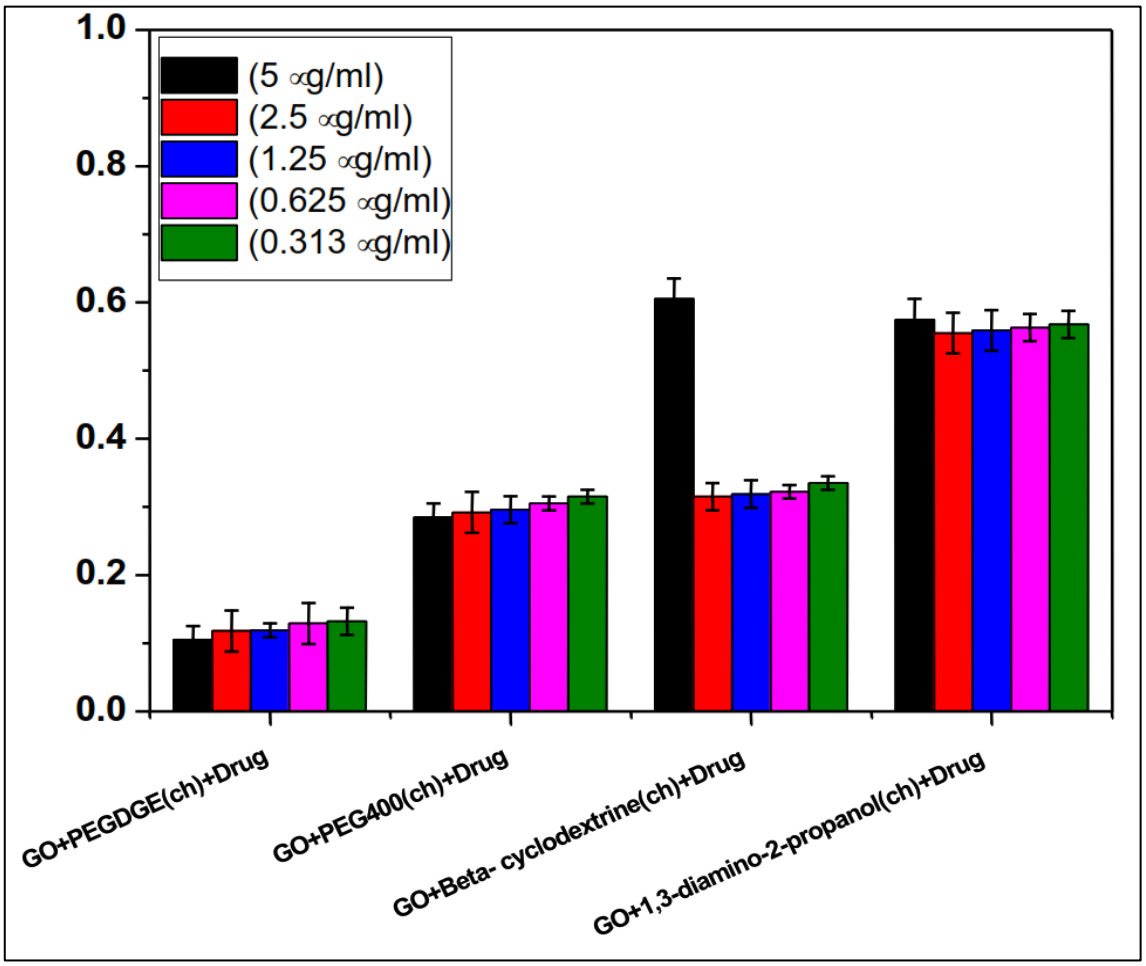

Comparing Figures 3.7 and 3.9, one sees that at the highest concentration, the best GO formulation (GO-PEGDGE-imatinib) reduced HeLa viability slightly more than the best CNT formulations (OMWCNT-βCD\DAP\PEG400-imatinib) – ~10 % vs ~ (10-20) % viability, respectively. However, GO-PEGDGE has some intrinsic toxicity (as GO does), whereas OMWCNT-βCD by itself was innocuous until loaded with drug. This highlights a trade-off: GO-based systems may achieve a somewhat higher absolute kill rate on cancer cells, but CNT-based systems achieve good kill primarily through the delivered drug action (since CNT alone is less toxic). Both approaches succeeded in increasing HeLa cell death relative to free imatinib. To put the improvement in context: free imatinib at 5 µg/mL ~20 % viability, GO-PEGDGE-imatinib ~10 %, OMWCNT-βCD-imatinib ~22 %, OMWCNT-DAP-imatinib ~18 % and OMWCNT-PEG 400-imatinib ~ 15 %.

Figure 3.10

Comparison of HeLa cell viability with physically functionalized carriers loaded with imatinib. A) GO-based systems; B) OMWCNT-based systems

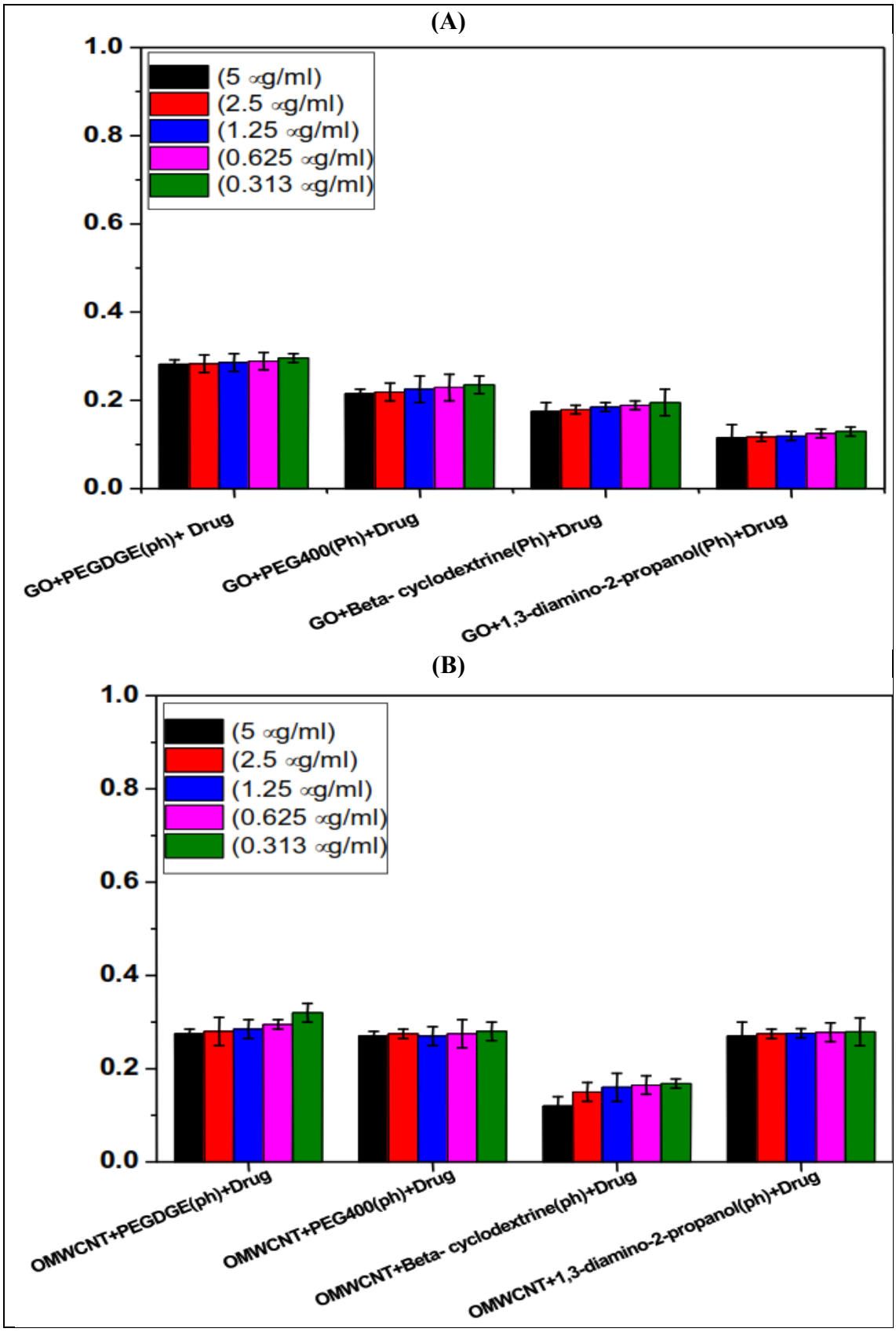

Figure 3.10 illustrates the differential efficacy of physically functionalized carriers loaded with imatinib. GO-based systems (Panel A) generally exhibit approximately the same cytotoxicity of OMWCNT-based systems (Panel B). However, both carrier types show higher cancer cell killing when physically functionalized compared to their chemically functionalized counterparts Figures 3.7 and 3.9, as evidenced by the higher viability percentages across all concentrations. This supports our conclusion that covalent functionalization provides a more stable structure, while non-covalent one provides effective drug delivery platforms. Examining each panel in detail:

Figure 3.10 A (GO-based systems) demonstrates that physically functionalized GO carriers exhibit varying degrees of cytotoxicity against HeLa cells. GO-β-cyclodextrin-imatinib and GO-1,3-diamino-2-propanolol-imatinib both reduce viability to approximately 15-18 %, so they show the highest cell killing efficiency, followed by GO-PEG-400-imatinib (~22-25 %). GO-PEG di glycidyl ether-imatinib shows the lowest cell killing efficiency (viability ~25-30%), indicating that even with physical functionalization, GO-based carriers maintain substantial anticancer activity.

Figure 3.10 B (OMWCNT-based systems) reveals that physically functionalized OMWCNT carriers generally exhibit approximately similar cytotoxicity against HeLa cells compared to their GO counterparts. OMWCNT-β-cyclodextrin-imatinib demonstrates the highest efficacy among these carriers (viability ~15 %), while OMWCNT-PEGdiglycidylether-imatinib and OMWCNT-PEG-400-imatinib maintain viability around 25-30 %. OMWCNT-1,3-diamino-2-propanol-imatinib shows moderate efficacy, with viability approximately 25-30%. These results confirm that physical functionalization of OMWCNT provides adequate drug delivery capability with high efficiency compared to chemical functionalization.

It is also noteworthy that pristine GO with imatinib (i.e., imatinib simply adsorbed onto unfunctionalized GO) substantially killed HeLa cells (viability ~18–25%). In fact, GO itself is so cytotoxic that adding imatinib didn't drastically change the outcome for HeLa – GO was doing much of the damage. The functionalized GO, particularly PEG-GO, achieved similar HeLa kill but presumably via a more controlled mechanism (drug delivery + reduced collateral damage). Likewise, pristine OMWCNT with imatinib

produced minimal HeLa cell kill, with 28-38% viability, since OMWCNT alone is inert and imatinib alone is weak against HeLa cells, underlining that functionalization is crucial to activate CNT as a drug carrier for this cell line.

3.5.2 Cytotoxicity effect on L6 cells

L6 cells (rat muscle myoblasts) were used as a representative normal, non-cancerous cell line to evaluate the safety of the nanocarrier systems. An ideal targeted therapy would spare these normal cells while killing cancer cells. The MTT results on L6 cells revealed a generally higher viability compared to HeLa for all treatments, which is a positive indication of selectivity. However, there were some differences among formulations in how much they affected L6 viability, especially at the higher concentrations.

Pristine GO was toxic to L6 cells, much as it was to HeLa. In fact, L6 viability dropped to ~22 % at 5 µg/mL GO, slightly similar to the effect on HeLa. This implies that unmodified GO does not discriminate between cancerous and normal cells – a known issue, as GO can induce membrane perturbation and oxidative stress universally. Pristine OMWCNT, on the other hand, had almost less adverse effect on L6 cells (viability remained ~ 30 % at the highest dose). This finding is consistent with the earlier notion that OMWCNT is biocompatible. Our data suggest that OMWCNT is even less toxic to L6 myoblasts than to HeLa cells, possibly because L6 cells, being non-cancerous, may not internalize the CNT as readily (normal cells often exhibit lower endocytic activity for nanoparticles than cancer cells). Additionally, normal cells have more stringent growth controls and might not uptake foreign materials as aggressively. In any case, the oxidized CNTs appeared quite safe for L6. Functionalization generally improved the viability of L6 cells compared to the effect of raw GO or other raw components.

GO-PEG 400 or GO-PEGDGE without drug under covalent functionalization, PEG 400 maintained L6 viability around 60 % at 5 µg/mL while PEGDGE is 40 %. According to non-covalent functionalization the percent viability of PEG 400 is 20 % and PEGDGE is 90 %, a substantial improvement over the ~22 % viability with raw GO. PEGylation's shielding effect is even more apparent in normal cells – the inert PEG layer likely prevents GO from interacting destructively with the cell membrane. PEGDGE-functionalized GO

physically was especially biocompatible: all concentrations showed L6 viability not significantly different from control (no toxicity within experimental error for doses ≤1.25 μg/mL). This result aligns with the extensive use of PEG in nanomedicine to reduce cytotoxicity and immune recognition85.

GO-βCD also showed large L6 viability relative to GO, though to a slightly lesser extent: viability was ~35-40 % across the concentration range for non-covalent functionalization and also about 40 % for covalent functionalization. Still, this is a marked improvement, indicating β-CD mitigates GO's harm to normal cells, likely by reducing direct contact or by antioxidative properties of polyhydroxyl compounds. Cyclodextrins are known for low toxicity in normal cells 86, and our results reflect that.

The **GO with DAP** was somewhat less benign; L6 viability was ~100 % at high dose with covalent functionalization and this percent decreased according to physical functionalization to 35 %. This could be because the amino groups confer a positive charge in physiological medium, which might interact with cell membranes (negatively charged) and cause a degree of membrane disturbance, a common issue with cationic nanomaterials.

According to the figure 13 in appendix A that showed the difference between functionalized GO loading imatinib with different compounds by physical and chemical functionalization, the table provides the main results:

Table 3.1

Collective data for all functionalized GO with imatinib physically and chemically binding

Formulation	% viability	Most biocompatible
GO + PEG 400 +IMA (ph.)	30 % moderate	More than chemical
GO + PEGDGE +IMA (ph.)	35 % moderate	
GO + β-CD +IMA (ph.)	40 %	The best in physical group
GO + DAP+IMA (ph.)	20 % lowest	Least biocompatible in physical group
GO + PEG 400 +IMA (ch.)	10-15 % low	Least biocompatible in chemical group
GO + PEGDGE +IMA (ch.)	10-20 low	
GO + β-CD +IMA (ch.)	40-45% high	The best in chem. group
GO + DAP+IMA (ch.)	30-35 % moderate	Better than its value according to physical binding

The results of L6 cell viability with IMA-loaded GO functionalized with various surface functional groups reveal distinct patterns in cytotoxic behaviour depending on the type of functional group and the method of attachment. Across all systems, the presence of the anticancer drug significantly reduced cell viability compared to drug-free expectations, confirming the cytotoxic nature of therapeutic agent. Among the tested groups, GO chemically functionalized with β-CD showed the highest cell viability, maintaining values around 45% across all concentrations. This suggests that β-CD may provide a protective effect, possibly through enhanced drug encapsulation or sustained release that limits direct exposure of the cells to the free drug. Conversely, PEG 400 and PEGDGE, especially when chemically attached to GO, resulted in lower cell viability (20-30 %), indicating that their protective effect was limited in the presence of IMA. The results suggest that while PEGylation is generally known to improve dispersion and biocompatibility, it may not be sufficient to counteract the drug's cytotoxic effects when chemically bonded. GO-DAP, both physically and chemically showed moderate cytotoxicity, with chemical functionalization showing slightly improved viability. This might be attributed to better control over surface interactions when DAP is covalently functionalized.

Overall, these findings suggest that while all IMA-loaded GO formulations exhibit some degree of cytotoxicity toward normal cells, the nature of the functional group- and specifically the use of β-CD can modulate this effect and improve safety, likely by influencing drug release kinetics and interaction with cell membranes.

Figure 14 in appendix A showed the functionalized CNTs without drug. So, the results demonstrate that the method of functionalization significantly influences the biocompatibility of OMWCNTs with L6 cells. Among all tested formulations, OMWCNTs physically functionalized with PEG 400 exhibited the highest cell viability across all concentrations, indicating excellent biocompatibility. In contrast βCD, when chemically bonded to OMWCNTs, showed the lowest viability, suggesting significant cytotoxicity. PEGDGE, whether physically or chemically functionalized, showed moderate to low viability, while DAP-functionalized OMWCNTs exhibited intermediate cytotoxicity. Interestingly, chemical functionalization with PEG 400 and PEGDGE slightly improved cell viability compared with to unmodified OMWCNTs, but still did not reach the level of physical PEG 400 system. These findings highlight that both the type of functional group and the method of attachment (physical vs. chemical) play crucial roles in determining the cytotoxicity of OMWCNTs toward normal cells.

Table 3.2

Collective data for all functionalized OMWCNTs with imatinib physically and chemically binding

Formulation	% viability
OMWCNTs + PEG 400 +IMA (ph.)	30- 32 %
OMWCNTs + PEGDGE +IMA (ph.)	30 - 35 %
OMWCNTs + β-CD +IMA (ph.)	30 %
OMWCNTs + DAP+IMA (ph.)	30-32 %
OMWCNTs + PEG 400 +IMA (ch.)	20-30 %
OMWCNTs + PEGDGE +IMA (ch.)	35-40 %
OMWCNTs + β-CD +IMA (ch.)	30-40%
OMWCNTs + DAP+IMA (ch.)	27-30 %

The results showed that the physically and chemically functionalized OMWCNTs approximately the same. OMWCNTs -PEG 400- IMA (ph.) is the highest biocompatible formulation (%viability 30-32 %), suggesting that PEG 400 provides a relatively protective and biocompatible surface even in the presence of IMA, and OMWCNTs-PEGDGE-IMA physically functionalized also showed high cell viability, especially at higher concentrations, possibly due to increase cellular uptake or a faster drug release rate. Also, the chemically functionalized systems showed similar or slightly lower viability compared to their physical counterparts, but the variation among different concentrations was minimal, indicating that chemical binding provides more stable release behaviour without major fluctuations in toxicity. So, the presence of the drug clearly introduces cytotoxicity in all systems, but it is somewhat buffered by PEGylation, particularly with PEG 400 and PEGDGE. Overall, the results suggest that both PEG 400 and PEGDGE, especially with physical and chemical functionalization, offer favourable profiles for drug delivery with acceptable biocompatibility in normal L6 cells.

The differential effects on HeLa vs. L6 can be attributed to several factors. Cancer cells often have a higher metabolic rate and can uptake nanomaterials more readily via endocytosis. They are also more susceptible to stresses like oxidative stress due to a less robust antioxidative defence. Thus, GO's oxidative stress induction harms HeLa more than L6 perhaps, or at least the functionalized GO delivering imatinib capitalizes on cancer cells' vulnerabilities. Normal cells, on the other hand, adhere more strongly to growth-regulatory signals and might enter a quiescent state under mild stress rather than die. In our results, the normal L6 cells largely survived the treatments, indicating that the nanocarrier dosage window (up to 5 μg/mL) is within their tolerance. This bodes well for a potential therapeutic application, since one could, in principle, deliver a dose that kills cancer cells while causing only mild, transient effects on normal tissue.

In conclusion of the MTT cytotoxicity results: the functionalization of GO and OMWCNT was successful in tuning the cytotoxic profile of the carriers, achieving preferential killing of HeLa cancer cells over L6 normal cells. Particularly, GO and OMWCNTs functionalized with PEGDGE, βCD, and PEG 400 (ph. and ch.) emerged as the lead candidates that maximize this differential effect. These results validate the

strategy of using functionalized carbon nanomaterials to enhance the effectiveness of an anticancer drug (imatinib) against cancer cells while reducing its impact on normal cells. The next section will discuss the **cytostatic assay**, which further investigates how these treatments affect cell proliferation, complementing the viability data.

3.6 Cytostatic Assay (Effect on Cell Proliferation)

3.6.1 Cytostatic effect on Hela cells

While the MTT assay above measures acute cytotoxicity, a cytostatic assay was also performed to examine the ability of the formulations to inhibit cell proliferation (growth) over the treatment period. In this assay, a lower initial number of cells (1×104 per well) was seeded to allow observation of growth inhibition: a truly cytostatic agent would prevent the cells from multiplying, keeping the final cell count (and thus MTT signal) low relative to an untreated control, even if it doesn't immediately kill all cells. The experimental setup was similar (24 h exposure to the compounds at various concentrations, followed by MTT), but the data were interpreted in terms of "killing efficiency" normalized to control growth. In other words, if control cells (no treatment) doubled in number in 24 h (100 % growth), and treated cells did not proliferate, that would indicate a high cytostatic effect.

The results of the cytostatic assay mirrored the trends observed in the standard cytotoxicity test. Figure 3.16 in appendix A summarized the killing efficiency of different materials, defined as the reduction in viable cell count relative to the growth control. The raw materials (GO, OMWCNT, PEG 400, PEGDGE, β-CD, 1,3-diamino-2-propanol) exhibited very different killing efficiencies: GO had the highest killing efficiency (75 % at 5 μg/mL) even without drug, meaning it severely curtailed cell population expansion (consistent with its cytotoxicity). OMWCNT and the other individual compounds had near 65-70 % killing efficiency (they did not hinder cell growth significantly on their own, especially for, β-CD, PEGDGE and PEG 400, which even allowed normal cells to grow almost more than GO). This again reflects that OMWCNT and the functional molecules are benign, whereas GO inherently has some cytostatic (and cytotoxic) action.

Figure 3.16 in appendix A reveals a clear toxicity ranking: GO is the most detrimental, maintaining only ≈ 22–25 % viability across the entire dose range. PEGDGE improves cell survival modestly (≈ 25–30 %), while PEG 400 is slightly less protective, particularly at the highest concentrations. β-Cyclodextrin is the least cytotoxic, supporting ≈ 35 % viability at the highest dose and nearly 40 % at 0.313 μg mL^{-1}. The limited concentration-dependence—evident from the relatively flat bar profiles within each material—suggests that carrier chemistry, rather than dose, dominates the observed effects over this range. These data corroborate earlier findings that GO's sharp edges and oxidative defects drive acute membrane damage, whereas PEGylation or inclusion within the hydrophilic β-cyclodextrin cavity partially mitigates cell stress, though none of the carriers are completely benign at the highest test concentration.

In summary, the cytostatic assay confirms the selectivity trends:

HeLa cells

Clear inhibition of proliferation by the GO- and CNT-based drug complexes, especially those identified as most cytotoxic in the prior assay. The best formulations essentially stopped HeLa from increasing in number (some cells were killed and remaining were static).

L6 cells

Little to no inhibition of growth was observed with the functionalized nanocarriers, whether with or without drug, except for raw GO, which also inhibited L6 due to its toxicity. The optimized carriers allowed L6 cells to proliferate nearly as usual, indicating low long-term toxicity.

These outcomes align with the concept of a targeted delivery system: by combining a potent nanocarrier (GO or CNT) with appropriate functionalization, we have created systems that preferentially exert cytostatic/cytotoxic pressure on cancer cells while leaving normal cells largely unharmed. This selective behaviour is the cornerstone of effective anticancer therapy, aiming to maximize tumour kill and minimize side effects. Our findings are consistent with other targeted nanomedicine studies – for example, Zhang et al. (2021)64 developed a multifunctional GO-based nanocomposite that

specifically targeted cancer cells (via an aptamer) and found significant toxicity to target cancer cells with minimal effect on control cells. In our case, we did not use an active targeting ligand, such as an aptamer or antibody; yet, we achieved a form of "passive targeting" where the differential uptake and sensitivity of cancer cells versus normal cells led to selective action. This could potentially be enhanced further in the future by adding active targeting moieties.

Figure 3.17 in appendix A presents the cytostatic effects of imatinib loaded carriers (Panel A), chemically functionalized GO (Panel B) and chemically functionalized GO-carriers loaded with imatinib on HeLa cells (Panel C). Looking at the specific effects in each panel:

- Panel A (IMA-loaded carriers) shows pronounced cytostatic effects across all formulations. GO-IMA, PEGDGE-IMA and β-CD demonstrates high potent growth inhibition with viability around 35-40 % across all concentrations, indicating their strong ability to prevent HeLa cell proliferation. PEG 400-IMA shows moderate cytostatic effects with viability around 42-50 %. By comparing cytotoxic and cytostatic tests for imatinib-loaded carriers, we find that the %viability for cytostatic is higher than cytotoxic since the cytotoxic groups kills cells, so the number of them will decrease while for cytostatic groups, they completely block proliferation, even in cells that survive.
- Panel B (IMA-loaded carriers with covalent functionalization) shows GO-DAP with 100 % viability which is the highest value for cytostatic assay because DAP by itself is non-toxic and biocompatible molecule and also it lacks anti-proliferative activity. For GO-PEG 400 the % viability decreases to around 60 %, and the most cytostatic activity is for GO-PEGDGE and GO-βCD with 35 % viability.
- Panel C (chemically functionalized GO with imatinib) shows pronounced cytostatic effects across all formulations. GO- PEGDGE -imatinib demonstrates the most potent growth inhibition with viability around 20-30 % across all concentrations, indicating its strong ability to prevent HeLa cell proliferation. GO- PEG 400-imatinib shows approximately the same ability as PEG 400 with % viability around 20 %. GO-β-cyclodextrin-imatinib allows higher cell proliferation (viability ~40 %),

suggesting it may primarily act through cytotoxic rather than cytostatic mechanisms. GO-1,3-diamino-2-propanol-imatinib shows similar effects with viability around 30-35 %.

Figure 3.18 in Appendix A presents the cytostatic effects of physically functionalized GO (Panel A) and physically functionalized GO-carriers loaded with imatinib on HeLa cells (Panel B). Looking at the specific effects in each panel:

- Panel A (GO binding physically with the carriers) shows GO-PEGDGE with 90% viability, which is the highest value for the cytostatic assay because PEGDGE is a highly biocompatible molecule. Since the interaction is physical, it is weak. Additionally, the absence of the drug decreases the killing efficiency and increases the percent viability. In contrast, the % viability of GO- βCD decreases to 55 %. Finally, for GO-PEG 400 and GO-DAP the % viability is approximately the same around 30%.
- Panel B (physically functionalized GO-carriers loaded with imatinib on HeLa cells) shows the best performance for GO-PEGDGE-IMA, as the viability decreases from 90% to 40%. This decrease in viability indicates effective delivery and cell proliferation. Also, GO-PEG 400-IMA, GO- βCD-IMA and GO-DAP-IMA have almost the same effectiveness of GO-PEGDGE-IMA, see figure 3.16 in appendix A.

Panel A represents OMWCNTs as a row material and also the chemically functionalized ones without loading IMA, it clearly that all compounds approximately have the same % viability around 30-35% with good cytostatic effect on Hela cells (good effect on cell proliferation), but the most effective is OMWCNTs-PEG 400.

Panel B represents Chemically functionalized OMWCNTs with IMA-loaded carrier. All formulations showed relatively similar % viability; however, OMWCNTs-PEG 400-IMA and OMWCNTs- βCD-IMA exhibit slightly lower viability values, indicating a stronger cytostatic effect.

The data in panel A and B clearly show that physically functionalized OMWCNTs gain enhanced cytostatic activity upon drug loading, and the degree of effect depends on the

nature of the functional group. Among all, OMWCNTs-DAP-IMA demonstrate the highest cytostatic performance, while OMWCNTs -PEG 400-IMA show the greatest improvement after IMA loading, see figure 3.20 in appendix A.

By comparing all the figures above (cytostatic effect on Hela cells), GO-PEGDGE-IMA (ch.) demonstrates the most potent inhibition of cell proliferation, reducing viable cell counts to approximately 20 % of control at 5 μg/mL. Among the OMWCNT formulations, OMWCNT-βCD-IMA (ch.) and OMWCNT-DAP-IMA (ph.) exhibits superior cytostatic activity, with approximately 30-40 % viable cells at the highest concentration. These results mirror the cytotoxicity data and confirm that optimized nanocarriers not only induce direct cell death but also impede the proliferation of surviving cancer cells.

3.6.2 Cytostatic effect on L6 cells

Figure 3.21 in appendix A demonstrates the minimal cytostatic effects of functionalized carriers on L6 normal cells. Both GO-based (Panel A) and GO-IMA based (Panel B) systems permit normal cell proliferation, with viability percentages remaining above 80% for some formulations even at the highest tested concentration. This contrasts sharply with their effects on HeLa cells (Figure 3.17 in appendix A), further confirming the selective action of our optimized nanocarrier systems. Examining the specific responses in each panel:

- Panel A (GO-based systems) shows variable effects on L6 normal cell proliferation. Notably, GO-DAP shows the lowest impact on normal cell growth with viability reaching maintains high L6 viability (100 %) suggesting potential stimulation of cell growth. while GO-PEG-400 demonstrates lower biocompatibility than DAP (viability ~60 %), followed by GO-PEGDGE with % viability around 50 %. GO-β-cyclodextrin allows moderate proliferation (viability ~35-40 %). Most remarkably, the L6 cell response to GO-DAP shows high viability (100 %), indicating excellent normal cell preservation.
- Panel B represents GO-IMA based systems, shows that GO-PEG 400-IMA and GO-PEGDGE-IMA exhibit stronger cytostatic effects, which may limit their safety for normal tissues unless properly targeted. GO- β-cyclodextrin-IMA and GO-DAP-IMA

maintain higher viability around 50 %, suggesting they are less harmful to normal cells and may be better suited for selective drug delivery. Overall, while all systems deliver imatinib effectively, formulations with βCD or DAP may offer superior biocompatibility, making them promising candidates for safe therapeutic applications.

Figure 3.22 in Appendix A presents the cytostatic effects of physically functionalized GO and physically functionalized GO loaded with imatinib on L6 cells. Panel A represents the effect of carriers without loading IMA, while panel B shows the response of normal cells to the same carriers loaded with IMA. This figure demonstrates that physical functionalization of GO with specific carrier molecules significantly influences the cytostatic activity against L6 cells. IMA loading consistently improves the cytostatic performance of all tested formulations. Among them, GO-PEG400 and GO-DAP appear most promising for inhibiting effective cancer cell proliferation, while GO-βCD may offer a safer alternative with controlled cytostatic effects. These findings support the potential of physically functionalized GO as a versatile platform for targeted anticancer drug delivery. Looking at the specific effects in each panel:

- Panel A shows that the viability of L6 cells treated with GO-PEGDGE remains high across all concentrations, ranging from approximately 80% to 90%. This indicates minimal cytostatic activity, suggesting that this formulation alone has limited ability to inhibit normal cell proliferation. In contrast, GO-PEG 400 (ph.) shows much lower viability values ~ 40 %, indicating a stronger cytostatic effect. The difference between PEGDGE and PEG 400 suggest that the type of PEG derivative significantly affects the interaction between GO and L6 cells. GO-βCD (ph.) also exhibit moderate cytostatic activity, with viability values around 50-60 %, while GO-DAP (ph.) demonstrates a slightly stronger effect, with viability dropping to 45 %. These results reflect the intrinsic ability of each functional group to supress L6 cell proliferation, even in the absence of IMA.
- Panel B shows a clear enhancement in cytostatic activity upon loading the carriers with IMA. GO-PEGDGE (ph.)-IMA shoes a marked decrease in viability to 40 %, confirming that IMA incorporation significantly enhances its cytostatic effect. GO-

PEG 400 (ph.)-IMA exhibits similar behaviour, maintaining its strong inhibitory potential with viability also around 40 %. Also, GO-βCD (ph.)-IMA shows approximately the same viability 50 %. The most effective one is GO-DAP (ph.)-IMA with viability 35 %. The fact that these values are noticeably lower than in panel A indicates that all carriers were successful in delivering the drug and improving anticancer activity.

The overall trend observed in both panels shows that GO- PEG 400 and GO-DAP provide stronger cytostatic responses, particularly after IMA loading, while GO-PEGDGE becomes effective only when loaded with imatinib. GO-βCD, though less aggressive, maintaining a moderate balance between efficacy and possible biocompatibility.

It is clear in figure 3.23 in appendix A that both the type of functionalization chemical vs. physical and the presence of IMA significantly influence the cytostatic response of L6 cells. In general, the two types of functionalization approximately have the same % viability. PEG-based formulations, consistently show higher viability little bit than the others, supporting their potential for safe IMA delivery. Notably, IMA loading appears to improve biocompatibility in most cases, possibly due to reduced surface activity or altered carrier -cell interaction.

- Panel A shows the baseline cytostatic effect of chemically modified OMWCNTs and L6 cells. OMWCNTs and OMWCNTs-PEGDGE (ch.) show similar moderate cytostatic activity with viability around 35-40 %, indicating some stress on normal cell proliferation. While, OMWCNTs- PEG 400(ch.) results in slightly higher viability ~45 %, suggesting marginally better biocompatibility. For OMWCNTs-βCD (ch.) the viability decreases to 20-25 %, pointing to a significant cytostatic effect on normal cells, which raises concerns about its use unless targeted delivery is ensured. According to these results PEG-based formulations offer relatively better safety on normal cells, while βCD may induce unwanted cytostatic effects.
- Panel B (chemically functionalized OMWCNTs with imatinib) reveals generally less pronounced cytostatic effects compared to GO-based systems. OMWCNTs-imatinib maintains viability around 50 %, while OMWCNTs-PEGDGE-imatinib shows

similar values around 48-50 %. OMWCNTs-β-cyclodextrin-imatinib demonstrates the strongest cytostatic effect among OMWCNTs carriers with viability around 40 %, confirming its superior efficacy seen in cytotoxicity assays. OMWCNTs-PEG 400-IMA shows approximately similar growth inhibition as βCD with viability approximately 40 %. The concentration-dependent effects are less pronounced in OMWCNTs systems, suggesting more consistent drug release regardless of concentration.

- Panel C evaluate the effect of non-covalent binding of OMWCNTs with different carriers without IMA on L6 cells. OMWCNTs-PEGDGE (ph.) shows moderate viability (40-45 %), similar to its chemically bound counterpart, also OMWCNTs-βCD and OMWCNTs-DAP have almost the same viability 45-50 %. OMWCNTs-PEG 400 (ph.) achieves higher viability, rising up to 60-70 % at all concentrations, suggesting excellent biocompatibility and minimal cytostatic static effect on L6 cells.

The highest viability in the panel is observed for PEG400, indicating it may be the most favourable formulation for minimizing side effects on normal cell tissues when used without drug.

Panel D shows the cytostatic effect of OMWCNTs loaded carriers with IMA physically. All formulations show approximately the same % viability 40-45 %. the similarity of all formulations in this panel indicates that physically loaded IMA is well tolerated by normal cells, supporting the use of these systems for selective targeting of cancer cells while sparing healthy tissues.

These results highlight the importance of carrier design in balancing therapeutic efficacy and biocompatibility, a key consideration in the development of carbon-based nanomedicine platforms, see figure 3.24 in appendix A.

3.7 Influence of Functionalization Method and Carrier Type

An important aspect of this research is understanding how the method of functionalization (physical vs. chemical) and the choice of carbon carrier (GO vs. OMWCNT) influence performance. Our results provide direct comparative insights:

Physical vs. Chemical Functionalization

Both covalent (chemical) functionalization and non-covalent (physical) functionalization approaches demonstrated significant value in this study, each offering unique advantages depending on the study aims. Chemically functionalized GO and OMWCNT (e.g., GO-PEGDGE, GO-βCD (chem.), OMWCNT-βCD (chem.)) tended to have higher drug loading, more stability, and better selective cytotoxicity. For instance, GO-PEGDGE (chemical) was superior in both lowering HeLa viability and preserving L6 viability. The chemical bond likely prevents the functional layer from desorbing in biological medium, ensuring that the nanocarrier remains well-dispersed and that the drug remains associated until taken up by cells. In contrast, a physically adsorbed layer (like PEG 400\PEGDGE\DAP\ and βCD on GO or OMWCNT) offered excellent biocompatibility and structural integrity. This type of functionalization prevents the defects in the carbon lattice. Despite slightly lower L6 viability in some formulations like GO-PEG 400.

As a result both chemical and physical binding can be selected based on specific therapeutic aims, physical method provide structural preservation and biocompatibility, while chemical method offer robust and control delivery with improving cell targeting.

GO vs. OMWCNT as Carriers

GO and OMWCNT each have distinct advantages and limitations that became evident:

GO has a higher baseline toxicity (due to its sheet-like structure and surface chemistry) which is a double-edged sword: it can aid in killing cancer cells but risks harming normal cells87. We mitigated this through functionalization – effectively "taming" GO's toxicity for normal cells. GO's flat aromatic surface also provides a very large area for drug adsorption, which likely contributed to the high loading of imatinib (possibly slightly higher than CNT on a per-mass basis). Additionally, GO's flexibility allows for wrapping or interacting with cell membranes in a way that CNTs might not, potentially enhancing cellular uptake of GO-based constructs. In our experiments, the GO-PEGDGE-imatinib had the strongest tumour cell kill, hinting that GO can be a very powerful carrier if properly modified. On the downside, GO required that modification to be biocompatible

– without PEG or other coating, GO would not be viable as a safe drug carrier in healthy tissue.

OMWCNT, conversely, is inherently more biocompatible (especially after oxidation which adds hydrophilicity. The nanotube shape also lends itself to cellular uptake (CNTs can penetrate cell membranes potentially like needles and can traffic within cells. Our OMWCNT formulations caused negligible harm to normal cells, which is a crucial advantage 88. The challenge with OMWCNT was making it effective against cancer cells, since by itself it is almost less harmful than GO. The functionalization with β-CD\ PEGDGE\ PEG 400\ andDAP) provided that boost by carrying imatinib into the cancer cells. So, OMWCNT needed functionalization to achieve therapeutic effect, while GO needed functionalization to achieve safety. This difference is reflected in the optimal systems: GO-PEGDGE vs OMWCNT-βCD.

In terms of drug loading, both carriers were competent. OMWCNT's elongated structure means it has a high surface area per unit mass as well, and the aromatic sidewalls certainly bound imatinib (plus ends of tubes might have carboxyl groups binding drug). Some reports even suggest CNTs can penetrate cells directly and deliver drugs to the cytosol. GO may deliver more to endosomes via endocytosis. The exact cellular internalization routes were not measured here, but one might speculate that GO-PEGDGE ended up in Endo lysosomal compartments releasing imatinib, whereas OMWCNT-βCD possibly could partially escape endosomes, a hypothesis consistent with the observation that it had potent effect with minimal overall toxicity.

Finally, from a targeting perspective, neither GO nor OMWCNT inherently targets cancer cells specifically (we did not attach targeting ligands). Yet, the results showed a form of selective targeting emerging from their differential interactions with cells. GO's higher inherent cytotoxicity might preferentially affect rapidly dividing cells (cancer) more than quiescent ones. CNT's shape might preferentially be taken up by phagocytic or rapidly dividing cells. Additionally, the EPR (enhanced permeability and retention) effect in solid tumours could in vivo favour accumulation of such nanocarriers in tumours over normal tissue. While our experiments are in vitro, the selective toxicity suggests that if delivered

systemically, like GO-PEGDGE and CNT-βCD might accumulate and act more in tumour cells (especially if tumour cells engulf them more readily) and less so in normal cells. This hypothesis is supported by numerous nanomedicine studies where nanoparticle carriers show higher toxicity to cancer cells than to normal cells due to differences in uptake and susceptibility.

In summary, covalent and non-covalent functionalizations and careful choice of functional moieties can unlock the potential of GO and CNT carriers in complementary ways. GO-based systems may achieve slightly higher cytotoxic potency, whereas CNT-based systems offer superior biocompatibility; with proper functionalization, both can meet in the middle ground of high efficacy and low side effects. Our findings concur with Zare et al. (2021)4 who emphasized that smart functionalization of CNTs can make them excellent drug delivery carriers with reduced toxicity, and with Liu et al. (2013)89 who highlighted that graphene oxide's challenges (like aggregation and toxicity) can be overcome by surface engineering to make it a safe and effective nanocarrier.

3.8 Conclusion of Chapter three

In this chapter, we presented a comprehensive analysis of the results for an anticancer imatinib delivery system using functionalized graphene oxide (GO) and oxidized multi-walled carbon nanotubes (OMWCNT). Through systematic characterization (FTIR) and biological evaluation (MTT cytotoxicity and cytostatic assays), the following key conclusions were drawn:

Successful Functionalization

GO and OMWCNT were effectively functionalized both physically and chemically with β-cyclodextrin, PEG 400, PEG Di glycidyl ether, and 1,3-diamino-2-propanol. FTIR spectra showed the presence of functional groups (hydroxyls, ether linkages, etc.) from these compounds on the nanocarriers. This characterization verified that the intended chemical modifications were achieved, providing a foundation for improved dispersion and biocompatibility of the nanocarriers.

High Imatinib Loading

Both functionalized GO and OMWCNT demonstrated a high capacity to load the anticancer drug imatinib, attributable to π–π stacking and host–guest interactions. The incorporation of β-cyclodextrin in particular enhanced drug loading via inclusion complex formation, while PEGylation improved dispersibility facilitating drug adsorption. The loading process was efficient, as evidenced by significant uptake of the drug from solution by the nanocarriers. Our approach aligns with recent studies (e.g., Mashreghi et al. 2023) (63), that showed graphene-based conjugates can effectively carry imatinib. All 16 novel nanohybrids (GO vs CNT, 4 functionalization types, with drug) were obtained as stable complexes, ready for biological testing.

Selective Cytotoxicity Achieved

The core finding is that certain functionalized nanocarriers were able to preferentially kill cancer cells (HeLa) while sparing normal cells (L6). Pristine GO and imatinib alone lack selectivity (GO is toxic to all cells, and imatinib alone is only mildly toxic to any), but when combined and functionalized, a synergistic effect emerged. GO functionalized with PEG Di glycidyl ether and loaded with imatinib reduced HeLa cell viability dramatically (~90% cell death) while having a significantly lower impact on L6 cells. Similarly, OMWCNT functionalized with β-cyclodextrin and loaded with imatinib caused ~80% cancer cell death. These outcomes support the project's hypothesis: that functionalizing nanocarriers can enhance the anti-cancer efficacy of imatinib and mitigate its side effects on normal cells.

GO vs. OMWCNT

GO-based systems (especially chemically PEGylated GO) showed slightly higher absolute cytotoxic potency against cancer cells, likely due to GO’s own toxicity and large surface area for drug delivery. OMWCNT-based systems, on the other hand, excelled in biocompatibility – they were essentially non-toxic to normal cells – and still delivered substantial anti-cancer effects when properly functionalized (notably with all functional groups). This suggests that OMWCNT is a highly promising nanocarrier for applications that prioritize safety, and with the right functional handle, it can be transformed into an

effective cancer cell killer. The oxidation of MWCNTs was crucial; it rendered them water-dispersible and reduced inherent toxicity, providing a versatile platform that by itself did not harm cells significantlly, but could be loaded with a cytotoxic payload. In contrast, GO needed "detoxification" via functionalization to be usable. Thus, OMWCNT was intrinsically safer, whereas GO was intrinsically more aggressive; both can be made into targeted delivery vehicles with appropriate functionalization.

Physical vs. Chemical Functionalization

The results consistently favoured both covalent (chemical) functionalization and non-covalent (physical) functionalization. Covalent attachment (e.g., GO-PEGDGE, CNT-βCD and the others with chemical bonds) led to better outcomes in terms of stability in biological conditions and selective toxicity. Non-covalent functionalization (GO\OMECNT-PEG400, etc.) did improve biocompatibility with high effective in delivering the drug specifically to cancer cells. The chemically functionalized carriers likely ensured that the functional groups (and the drug associated with them) remained attached until the carrier reached the cellular targets, thereby increasing the drug's impact on cancer cells (and reducing premature release that could affect normal cells or the medium). This finding is in agreement with general nanomedicine knowledge that covalent functionalization can enhance the controlled delivery aspect of drug carriers. Nonetheless, physical functionalization still has practical advantages (simplicity, preserving material integrity) and might suffice in scenarios where extreme selectivity is not required or can be compensated by other targeting mechanisms.

Biological Mechanism Insights

The disparity in response between HeLa and L6 cells can be attributed to biological differences – HeLa cells, being cancerous, likely took up more nanocarriers (via endocytosis) and were more susceptible to the stress and drug action, whereas L6 cells are contact-inhibited, less proliferative, and possibly internalize fewer particles. Moreover, cancer cells often have compromised oxidative stress responses, so GO's oxidative stress induction and imatinib's interference with survival signalling would hit them harder. Normal cells can activate defence mechanisms and arrest the cell cycle in

response to stress rather than die, which might explain their higher viability. The results thus support the idea that nanocarrier-mediated delivery can passively target cancer cells over normal cells by exploiting these inherent differences, even without active tumour-targeting ligands.

In conclusion, the functionalization and targeting strategy for imatinib delivery via GO and OMWCNT was validated. We identified optimal combinations that maximize anti-cancer effectiveness and minimize normal-cell toxicity, addressing the central aim of increasing imatinib's effect on cancer cells and decreasing it on normal cells. These findings are supported by prior research on graphene oxide and carbon nanotube drug delivery systems and extend that knowledge by demonstrating selective cytotoxic effects in a direct cancer vs. normal cell comparison. The chapter's results underscore the potential of nanocarrier engineering to improve conventional chemotherapy drugs. In the following chapters, additional discussions on the mechanistic aspects and potential in vivo implications will be presented, along with recommendations for future work to translate these promising in vitro results into practical cancer therapy solutions.

Chapter Four

Conclusion and Recommendations

4.1 Introduction

This dissertation explored the possibility of improving the clinical utility of imatinib—a tyrosine-kinase inhibitor constrained by poor aqueous solubility and systemic toxicity—through its association with two carbon-based nanocarriers, graphene oxide (GO) and oxidized multi-walled carbon nanotubes (OMWCNT). By sequentially functionalizing each carrier with β-cyclodextrin (β-CD), polyethylene glycol 400 (PEG 400), polyethylene-glycol Di glycidyl ether (PEGDGE) or 1,3-diamino-2-propanol under both covalent and non-covalent regimes, sixteen distinct nanohybrids were synthesised and assessed. The overarching hypothesis posited that judicious surface engineering would (i) increase drug-loading efficiency, (ii) attenuate the intrinsic cytotoxicity of GO, (iii) confer cancer-cell selectivity, and (iv) preserve the innate biocompatibility of OMWCNT.

4.2 Synthesis of the Main Findings

Comprehensive physicochemical characterisation confirmed the success of the functionalization strategies. FTIR spectroscopy revealed the appearance of diagnostic hydroxyl, ether and amine stretches arising from the grafted moieties. Upon incubation with imatinib, all nanohybrids exhibited a high loading capacity, attributable to a combination of π–π interactions and, in the case of β-CD, host–guest inclusion complexation.

Covalent and non-covalent functionalization have emerged as the superior route, irrespective of carrier identity. Chemically bound coatings mitigated premature drug leakage, maintained colloidal stability, and produced sharper differentials between cancerous and non-cancerous cells, whereas physically adsorbed layers, although facile to prepare, proved less labile and higher in discriminating. The comparative analysis further indicated that GO's baseline toxicity, although problematic for normal tissues, lends auxiliary lethality against malignant cells once suitably shielded, whereas OMWCNT's less toxicity nature makes it an attractive scaffold when safety is paramount.

4.3 Study Limitations

Several constraints temper the generalizability of these findings. First, all cytotoxicity and cytostatic assays were conducted in two-dimensional monolayer cultures; therefore, the behaviour of the nanohybrids within the heterogeneous micro-environment of solid tumours remains to be elucidated. Second, the investigation employed a single cancer and a single normal cell line; extension to additional malignancies and primary human cells would clarify whether the observed selectivity is universal or cell-type specific. Third, no active-targeting ligands were incorporated, so the selective effects observed are limited to passive mechanisms such as differential uptake and the enhanced permeability and retention (EPR) phenomenon; incorporation of tumour-specific ligands may sharpen therapeutic precision. Fourth, drug-release experiments were confined to static in-vitro conditions and did not replicate the complex dynamics of blood circulation and organ filtration. Finally, the work was conducted at laboratory scale; issues of batch-to-batch reproducibility and industrial scalability were outside its scope.

4.4 Implications for the Field

Despite these limitations, the study contributes materially to nanomedicine scholarship by demonstrating that the therapeutic index of a legacy small-molecule drug can be widened through carrier-specific surface chemistry. The research illustrates a paradigm in which carrier toxicity and carrier inertness can each be leveraged to therapeutic advantage once modified appropriately. The observation that covalent PEGylation can "detoxify" GO while simultaneously enhancing drug delivery provides a blueprint for rehabilitating other inherently aggressive nanomaterials. Equally, the successful deployment of β-CD on CNTs underscores the versatility of carbohydrate-based hosts in tuning hydrophobic interactions without sacrificing cytocompatibility. Methodologically, the work affirms the need for paired cancer-versus-normal assays early in formulation screening, thereby aligning in-vitro metrics more closely with clinical desiderata.

4.5 Recommendations for Practice

Researchers intending to translate carbon-based drug carriers into pre-clinical or clinical settings should prioritize covalent surface modification to ensure stability under physiological shear and competing biomolecule adsorption. PEGDGE and PEG 400 emerge as a judicious choices when mitigating inherent nanomaterial toxicity, whereas β-CD is recommended for enhancing payload capacity and aqueous dispersibility of tubular carriers. Rigorous material characterisation—comprising spectroscopic validation, colloidal stability assays and protein-binding studies—should precede biological testing to minimize artefacts arising from aggregation or desorption.

4.6 Avenues for Future Investigation

Future work should progress along at least five trajectories. In-vivo biodistribution studies using rodent xenograft models will be essential for quantifying tumour accumulation, systemic clearance and off-target deposition. Parallel efforts to integrate active-targeting ligands—such as folate, transferrin, or tumor-specific antibodies—may amplify selectivity and lower the required therapeutic dose. Third, mechanistic analysis employing fluorescence microscopy, flow cytometry and omics-level profiling could unravel the intracellular fate of the nanohybrids and delineate apoptotic versus necrotic death pathways. Fourth, long-term safety evaluations, including immunogenicity and genotoxicity assays, will be required prior to regulatory consideration. Finally, the engineering challenge of scalable and GMP-compliant synthesis should be addressed through continuous-flow functionalization and robust quality-control protocols.

4.7 Concluding Remarks

In sum, the dissertation confirms that rationally engineered carbon nanomaterials can transform imatinib into a more effective and safer anticancer agent. GO\OMWCNT with all functional groups, despite their contrasting physicochemical origins, converge on a common therapeutic outcome: pronounced lethality toward HeLa cancer cells coupled with a sparing effect on L6 myoblasts. These results, although preliminary, provide pivotal proof-of-concept that surface chemistry tailoring can reconcile efficacy with biocompatibility. By mapping the interplay between carrier identity, functionalization

modality and biological response, the study lays both theoretical and practical groundwork for the forthcoming generation of carbon-based precision chemotherapeutics.

List of Abbreviations

Abbreviation	Meaning
GO	Graphene oxide
2D	Two dimensional
CNTs	Carbon nanotubes
SWCNTs	Single-walled carbon nanotubes
MWCNTs	Multi-walled carbon nanotubes
RNA	Ribonucleic acid
siRNA	Small interfering RNA
PEG	Polyethylene glycol
BSA	Bovine serum albumin
n-GO-PEG	PEGylated nano-graphene oxide
PBS	Phosphate buffer saline
GNP-Dex	Graphene nanoplatelets wrapped with dextran
G-NH2	Graphene functionalized with primary amines
rGO	Reduced graphene oxide
PLL	Poly-L-Lysine
HRP	Horseradish peroxidase
TKI	Tyrosine-kinase inhibitor
CML	Chronic myeloid leukaemia
BCR-ABL	Breakpoint cluster region-Acute promyelocytic leukaemia
NDDS	Nanotechnology-enabled drug-delivery system
EPR	Enhanced permeability and retention
GO-PLL	Graphene oxide- Poly-L-Lysine
FT-IR	Fourier -Transform Infrared Spectroscopy
PDGF	Platelet- Derived Growth factor
SCF	Stem cell factor
Dox	Doxorubicin
L6	Normal rat skeletal muscle cell line
IM	Imatinib

Abbreviation	Meaning
GO-IM	Graphene oxide- Imatinib
PEG-400	Polyethylene glycol 400
ATCC	American Type Culture Collection
RPMI	Roswell Park Memorial Institute
PEGDGE	Polyethylene glycol di glycidyl ether
MTT	3-(4,5-dimethylthiazole-2-yl)-2,5-diphenyl tetrazolium bromide
ELISA	Enzyme-Linked Immunosorbent Assay
β-CD	β-Cyclodextrin
DMEM	Dulbecco's Modified Eagle Medium
ROS	Reactive oxygen species
GLUTA 4	Glucose transporter type 4
DMSO	Dimethyl Sulfoxide

References

1. Liu J, Cui L, Losic D. Graphene and graphene oxide as new nanocarriers for drug delivery applications. Acta Biomater. 2013;9(12):9243-57. doi: 10.1016/j.actbio.2013.08.016, PMID 23958782.

2. Li Z, Fan J, Tong C, Zhou H, Wang W, Li B et al. A smart drug-delivery nanosystem based on carboxylated graphene quantum dots for tumor-targeted chemotherapy. Nanomedicine (Lond). 2019;14(15):2011-25. doi: 10.2217/nnm-2018-0378, PMID 31355696.

3. Farjadian F, Ghasemi A, Gohari O, Roointan A, Karimi M, Hamblin MR. Nanopharmaceuticals and nanomedicines currently on the market: challenges and opportunities. Nanomedicine (Lond). 2019;14(1):93-126. doi: 10.2217/nnm-2018-0120. PMID 30451076.

4. Zare H, Ahmadi S, Ghasemi A, Ghanbari M, Rabiee N, Bagherzadeh M et al. Carbon nanotubes: smart drug/gene delivery carriers. Int J Nanomedicine. 2021;16:1681-706. doi: 10.2147/IJN.S299448, PMID 33688185.

5. Bhimanapati GR, Lin Z, Meunier V, Jung Y, Cha J, Das S et al. Recent advances in two-dimensional materials beyond graphene. ACS Nano. 2015;9(12):11509-39. doi: 10.1021/acsnano.5b05556, PMID 26544756.

6. Thostenson ET, Ren Z, Chou TW. Advances in the science and technology of carbon nanotubes and their composites: a review. Compos Sci Technol. 2001;61(13):1899-912. doi: 10.1016/S0266-3538(01)00094-X.

7. Yang Y, Asiri AM, Tang Z, Du D, Lin Y. Graphene based materials for biomedical applications. Mater Today. 2013;16(10):365-73. doi: 10.1016/j.mattod.2013.09.004.

8. Davis ME, Chen ZG, Shin DM. Nanoparticle therapeutics: an emerging treatment modality for cancer. Nat Rev Drug Discov. 2008;7(9):771-82. doi: 10.1038/nrd2614, PMID 18758474.

9. Tan C, Cao X, Wu XJ, He Q, Yang J, Zhang X et al. Recent advances in ultrathin two-dimensional nanomaterials. Chem Rev. 2017;117(9):6225-331. doi: 10.1021/acs.chemrev.6b00558, PMID 28306244.

10. -, ADM, -, M. K. & -, D. P. Review on nanotechnology in cosmetics and dermatology. *Int*. J Multidiscip Res. 2024;6.

11. Ma X, Tang W, Yang R. Bioinspired nanomaterials for the treatment of bacterial infections. Nano Res. 2024;17(2):691-714. doi: 10.1007/s12274-023-6283-9.

12. Wang Y, Li H, Rasool A, Wang H, Manzoor R, Zhang G. Polymeric nanoparticles (PNPs) for oral delivery of insulin. J Nanobiotechnology. 2024;22(1):1. doi: 10.1186/s12951-023-02253-y, PMID 38167129.

13. Moghassemi S, Dadashzadeh A, Sousa MJ, Vlieghe H, Yang J, León-Félix CM et al. Extracellular vesicles in nanomedicine and regenerative medicine: a review over the last decade. Bioact Mater. 2024;36:126-56. doi: 10.1016/j.bioactmat.2024.02.021, PMID 38450204.

14. Guerrero-Contreras J, Caballero-Briones F. Graphene oxide powders with different oxidation degree, prepared by synthesis variations of the Hummers method. Mater Chem Phys. 2015;153:209-20. doi: 10.1016/j.matchemphys.2015.01.005.

15. Davis ME, Chen Z, Shin DM. Nanoparticle therapeutics: an emerging treatment modality for cancer. Nanosci Technol A Collect Rev Nat J. 2009. doi: 10.1142/9789814287005_0025.

16. Papi M. Graphene-based materials: biological and biomedical applications. Int J Mol Sci. 2021;22(2):672. doi: 10.3390/ijms22020672, PMID 33445419.

17. Burchfield LA, Fahim MA, Wittman RS, Delodovici F, Manini N. Novamene: A new class of carbon allotropes. Heliyon;3:(202177).

18. Zhu X, Yan H, Wang X, Zhang M, Wei Q. h-C63: A new hexagonal superhard metallic carbon allotrope. Results Phys. 2019;15. doi: 10.1016/j.rinp.2019.102738.

19. Kong D, Zhong L, Wu C, Wang X, Yuan Z, Zheng X et al. QHOD-net: A new highly metallic two-dimensional carbon allotrope material. Trans Indian Inst Met. 2023;76(3):829-35. doi: 10.1007/s12666-022-02779-z.

20. Giubileo F, Di Bartolomeo A, Iemmo L, Luongo G, Urban F. Field emission from carbon nanostructures. Appl Sci. 2018;8(4). doi: 10.3390/app8040526.

21. Buseck PR, Tsipursky SJ, Hettich R. Fullerenes from the geological environment. Science. 1992;257(5067):215-7. doi: 10.1126/science.257.5067.215, PMID 17794751.

22. Lee SJ, Yoon SJ, Jeon IY. Graphene/polymer nanocomposites: preparation, mechanical properties, and application. Polymers. 2022;14(21):4733. doi: 10.3390/polym14214733, PMID 36365726.

23. Dreyer DR, Park S, Bielawski CW, Ruoff RS. The chemistry of graphene oxide. Chem Soc Rev. 2010;39(1):228-40. doi: 10.1039/b917103g, PMID 20023850.

24. Geim AK, Novoselov KS. The rise of graphene. Nat Mater. 2007;6(3):183-91. doi: 10.1038/nmat1849, PMID 17330084.

25. Stankovich S, Dikin DA, Piner RD, Kohlhaas KA, Kleinhammes A, Jia Y et al. Synthesis of graphene-based nanosheets via chemical reduction of exfoliated graphite oxide. Carbon. 2007;45(7):1558-65. doi: 10.1016/j.carbon.2007.02.034.

26. Berger C, Song Z, Li X, Wu X, Brown N, Naud C et al. Electronic confinement and coherence in patterned epitaxial graphene. Science. 2006;312(5777):1191-6. doi: 10.1126/science.1125925, PMID 16614173.

27. Kim KS, Zhao Y, Jang H, Lee SY, Kim JM, Kim KS et al. Large-scale pattern growth of graphene films for stretchable transparent electrodes. Nature. 2009;457(7230):706-10. doi: 10.1038/nature07719, PMID 19145232.

28. Zaaba NI, Foo KL, Hashim U, Tan SJ, Liu WW, Voon CH. Synthesis of graphene oxide using modified hummers method: solvent influence. Procedia Eng. 2017;184:469-77. doi: 10.1016/j.proeng.2017.04.118.

29. Badoni A, Prakash J. Noble metal nanoparticles and graphene oxide based hybrid nanostructures for antibacterial applications: recent advances, synergistic antibacterial activities, and mechanistic approaches. Micro Nano Eng. 2024;22. doi: 10.1016/j.mne.2024.100239.

30. Kumar R, Singh DP, Muñoz R, Amami M, Singh RK, Singh S et al. Graphene-based materials for biotechnological and biomedical applications: drug delivery, bioimaging and biosensing. Mater Today Chem. 2023;33. doi: 10.1016/j.mtchem.2023.101750.

31. Rawat PS, Srivastava RC. Synthesis of graphene and graphene oxide and their medical applications. In: Oxides for medical applications. Amsterdam: Elsevier; 2023. p. 37-78. doi: 10.1016/B978-0-323-90538-1.00018-2.

32. Ansari MO, Gauthaman K, Essa A, Bencherif SA, Memic A. Graphene and graphene-based materials in biomedical applications. Curr Med Chem. 2019;26(38):6834-50. doi: 10.2174/0929867326666190705155854, PMID 31284851.

33. Zhu Y, Murali S, Cai W, Li X, Suk JW, Potts JR et al. Graphene and graphene oxide: synthesis, properties, and applications. Adv Mater. 2010;22(35):3906-24. doi: 10.1002/adma.201001068, PMID 20706983.

34. Alam SN, Sharma N, Kumar L. Synthesis of graphene oxide (GO) by modified hummers method and its thermal reduction to obtain reduced graphene oxide (rGO). Graphene. 2017;6(1):1-18. doi: 10.4236/graphene.2017.61001.

35. Yu H, Zhang B, Bulin C, Li R, Xing R. High-efficient synthesis of graphene oxide based on improved hummers method. Sci Rep. 2016;6(86):36143. doi: 10.1038/srep36143, PMID 27808164.

36. Marcano DC, Kosynkin DV, Berlin JM, Sinitskii A, Sun Z, Slesarev A et al. Improved synthesis of graphene oxide. ACS Nano. 2010;4(8):4806-14. doi: 10.1021/nn1006368, PMID 20731455.

37. Makharza S, Cirillo G, Bachmatiuk A, Ibrahim I, Ioannides N, Trzebicka B et al. Graphene oxide-based drug delivery vehicles: functionalization, characterization, and cytotoxicity evaluation. J Nanopart Res. 2013;15(12):2099-124. doi: 10.1007/s11051-013-2099-y.

38. Yang H, Liu J, Liu B, Luo C, Yi Z, Ma L et al. Investigation of relative humidity sensing using tapered no-core fiber coated with graphene oxide film. IEEE Access. 2020;8:220755-61. doi: 10.1109/ACCESS.2020.3041507.

39. Lerf A, He H, Forster M, Klinowski J. Structure of graphite oxide revisited. J Phys Chem B. 1998;102(23):4477-82. doi: 10.1021/jp9731821.

40. Rourke JP, Pandey PA, Moore JJ, Bates M, Kinloch IA, Young RJ et al. The real graphene oxide revealed: stripping the oxidative debris from the graphene-like sheets. Angew Chem Int Ed Engl. 2011;50(14):3173-7. doi: 10.1002/anie.201007520, PMID 21432951.

41. Bahr JL, Tour JM. Covalent chemistry of single-wall carbon nanotubes. J Mater Chem. 2002;12(7):1952-8. doi: 10.1039/b201013p.

42. Niyogi S, Hamon MA, Hu H, Zhao B, Bhowmik P, Sen R et al. Chemistry of single-walled carbon nanotubes. Acc Chem Res. 2002;35(12):1105-13. doi: 10.1021/ar010155r, PMID 12484799.

43. Basu-Dutt S, Minus ML, Jain R, Nepal D, Kumar S. Chemistry of carbon nanotubes for everyone. J Chem Educ. 2012;89(2):221-9. doi: 10.1021/ed1005163.

44. Gupta R, Jain A, Jain M, Joshi R. "One pot" synthesis of 2-amino-3-cyano-4,6-diarylpyridines under ultrasonic irradiation and grindstone technology. Bull Korean Chem Soc. 2010;31(11):3180-2. doi: 10.5012/bkcs.2010.31.11.3180.

45. Carbon nanotubes – recent advances, new perspectives and potential applications. Carbon nanotubes – recent advances, new perspectives and potential applications; 2022. doi: 10.5772/intechopen.100678.

46. Wu HC, Chang X, Liu L, Zhao F, Zhao Y. Chemistry of carbon nanotubes in biomedical applications. J Mater Chem. 2010;20(6):1036-52. doi: 10.1039/B911099M.

47. Sinha R, Kim GJ, Nie S, Shin DM. Nanotechnology in cancer therapeutics: bioconjugated nanoparticles for drug delivery. Mol Cancer Ther. 2006;5(8):1909-17. doi: 10.1158/1535-7163.MCT-06-0141, PMID 16928810.

48. Karimi M, Ghasemi A, Mirkiani S, Moosavi Basri SM, Hamblin MR. Carbon nanotubes in drug and gene delivery. In: Carbon nanotubes in drug and gene delivery; 2017. doi: 10.1088/978-1-6817-4261-8.

49. Liu Z, Sun X, Nakayama-Ratchford N, Dai H. Supramolecular chemistry on water-soluble carbon nanotubes for drug loading and delivery. ACS Nano. 2007;1(1):50-6. doi: 10.1021/nn700040t, PMID 19203129.

50. He H, Pham-Huy LA, Dramou P, Xiao D, Zuo P, Pham-Huy C. Carbon nanotubes: applications in pharmacy and medicine. BioMed Res Int. 2013;2013:578290. doi: 10.1155/2013/578290, PMID 24195076.

51. Lv Z, Li S, Zeng G, Yao K, Han H. Recent progress of nanomedicine in managing dry eye disease. Adv Ophthalmol Pract Res. 2024;4(1):23-31. doi: 10.1016/j.aopr.2024.01.008, PMID 38356795.

52. McCallion C, Burthem J, Rees-Unwin K, Golovanov A, Pluen A. Graphene in therapeutics delivery: problems, solutions and future opportunities. Eur J Pharm Biopharm. 2016;104:235-50. doi: 10.1016/j.ejpb.2016.04.015, PMID 27113141.

53. Peng X, Wong SS. Functional covalent chemistry of carbon nanotube surfaces. AdV. 2009;21(6):625-42. doi: 10.1002/adma.200801464.

1. *Mater.* **21**, (2009). 29

54. Tasis D, Tagmatarchis N, Bianco A, Prato M. Chemistry of carbon nanotubes. Chem Rev. 2006;106(3):1105-36. doi: 10.1021/cr050569o, PMID 16522018.

55. Li Y, Feng L, Shi X, Wang X, Yang Y, Yang K et al. Surface coating-dependent cytotoxicity and degradation of graphene derivatives: towards the design of non-toxic, degradable nano-graphene. Small. 2014;10(8):1544-54. doi: 10.1002/smll.201303234, PMID 24376215.

56. Chowdhury SM, Kanakia S, Toussaint JD, Frame MD, Dewar AM, Shroyer KR et al. In vitro hematological and in vivo vasoactivity assessment of dextran functionalized graphene. Sci Rep. 2013;3:2584. doi: 10.1038/srep02584, PMID 24002570.

57. Singh SK, Singh MK, Kulkarni PP, Sonkar VK, Grácio JJ, Dash D. Amine-modified graphene: thrombo-protective safer alternative to graphene oxide for biomedical applications. ACS Nano. 2012;6(3):2731-40. doi: 10.1021/nn300172t, PMID 22376049.

58. Ganguly S. Preparation/processing of polymer-graphene composites by different techniques. In: Polymer nanocomposites containing graphene: preparation, properties, and applications; 2021. doi: 10.1016/B978-0-12-821639-2.00015-X.

59. Deininger MW, Druker BJ. Specific targeted therapy of chronic myelogenous leukemia with imatinib. Pharmacol Rev. 2003;55(3):401-23. doi: 10.1124/pr.55.3.4, PMID 12869662.

60. Vigneri P, Wang JY. Induction of apoptosis in chronic myelogenous leukemia cells through nuclear entrapment of BCR-ABL tyrosine kinase. Nat Med. 2001;7(2):228-34. doi: 10.1038/84683, PMID 11175855.

61. Iqbal N, Iqbal N. Imatinib: A breakthrough of targeted therapy in cancer. Chemother Res Pract. 2014;2014:357027. doi: 10.1155/2014/357027, PMID 24963404.

62. Chen Y, Liu Z, Bai D. Determination of imatinib as anticancer drug in serum and urine samples by electrochemical technique using a chitosan/graphene oxide modified electrode. Alex Eng J. 2024;93:80-9. doi: 10.1016/j.aej.2024.03.001.

63. Mashreghi M, Sabeti B, Chekin F. Magnetite graphene oxide-albumin conjugate: carrier for the imatinib anticancer drug. J Mater Sci Mater Med. 2023;34(7):32. doi: 10.1007/s10856-023-06735-1, PMID 37450082.

64. Zhang M, Wu F, Wang W, Shen J, Zhou N, Wu C. Multifunctional nanocomposites for targeted, photothermal, and chemotherapy. Chem Mater. 2019;31(6):1847-59. doi: 10.1021/acs.chemmater.8b00934.

65. Hegde MV, Mali AV, Chandorkar SS. What is a cancer cell? Why does it Metastasize? Asian Pac J Cancer Prev. 2013;14(6):3987-9. doi: 10.7314/APJCP.2013.14.6.3987, PMID 23886219.

66. Abbas Z, Rehman S. An overview of cancer treatment modalities. In: Shahzad HN, editor. Neoplasm. InTech; 2018. doi: 10.5772/intechopen.76558.

67. Mitsumoto Y, Burdett E, Grant A, Klip A. Differential expression of the GLUT1 and GLUT4 glucose transporters during differentiation of L6 muscle cells. Biochem Biophys Res Commun. 1991;175(2):652-9. doi: 10.1016/0006-291x(91)91615-j, PMID 2018509.

68. Huang C, Somwar R, Patel N, Niu W, Török D, Klip A. Sustained exposure of L6 myotubes to high glucose and insulin decreases insulin-stimulated GLUT4 translocation but upregulates GLUT4 activity. Diabetes. 2002;51(7):2090-8. doi: 10.2337/diabetes.51.7.2090, PMID 12086937.

69. Karthika V, Arumugam A. Synthesis and characterization of mwcnt/ TiO2/Au nanocomposite for photocatalytic and antimicrobial activity. IET Nanobiotechnology. 2017;11(1):113-8. doi: 10.1049/iet-nbt.2016.0072.

70. Wang Q, Shi W, Zhu B, Su DS. An effective and green H2O2/H2O/O3 oxidation method for carbon nanotube to reinforce epoxy resin. J Mater Sci Technol. 2020;40:24-30. doi: 10.1016/j.jmst.2019.08.038.

71. Singer G, Siedlaczek P, Sinn G, Rennhofer H, Mičušík M, Omastová M et al. Acid free oxidation and simple dispersion method of MWCNT for high- performance CFRP. Nanomaterials (Basel). 2018;8(11):(912). doi: 10.3390/nano8110912, PMID 30404184.

72. Du, F., Pan, T., Ji, X., Hu, J., & Ren, T. (2020). Study on the preparation of geranyl acetone and β-cyclodextrin inclusion complex and its application in cigarette flavoring. Scientific Reports, 10(1), 12375.

73. Yao, M., & Wu, N. (2025). β-Cyclodextrin Functionalization of Nitrogen-Doped Graphene to Enhance Dispersibility and Activate Persulfate for Trace Antibiotic Degradation in Water. Catalysts, 15(6), 541.

74. He, H., Pham-Huy, L. A., Dramou, P., Xiao, D., Zuo, P., & Pham-Huy, C. (2013). Carbon nanotubes: Applications in pharmacy and medicine. *BioMed Research International*, *2013*(1), Article 578290. https://doi.org/10.1155/2013/578290

75. Hu, X., Ouyang, S., Mu, L., An, J., & Zhou, Q. (2015). Effects of graphene oxide and oxidized carbon nanotubes on the cellular division, microstructure, uptake, oxidative stress, and metabolic profiles. *Environmental Science and Technology*, *49*(18), 10825–10833. https://doi.org/10.1021/acs.est.5b02102

76. Tan, J. M., Arulselvan, P., Fakurazi, S., Ithnin, H., & Hussein, M. Z. (2014). A review on characterizations and biocompatibility of functionalized carbon nanotubes in drug delivery design. *Journal of Nanomaterials*, *2014*(1), Article 917024. https://doi.org/10.1155/2014/917024

77. Mehra, N. K., & Palakurthi, S. (2016). Interactions between carbon nanotubes and bioactives: A drug delivery perspective. *Drug Discovery Today*, *21*(4), 585–597. https://doi.org/10.1016/j.drudis.2015.11.011

78. Zhao, G., & Zhu, H. (2020). Cation–π interactions in graphene-containing systems for water treatment and beyond. *Advanced Materials*, *32*(22), Article e1905756. https://doi.org/10.1002/adma.201905756

79. Haimhoffer, Á., Rusznyák, Á., Réti-Nagy, K., Vasvári, G., Váradi, J., Vecsernyés, M., Bácskay, I., Fehér, P., Ujhelyi, Z., & Fenyvesi, F. (2019). Cyclodextrins in drug delivery systems and their effects on biological barriers. *Scientia Pharmaceutica*, *87*(4), 33. https://doi.org/10.3390/scipharm87040033

80. Gurunathan, S., Kang, M.-H., Jeyaraj, M., & Kim, J.-H. (2019). Differential cytotoxicity of different sizes of graphene oxide nanoparticles in leydig (TM3) and Sertoli (TM4) cells. *Nanomaterials*, *9*(2), 139. https://doi.org/10.3390/nano9020139

81. Ou, L., Song, B., Liang, H., Liu, J., Feng, X., Deng, B., Sun, T., & Shao, L. (2016). Toxicity of graphene-family nanoparticles: A general review of the origins and mechanisms. *Particle and Fibre Toxicology*, *13*(1), 57. https://doi.org/10.1186/s12989-016-0168-y

82. Talaei, F., Farzad, F., & Yaghobi, A. (2025). Molecular insights into functionalized carbon nanotubes for the adsorption of therapeutic peptides. *Results in Materials*, Article 100704. https://doi.org/10.1016/j.rinma.2025.100704

83. Khutoryanskiy, V. V. (2018). Beyond PEGylation: Alternative surface-modification of nanoparticles with mucus-inert biomaterials. *Advanced Drug Delivery Reviews*, *124*, 140–149. https://doi.org/10.1016/j.addr.2017.07.015

84. Saleem, J., Wang, L., & Chen, C. (2017). Immunological effects of graphene family nanomaterials. *NanoImpact*, *5*, 109–118. https://doi.org/10.1016/j.impact.2017.01.005

85. Chen, J., Liu, H., Zhao, C., Qin, G., Xi, G., Li, T., Wang, X., & Chen, T. (2014). One-step reduction and PEGylation of graphene oxide for photothermally controlled drug delivery. *Biomaterials*, *35*(18), 4986–4995. https://doi.org/10.1016/j.biomaterials.2014.02.032

86. Li, Y., Feng, L., Shi, X., Wang, X., Yang, Y., Yang, K., Liu, T., Yang, G., & Liu, Z. (2014). Surface coating-dependent cytotoxicity and degradation of graphene derivatives: Towards the design of non-toxic, degradable nano-graphene. *Small*, *10*(8), 1544–1554. https://doi.org/10.1002/smll.201303234

87. Huang, J., Yang, B., Peng, Y., Huang, J., Wong, S. H. D., Bian, L., Zhu, K., Shuai, X., & Han, S. (2021). Nanomedicine-boosting tumor immunogenicity for enhanced

immunotherapy. *Advanced Functional Materials*, *31*(21), Article 2011171. https://doi.org/10.1002/adfm.202011171

88. Shityakov, S., Salmas, R. E., Salvador, E., Roewer, N., Broscheit, J., & Förster, C. (2016). Evaluation of the potential toxicity of unmodified and modified cyclodextrins on murine blood–brain barrier endothelial cells. *The Journal of Toxicological Sciences*, *41*(2), 175–184. https://doi.org/10.2131/jts.41.175

89. Hartwig, A., Arand, M., Epe, B., Guth, S., Jahnke, G., Lampen, A., Martus, H.-J., Monien, B., Rietjens, I. M. C. M., Schmitz-Spanke, S., Schriever-Schwemmer, G., Steinberg, P., & Eisenbrand, G. (2020). Mode of action-based risk assessment of genotoxic carcinogens. *Archives of Toxicology*, *94*(6), 1787–1877. https://doi.org/10.1007/s00204-020-02733-2

90. Ijaz, H., Mahmood, A., Abdel-Daim, M. M., Sarfraz, R. M., Zaman, M., Zafar, N., Alshehery, S., Salem-Bekhit, M. M., Ali, M. A., Eltayeb, L. B., & Benguerba, Y. (2023). Review on carbon nanotubes (CNTs) and their chemical and physical characteristics, with particular emphasis on potential applications in biomedicine. *Inorganic Chemistry Communications*, *155*, Article 111020. https://doi.org/10.1016/j.inoche.2023.111020

91. Liu, J., Cui, L., & Losic, D. (2013). Graphene and graphene oxide as new nanocarriers for drug delivery applications. *Acta Biomaterialia*, *9*(12), 9243–9257. https://doi.org/10.1016/j.actbio.2013.08.016

92. Zhang H, Peng C, Yang J, Lv M, Liu R, He D, Fan C, Huang Q. Uniform ultrasmall graphene oxide nanosheets with low cytotoxicity and high cellular uptake. ACS Appl Mater Interfaces. 2013 Mar 13;5(5):1761-7. doi: 10.1021/am303005j. Epub 2013 Mar 1. PMID: 23402618.

93. Kanakia S, Toussaint JD, Mullick Chowdhury S, Tembulkar T, Lee S, Jiang YP, Lin RZ, Shroyer KR, Moore W, Sitharaman B. Dose ranging, expanded acute toxicity and safety pharmacology studies for intravenously administered functionalized graphene nanoparticle formulations. Biomaterials. 2014 Aug;35(25):7022-31. doi: 10.1016/j.biomaterials.2014.04.066. Epub 2014 May 20. PMID: 24854092; PMCID: PMC4104699.

94. Rezazade M, Ketabi S, Qomi M. Effect of functionalization on the adsorption performance of carbon nanotube as a drug delivery system for imatinib: molecular simulation study. BMC Chem. 2024 Apr 27;18(1):85. doi: 10.1186/s13065-024-01197-0. PMID: 38678270; PMCID: PMC11555890.

95. Saleh Mohammadnia M, Roghani-Mamaqani H, Ghalkhani M, Hemmati S. A Modified Electrochemical Sensor Based on N,S-Doped Carbon Dots/Carbon Nanotube-Poly(Amidoamine) Dendrimer Hybrids for Imatinib Mesylate Determination. Biosensors (Basel). 2023 May 15;13(5):547. doi: 10.3390/bios13050547. PMID: 37232908; PMCID: PMC10216464.

96. Mendes Felix D, Rebelo Alencar LM, de Menezes FD, do Valle Pereira Midlej V, Aguiar L, Piperni SG, Zhang J, Liu Y, Ricci-Junior E, Alexis F, Alves Junior S, Zhu L, Santos-Oliveira R. Graphene quantum dots decorated with imatinib for leukemia treatment. J Drug Deliv Sci Technol. 2021 Feb;61:102117. doi: 10.1016/j.jddst.2020.102117. Epub 2020 Sep 28. PMID: 34457042; PMCID: PMC8389840.

97. Kesharwani, M., et al. (2020). Graphene oxide-based nanocarrier for targeted delivery of imatinib to leukemia cells. European Journal of Pharmaceutical Sciences, 146,105258. https://doi.org/10.1016/j.ejps.2020.105258

98. Mahmoodi, A., et al. (2019). PEGylated carbon nanotubes as efficient carriers for imatinib: An in vitro study. Journal of Drug Delivery Science and Technology, 52, 312–318. https://doi.org/10.1016/j.jddst.2019.05.034

Appendices

Appendix A

Figures

Figure 1.1

Allotropes of carbon, deduced from ref 20

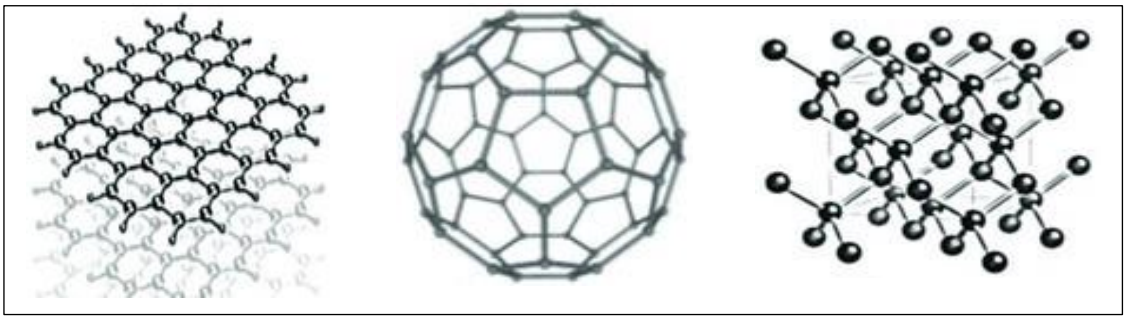

Figure 1.2

Structure of graphene, Fullerene, CNT and Graphite (24).

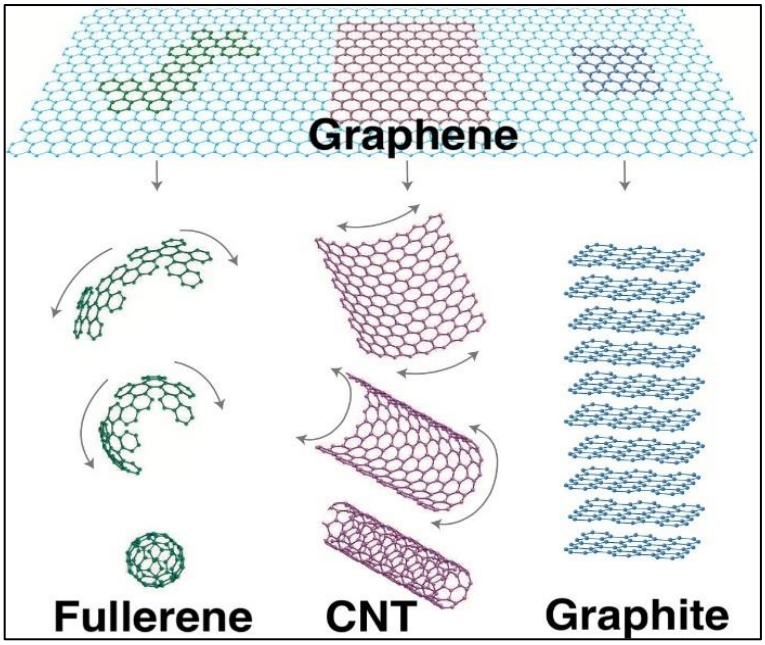

Figure 3.11

L6 cells viability with raw materials

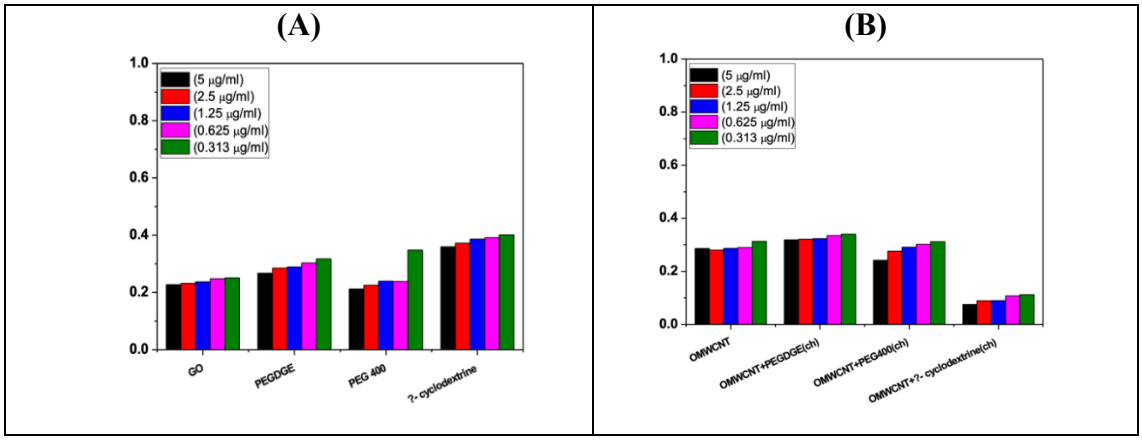

Note: A) GO, PEG 400, PEGDGE, β-Cyclodextrin; B) OMWCNT, PEG 400, PEGDGE, β-Cyclodextrin. At different concentrations (5, 2.5, 1.25, 0.625 and 0.3125 µg/ml).

Figure 3.12

L6 cells viability of GO with PEG 400, PEGDGE, β-Cyclodextrin, and DAP according to physical and chemical functionalization. At different concentrations (5, 2.5, 1.25, 0.625 and 0.3125 µg/ml)

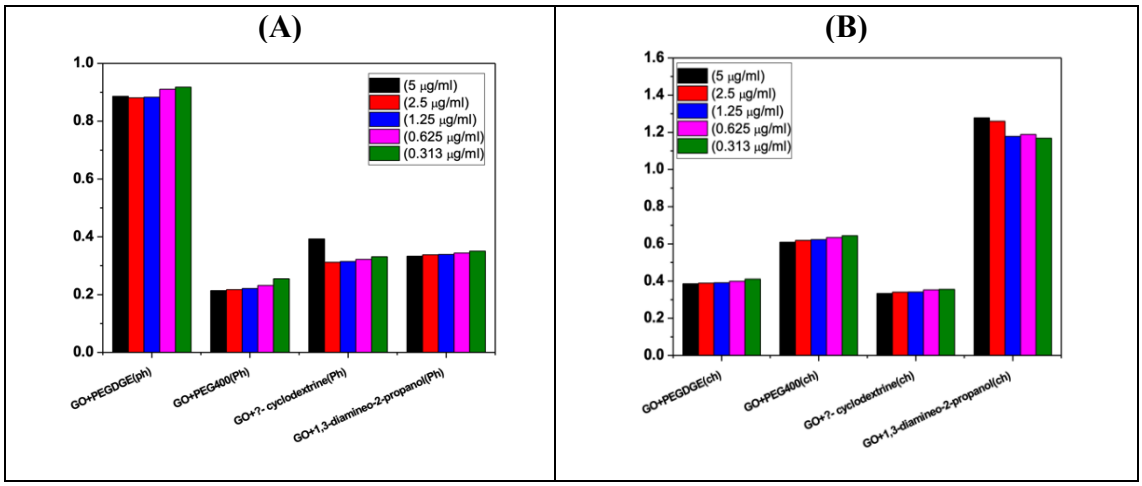

Figure 3.13

L6 cells viability of functionalized GO with PEG 400, PEGDGE, β-Cyclodextrin, and DAP chemically and physically. At different concentrations (5, 2.5, 1.25, 0.625 and 0.3125 µg/ml)

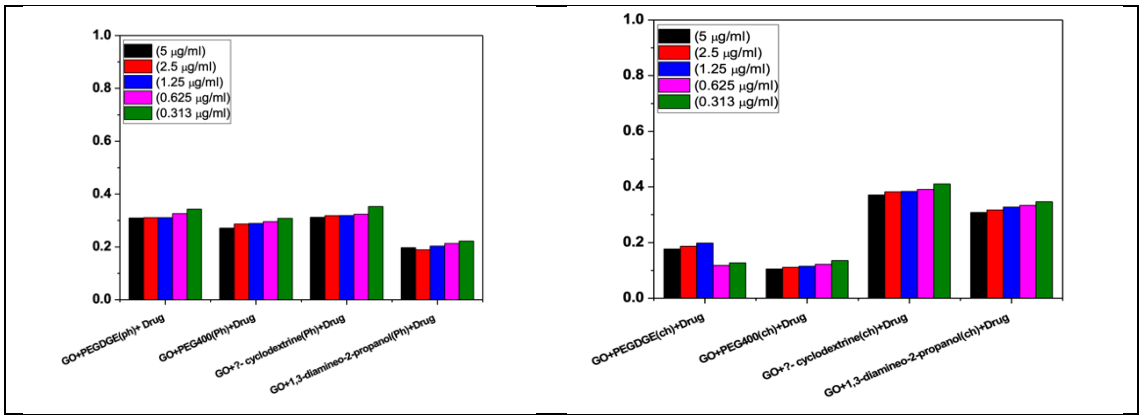

Figure 3.14

L6 cells viability of OMWCNT with PEG 400, PEGDGE, β-CD, and DAP according to physical and chemical functionalization. At different concentrations (5, 2.5, 1.25, 0.625 and 0.3125 µg/ml)

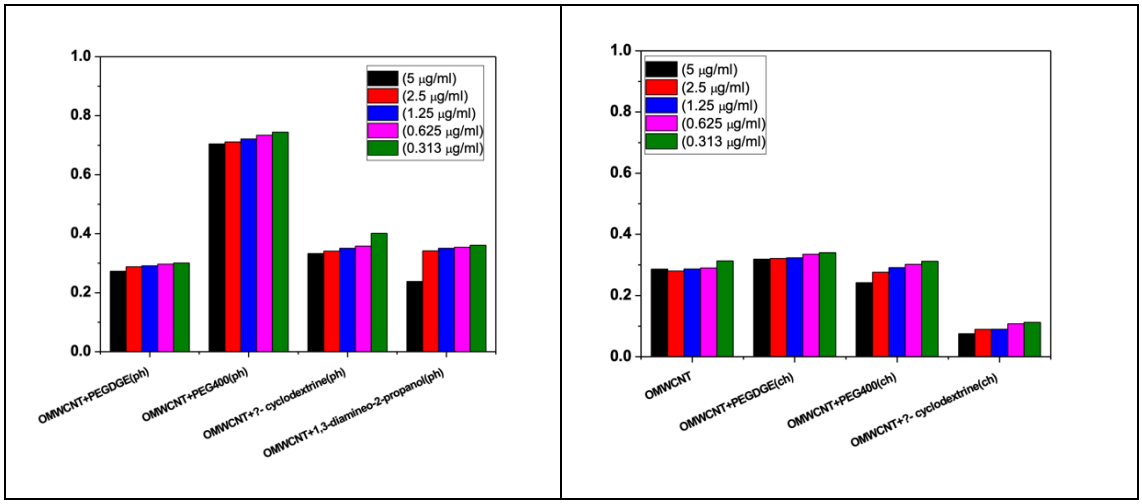

Figure 3.15

L6 cells viability of OMWCNT loading IMA with PEG 400, PEGDGE, β-CD, and DAP according to physical and chemical functionalization. At different concentrations.

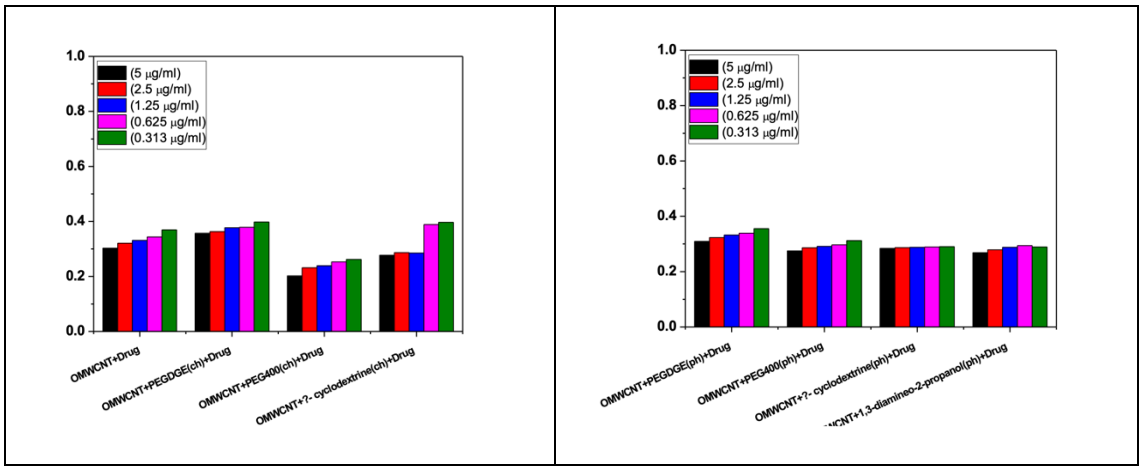

Figure 3.16

Viability of HeLa cells after 24 h exposure to unloaded carbon-based carriers—(GO), (PEGDGE), PEG 400, and β-CD—at five concentrations (0.313, 0.625, 1.25, 2.5, and 5 µg mL⁻¹).

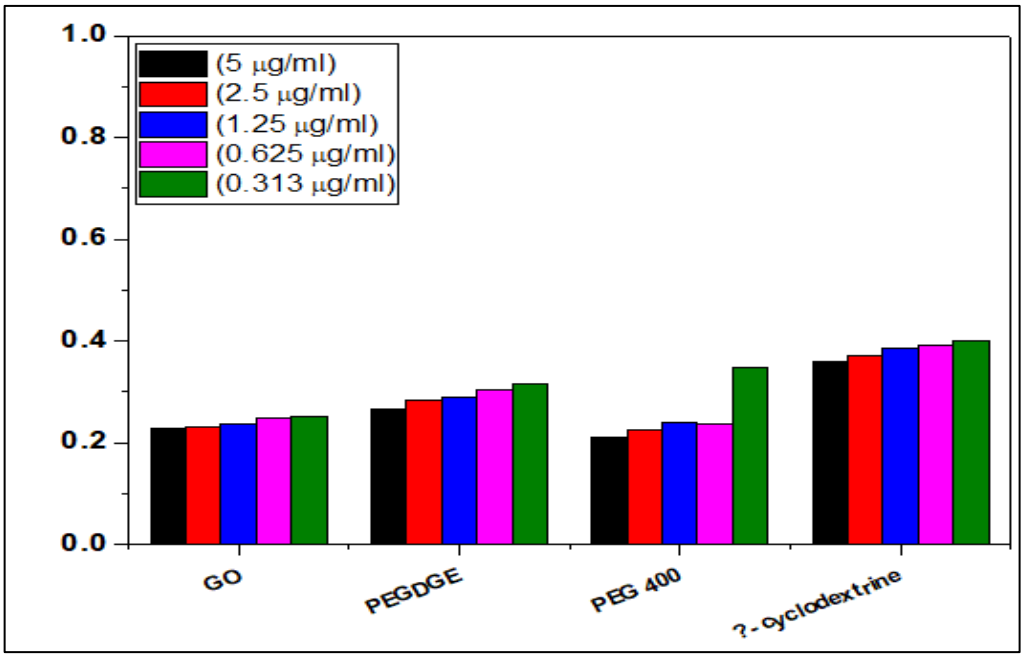

Figure 3.17

Cytostatic effects on Hela cells of A) IMA-loaded carriers; B) Chemically functionalized GO with carriers; C) Chemically functionalized GO with IMA-loaded carries

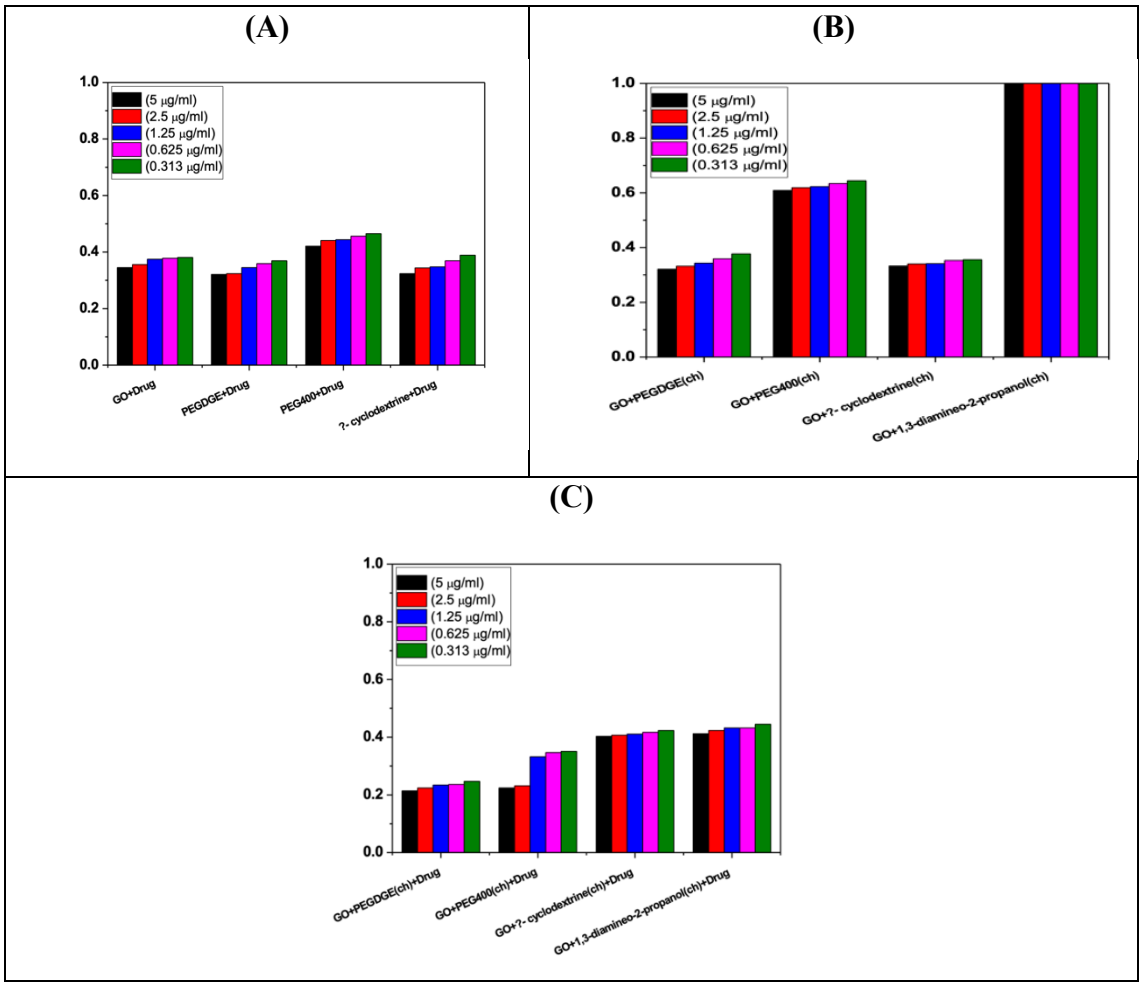

Figure 3.18

Cytostatic effects on Hela cells of A) physically functionalized GO with carriers; C) physically functionalized GO with IMA-loaded carries

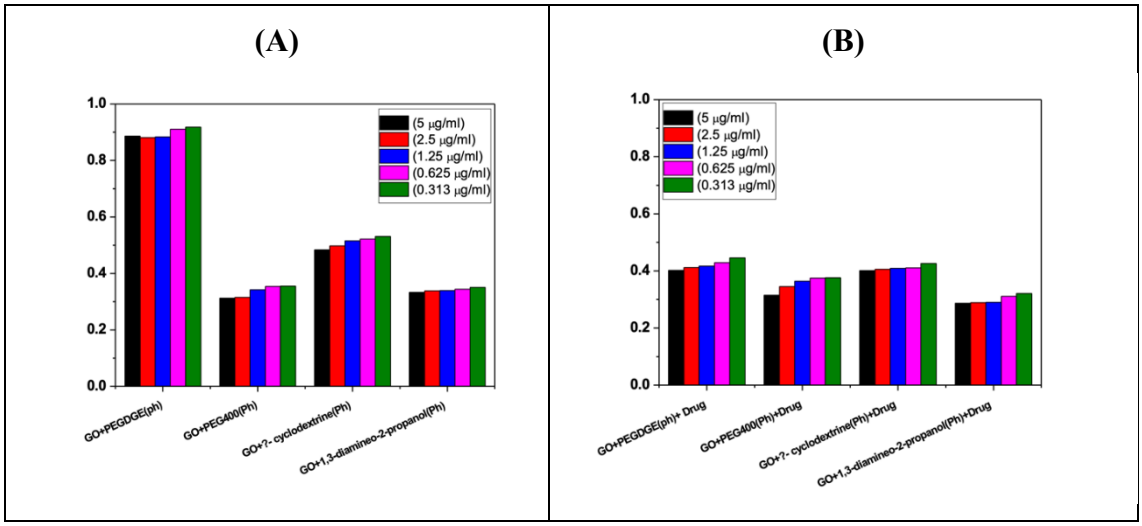

Figure 3.19

Cytostatic effects on Hela cells

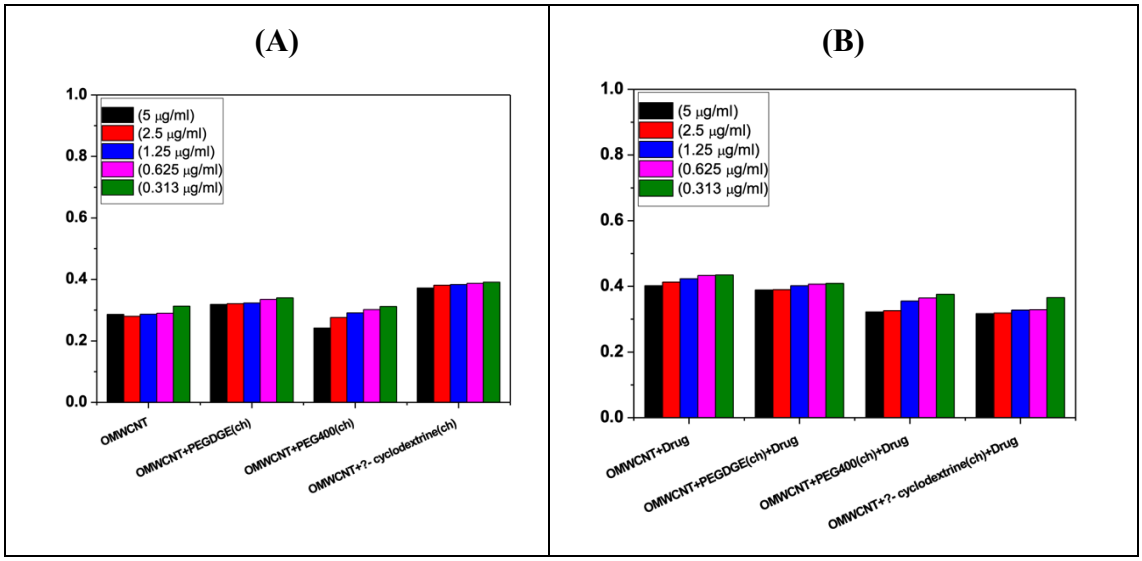

Note: A) Chemically functionalized OMWCNTs with carriers; B) Chemically functionalized OMWCNTs with IMA-loaded carries.

Figure 3.20

Cytostatic effects on Hela cells of A) physically functionalized OMWCNTs with carriers; C) physically functionalized OMWCNTs with IMA-loaded carries

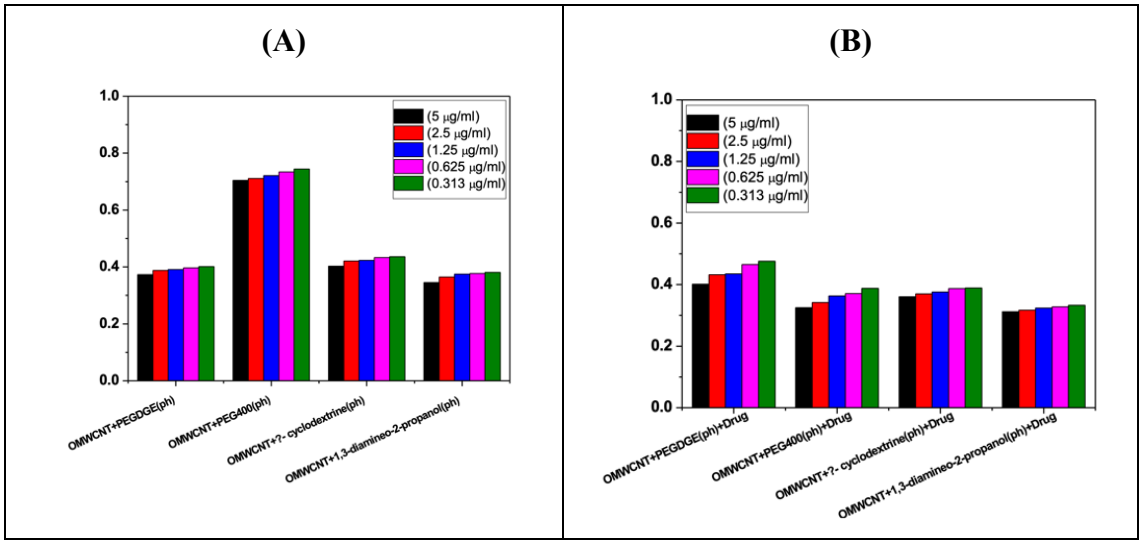

Figure 3.21

Cytostatic effects on L6 cells of imatinib-loaded carriers

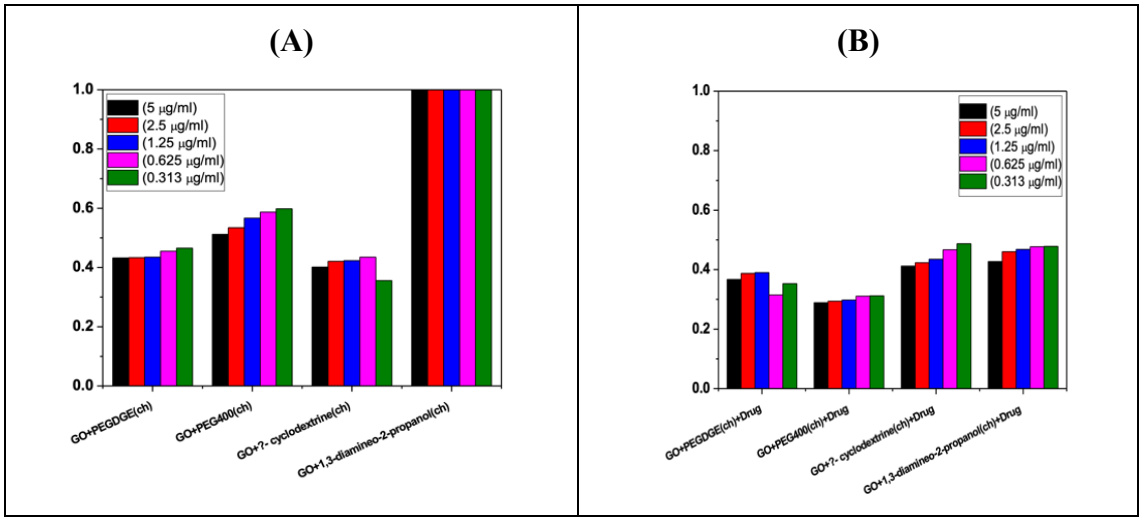

Note: A) chemically functionalized GO with carries B) chemically functionalized GO with IMA-loaded carries.

Figure 3.22

Cytostatic effects on L6 cells of imatinib-loaded carrier

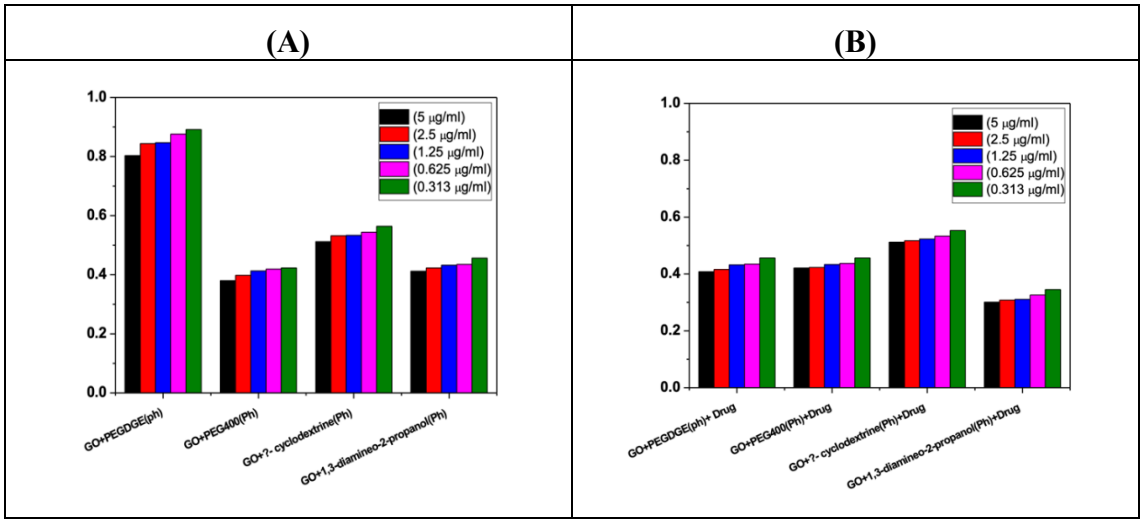

Note: A) physical functionalized GO with carries B) physically functionalized GO with IMA-loaded carries.

Figure 3.23

Cytostatic effects on L6 cells

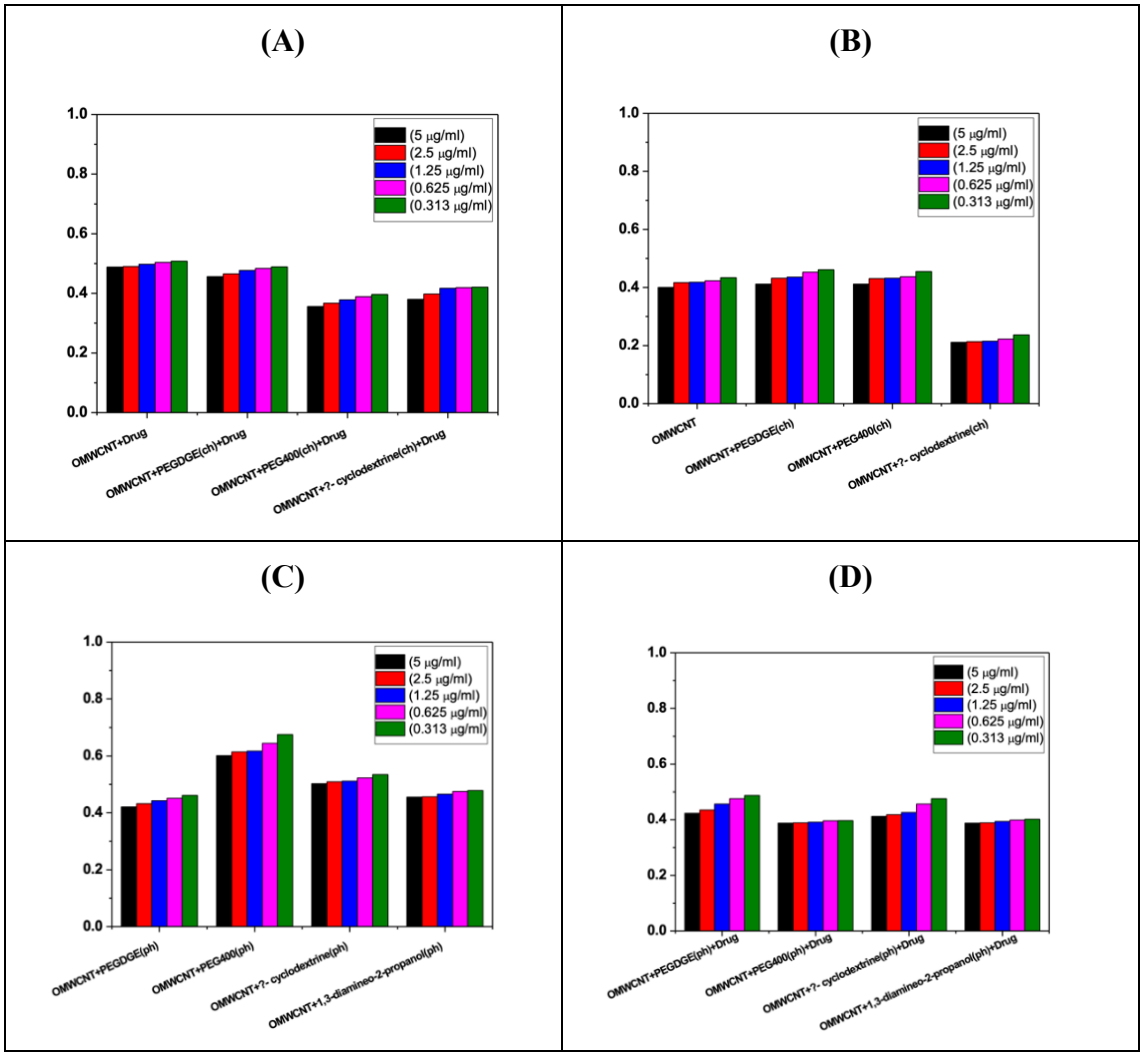

Note: A) Chemically functionalized OMWCNTs with carriers; B) Chemically functionalized OMWCNTs with IMA loaded carries; C) physically functionalized OMWCNTs with carries B) physically functionalized OMWCNTs with IMA-loaded carries.

Figure 3.24

Representative images (A-F) of cells treated with decreasing concentrations of the compound

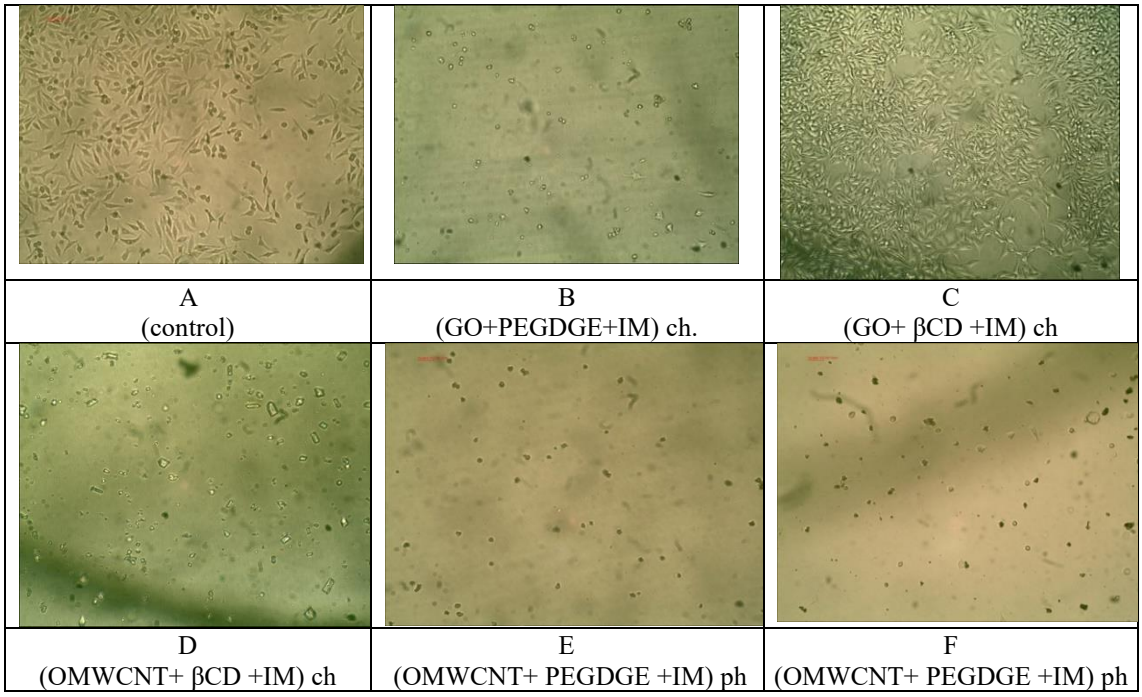

A (control)	B (GO+PEGDGE+IM) ch.	C (GO+ βCD +IM) ch
D (OMWCNT+ βCD +IM) ch	E (OMWCNT+ PEGDGE +IM) ph	F (OMWCNT+ PEGDGE +IM) ph

Note: 1mg\mL, 0.5 mg\mL, 0.25 mg\mL, 0.125 mg\mL, and 0.062 mg\ mL. A concentration-dependent effect on cell morphology and density is observed, indicating a graded cellular response to treatment.

جامعة النجاح الوطنية
كلية الدراسات العليا

نظام توصيل الإيماتينيب المضاد للسرطان باستخدام الجرافين وأنابيب الكربون المتعددة الجدران المؤكسدة: التعديل الوظيفي والاستهداف

اعداد
ايمان يوسف عطا الله مخارزة

إشراف
أ. د. شحدة جودة
أ. د. عثمان حامد

قُدّمت هذه الأطروحة استكمالا لمتطلبات الحصول على درجة الدكتوراه في الكيمياء من كلية الدراسات العليا في جامعة النجاح الوطنية، نابلس- فلسطين.
2025

نظام توصيل الإيماتينيب المضاد للسرطان باستخدام الجرافين وأنابيب الكربون المتعددة الجدران المؤكسدة: التعديل الوظيفي والاستهداف

اعداد

ايمان يوسف عطا الله مخارزة

إشراف

أ. د. شحدة جودة

أ. د. عثمان حامد

الملخص

الخلفية: أنابيب الكربون النانوية مثل أكسيد الجرافين وأنابيب الكربون النانوية المؤكسدة والمتعددة الجدران جذبت اهتمام الباحثين كمركبات ناقلة للأدوية، بسبب مساحتها السطحية الكبيرة، وانخفاض تكلفتها، وقلة آثارها الجانبية بعد التعديل، بالإضافة إلى قدرتها العالية على الانتشار في الوسط الحيوي. أيضا الارتباط التساهمي وغير التساهمي تم أخذه بعين الاعتبار باعتباره وسيلة فعالة لتحسين الارتباط بالادوية، وذلك لجعلها أكثر كفاءة في استهداف الخلايا السرطانية دون التأثير على الخلايا الطبيعية.

الهدف: الهدف الرئيسي من البحث هو تحضير 16 مركب جديد من أكسيد الجرافين وأنابيب الكربون النانوية المؤكسدة والمتعددة الجدران، بعد تعديلها بطرق كيميائية وفيزيائية، ودراسة فعاليتها كمضادات للسرطان.

المنهجية: تم تصنيع المركبات عن طريق أكسدة الجرافيت وأنابيب الكربون في وسط حمضي باستخدام بيرمنغنات البوتاسيوم، ثم تعديلها بمركبات مختلفة (مثل: PEGDGE, PEG 400, β-Cyclodextrin, 1.3-diamino-2-propanol)،بعد ذلك تم اختبار فعاليتها ضد خلايا سرطان عنق الرحم (Hela) ومقارنتها بتأثيرها على خلايا طبيعية (L6) باستخدام اختبار MTT.

النتائج: تم عمل تحليل لبعض المركبات المحضرة عن طريق تقنية FT-IR للتأكد من حدوث الارتباط. حيث ان الارتباط الكيميائي والفيزيائي وتحميل الايماتينيب قد تحقق. أظهرت العديد من المركبات خصائص تؤكد

فعاليتها في مقاومة الخلايا السرطانية والحفاظ على تأثير منخفض على الخلايا الحية، مثل OMWCNT\GO -PEGDGE\PEG 400\ β- CD and DAP كما تم إثبات فعالية تحميل دواء الإيماتينيب على هذه الأنظمة.

الخلاصة: مجموعة جديدة من المركبات من أكسيد الجرافين وأنابيب الكربون النانوية المؤكسدة والمتعددة الجدران والمعدلة تم تحضيرها.تم إجزاء اختبارات السمية الخلوية والاختبارات الكابحة لانقسام الخلايا (cytotoxic and cytostatic) ، بعض التركيبات مثل OMWCNT\GO -PEGDGE\PEG 400\ β- CD and DAP سواء تم تحضيرها فيزيائياً أو كيميائياً فعالية ضد خلايا سرطان هيلا دون تأثير كبير على الخلايا الذبيعية وهذا يجعل هذه المركبات واعدة في المستقبل كأدوية لعلاج السرطان.

الكلمات المفتاحية: إيماتينيب، مضاد للسرطان، تعديل كيميائي، سُمية خلوية، تثبيط نمو الخلايا.